LINKING TWO SEEMINGLY UNRELATED DISEASES, CANCER AND

ACUTE RESPIRATORY DISTRESS SYNDROME, THROUGH A

DICTYOSTELIUM SECRETED PROTEIN

A Dissertation

by

SARAH E. HERLIHY

Submitted to the Office of Graduate and Professional Studies of
Texas A&M University
in partial fulfillment of the requirements for the degree of

DOCTOR OF PHILOSOPHY

Chair of Committee,	Richard Gomer
Committee Members,	Michael Criscitiello
	Luis Rene Garcia
	Michael Polymenis
	Kathryn Ryan
Head of Department,	Thomas McKnight

August 2014

Major Subject: Biology

ABSTRACT

The work in this dissertation links two diseases through a protein secreted by *Dictyostelium discoideum* cells. The protein, AprA, inhibits cell proliferation and induces chemorepulsion (movement away) of *Dictyostelium* cells. This has implications in both cancer research and the study of Acute Respiratory Distress Syndrome.

Cancer is a misregulation of cellular proliferation. Often the removal of a primary tumor results in rapid metastatic cell proliferation. The rapid proliferation of metastatic cells indicates the presence of a factor, called a chalone, secreted by the primary tumor cells, that inhibits metastatic cell proliferation. The ability of AprA to inhibit proliferation of the cells that secretes it classifies it as a chalone. Using the model organism *Dictyostelium* and the protein AprA allows us to study chalone signaling mechanisms.

Acute Respiratory Distress Syndrome (ARDS) is characterized by an excess influx of neutrophils into the lungs. Neutrophils damage the lung tissue and ultimately recruit more neutrophils that repeat the process. A need exists to remove these cells and allow resolution to occur. One way to accomplish this is through chemorepulsion, the directional movement of cells away from an external cue. We can use AprA to study the mechanisms of chemorepulsion.

In this dissertation, I have found that the PTEN-like protein CnrN, which is an inhibitor of proliferation and chemotaxis, is involved in both AprA proliferation inhibition and chemorepulsion of *Dictyostelium* cells. I have shown that the human

ii

protein DPPIV, which is structurally similar to AprA, causes chemorepulsion of human neutrophils. Additionally, aspirated DPPIV reduces the accumulation of neutrophils in the lungs of a mouse model of ARDS. Work shown in the appendices suggests that AprA signals through specific G protein-coupled receptors.

The work in this dissertation studies the role of chalones and chemorepellents. It allows the unique opportunity to study chemorepulsion in both *Dictyostelium* and human cells. The hope and goal is that the work in this dissertation could lead to novel therapies for diseases such as cancer and ARDS.

DEDICATION

I would like to dedicate this dissertation first to my husband, Kevin Herlihy, without whom I would not have been so successful. Secondly, I would like to dedicate this to my families who have supported and encouraged me. Thank you all.

ACKNOWLEDGEMENTS

I would like to thank my committee chair, Dr. Gomer for his support, guidance, and patience throughout my graduate career. I also would like to thank my committee members, Dr. Criscitiello, Dr. Garcia, Dr. Polymenis, and Dr. Ryan, for their advice and support throughout the course of this research.

I also want to extend my gratitude to Dr. Robert Insall who provided the Insall chambers, which were essential to this work. A huge thanks to my current and past undergraduates with their contributions to my work including Hannah Strake, Jose Ting, Francisco Brito, and Michael Teach. Thanks also go to my friends and colleagues and the department faculty and staff for making my time at Texas A&M University a great experience. A special thanks to my former and current lab mates who make each day unique (Nehemiah Cox, Dr. Jeff Crawford, Dr. Anu Maharjan, Dr. Jonathan Phillips, Dr. Darrell Pilling, Patrick Suess, Rachel Sterling, Michael White, and Ivy Zheng). Thanks to Simone Lepage for her constant support and Dr. Lindsay Bennett for guiding me through the dissertation writing process.

Finally, thank you to my two wonderful families for their encouragement and to my husband for his patience, love, and unfailing support.

TABLE OF CONTENTS

LIST OF FIGURES

LIST OF TABLES

CHAPTER I

INTRODUCTION AND LITERATURE REVIEW

Chalones

The ability of tissues or a group of cells to regulate their number of cells can be explained simply by the chalone theory. A chalone is a factor, secreted by cells, that acts by inhibiting cell division (1, 2). Historically, chalones referred to small oligopeptides, purified from homogenates, that inhibited cellular division of a specific tissue (2). These factors included chalones for tissues such as bone marrow, liver, epidermis, and thymus, but researchers were unable to verify these factors were actually secreted (2-7). The discovery of factors other than oligopeptides, such as the protein myostatin, revived the chalone theory (8).

The most well characterized chalone is myostatin, which regulates the amount of muscle an organism has (9). Myostatin belongs to the TGF-β superfamily, which is thought to contain several chalones, including an olfactory epithelium chalone (10). Significant increases in muscle mass are observed in myostatin knockout mice and cattle with mutations of the myostatin gene (11, 12). Overexpression of myostatin in mice causes a dramatic loss of muscle mass and wasting (13). Myostatin acts by inhibiting the proliferation of myoblasts, the muscle cells precursors, mediated through various downstream signals, some of which have been identified (14-17).

Although we know how myostatin functions to inhibit myoblast proliferation, much less is known about the chalones and their mechanisms within the larger field of

chalones. The theory suggests that as a tissue size increases, the concentration of chalone will increase to stop or slow proliferation until a tissue or group of cells reaches its ideal size (10). The evidence for factors that regulate cell division is widespread. Unlike the case for myostatin, for many tissues the chalone and associated signal transduction pathways are unknown. For example, the melanocyte chalone can be injected into the skin, under a melanoma and the chalone will inhibit further proliferation of the melanoma through unknown mechanisms (18, 19). An unknown liver chalone regulates the division of cells in damaged livers to regrow the liver to its original size (20, 21). A splenectomized mouse regrows implanted pieces of spleen to the exact mass of its removed spleen (22). One of the most intriguing examples of the existence of chalones is observed in cancer patients who have their primary tumors removed. In these patients, metastases begin to proliferate rapidly after the primary tumor is removed (23-28). All of these examples point toward the existence of factors, such as chalones, that sense cell density and can regulate cell proliferation.

Dictyostelium discoideum

Dictyostelium discoideum diverged on the evolutionary tree following plants but prior to fungi (29). Despite its early divergence, *Dictyostelium* shares more homologous genes with mammals than yeast does with mammals (29-31). In 2005, the entire 34 Mb *Dictyostelium discoideum* haploid genome was sequenced and recently genome-wide RNA-seq was completed (32, 33). Both of these, along with gene annotations, are provided on a NIH-funded, open-access webpage http://dictybase.org/. Additionally, the

site offers strains, transformants, and vectors through an NIH-funded stock center. A number of features make *Dictyostelium* an ideal eukaryotic model. Axenic strains (Ax) can grow in simple media with a doubling time of approximately twelve hours, making *Dictyostelium* inexpensive and easy to maintain in the laboratory. *Dictyostelium* cells can also be grown on agar plates, where they chemotax toward and ingest bacteria. Cells can be manipulated easily; mutagenesis can be done through restriction enzyme-mediated insertion or shotgun antisense and vectors can be expressed through simple transfection (34-37). In addition to its vegetative growth in the presence of nutrients, *Dictyostelium* cells can undergo development. When starved, *Dictyostelium* cells chemotax toward relayed pulses of cAMP and form fruiting bodies which each contain approximately 20,000 cells. These attributes make *Dictyostelium* a good model to study tissue size regulation, chemotaxis, and signal transduction (38).

Dictyostelium **Chalones**

Dictyostelium produces two chalones, AprA and CfaD (39, 40). AprA and CfaD act as inhibitors of vegetative *Dictyostelium* proliferation (39, 40). Cells lacking either AprA or CfaD proliferate faster than wild type cells (39, 40). Mutant fast proliferation phenotypes can be rescued by expressing AprA or CfaD in their respective mutant backgrounds (39, 40). In agreement with the chalone theory, the concentrations of AprA and CfaD increase as the *Dictyostelium* cell density increases (40, 41). The translation of AprA and CfaD proteins is regulated by eIF2α phosphorylation (42). When recombinant AprA (rAprA) or recombinant CfaD (rCfaD) are added to wild type cells, they slow the

proliferation of wild type cells (40, 41). rAprA rescues the $aprA^-$ phenotype, but not $cfaD^-$ phenotype, and rCfaD rescues the $cfaD^-$ phenotype but not $aprA^-$ (40, 41). Both proteins are therefore necessary for the inhibition of proliferation. Although AprA and CfaD are both necessary, they appear to activate separate G protein-coupled receptors (unpublished data) and downstream signaling molecules (43). This is in agreement with the observation in other systems that some chalones may function through G protein-coupled receptors (2, 44). AprA signals through the Gα protein Gα8 and an unidentified G protein-coupled receptor, while CfaD appears to function through Gα1 and an unknown G protein-coupled receptor (43). Several downstream signaling components of AprA and CfaD have been identified including BzpN, a leucine zipper transcription factor, and QkgA, a tyrosine kinase-like ROCO kinase, and RblA, the tumor suppressor retinoblastoma (45-47).

Apart from its role as a chalone, AprA functions as a chemorepellent of *Dictyostelium* cells (48). When wild type *Dictyostelium* cells are plated on agar, cells tend to move outward away from the dense colony center (46). Cells lacking AprA maintain a tight colony edge and do not move outward from the colony (46). Cells move in a biased direction away from a source of rAprA, but not in a biased direction from buffer alone or buffer containing the chalone rCfaD (48). While AprA affects the direction of cell movement, AprA does not affect the speed at which the cells move (48). The chemorepellent activity of AprA is dependent on CfaD, the ROCO kinase QkgA, and the Gα protein Gα8 (48). AprA does not require BzpN, phospholipase C (PLC), or the *Dictyostelium* phosphatidylinositol 3-kinase (PI3K) 1 or 2 to induce chemorepulsion

4

(48). Similar to *Dictyostelium* cell movement outward from a colony, some researchers have suggested that chemorepellents exist within tumors to cause these cells to move away from the cell-dense tumor and promote invasion and metastases (49).

Chemotaxis

The directed movement of cells, or chemotaxis, can occur when a cell senses a gradient of an external cue. Eukaryotic cell chemotaxis has been most extensively studied in *Dictyostelium* and its mammalian counterpart, the neutrophil (38, 50-52). Both types of cells can bias their directional movement based on external cues. *Dictyostelium* offers the advantage of genetic manipulation, which is difficult in the short-lived neutrophil. Chemoattraction, the movement of cells toward an external cue, is well studied in both models. *Dictyostelium* cells migrate toward the bacterial product folate in their vegetative state and cAMP during development (53). Neutrophils migrate toward a number of chemoattractants including the bacterial product f-Met-Leu-Phe (fMLP) and interleukin-8 (IL-8) secreted by macrophages and epithelial cells (54, 55).

The signal transduction pathways mediating *Dictyostelium* and neutrophil chemotaxis are highly conserved (51, 56). Chemotaxis begins with the ability to sense a gradient of chemoattractant. Typically, chemoattractants are sensed by detecting higher concentrations of the chemoattractant on one side of the cell through uniformly expressed G protein-coupled receptors (51, 57). Directional movement is dependent on the maintenance of cell polarity and the formation of pseudopods to move the cell forward (50, 51). When a cell polarizes, the cell becomes elongated and alters the

localization of protein signals within the cell body (51). G protein-coupled receptors signal to PI3K which phosphorylates the membrane lipid phosphatidylinositol 4,5-bisphosphate (PIP_2) to phosphatidylinositol 3,4,5-trisphosphate (PIP_3) and increases PIP_3 at the leading edge (end of the cell closest to the attractant) of the cell where it promotes pseudopod formation to move the cell forward (38, 51, 58-60). Sites of actin filament rearrangement are induced by PIP_3 and these sites are locations of pseudopod formation (61). At the rear of the cell, phosphatase and tensin homolog (PTEN) prevents the buildup of PIP_3 by dephosphorylating PIP_3 back into PIP_2 (38, 51, 58, 62). In this way, PTEN inhibits the formation of pseudopods in the opposite direction of the chemoattractant signal (38, 51, 58, 62). An effector of PI3K signaling and a small GTPase, Rac, helps regulate pseudopod formation at the leading edge through actin polymerization (51). Additionally, Rac inhibits Rho, another small GTPase at the leading edge (51). Consequently, Rho becomes polarized to the trailing edge where it interacts with PTEN to promote myosin filament formation and inhibit actin formation, thereby inhibiting pseudopod formation (51). By maintaining or altering the polarization of these internal signals, cells can manipulate their directional movement toward a chemoattractant.

Another form of direct cell movement is chemorepulsion, where cells move away from a given signal. Although many cell types have the ability to undergo both chemoattraction and chemorepulsion, the mechanisms are not as well characterized for chemorepulsion as they are for chemoattraction. Many cells have been observed chemotaxing toward (chemoattraction) and away from (chemorepulsion) external cues

including *Dictyostelium* cells, neutrophils, mast cells, neuronal cells, and cancerous cells (49, 63-66). In the developing brain, neuronal chemorepellents such as semaphorins, netrin-1, and Slit help guide axon growth (66-68). Later axon growth is blocked by migratory inhibitory cues such as myelin-associated glycoprotein (MAG) (69). Recently, MAG was shown to activate PTEN, indicating chemorepellents, at least in neurons, might function by potentiating inhibitory signals to induce polarity (69). An analog of cAMP causes chemorepulsion in *Dictyostelium* cells (65). Similar to neurons, these repulsed *Dictyostelium* cells show a reversal of chemoattractive signaling, where PTEN is localized nearest the cue to prevent movement/pseudopod formation in the direction of the repellent (65). At high concentrations, IL-8, usually a chemoattractant of neutrophils, becomes a chemorepellent of neutrophils (64). Cells in a gradient of high IL-8 also show a reverse of attractant signaling, suggesting neutrophils may also use similar pathways in chemoattraction and chemorepulsion (64). Akt, an effector of PI3K, is localized to the leading edge of the cells (the edge away from the highest concentration of IL-8) (64). During inflammation, neutrophils move from the bloodstream into a damaged/infected tissue (70). Most neutrophils are thought to undergo apoptosis within the tissue as resolution begins (70). Reverse migration, or movement of neutrophils back into the bloodstream, can be observed in the wounds of zebrafish (71). A number of groups have shown that mammalian neutrophils can undergo reverse migration identified by altered expression of proteins on the neutrophils (72, 73). Reverse migration may be caused by either chemoattractant or chemorepellent signals.

Dipeptidyl Peptidase IV

Dipeptidyl peptidase IV (DPPIV) is a protein belonging to a large group of "DPPIV activity and/or structure homology" (DASH) proteins (74-79). DPPIV is a 100 kDa serine protease which cleaves peptides with a proline or alanine in the second position at the N-terminus. The active site of DPPIV is a triad including Ser630, Asp708, and His740 (77). DPPIV is active as a dimer in the plasma membrane of some lymphocytes and epithelial cells and a heavily glycosylated soluble form of DPPIV is also found in plasma, serum, cerebrospinal fluid, synovial fluid, semen, and urine (75, 76, 79-81). The glycosylation has been predicted to be important for the enzymatic activity of DPPIV (75, 81).

The role of DPPIV is extensive. Functions of DPPIV can be broken down into two main categories proteolytic and cellular communication (82). In the blood, DPPIV cleaves a number of substrates. One of DPPIV's main substrates is glucagon-like peptide-1 (GLP-1), an incretin that regulates insulin levels (83). Incretins are increased in response to glucose ingestion (83). Incretins subsequently increase insulin secretion and therefore glucose uptake from the blood (83). DPPIV inhibits incretin function through enzymatic cleavage (83). Inhibitors of DPPIV are being used as treatment for type 2 diabetes where glucose uptake from the blood is misregulated (83). The inhibitors allow a longer half-life of the incretins to influence insulin secretion and glucose uptake (83). DPPIV also cleaves stromal-derived factor 1 (SDF-1) the ligand for CXCR4 (84). SDF-1 is a chemoattractant for CD34^{+} hematopoietic progenitor cells (HPCs) (85).

8

When cleaved by DPPIV, the affinity of SDF-1 for CXCR4 decreases, allowing HPCs to migrate into the bloodstream (85).

DPPIV binds to many binding partners to elucidate different cellular responses. The membrane form of DPPIV binds adenosine deaminase (ADA), which metabolizes adenosine (86). DPPIV-ADA binding and ADA accumulation at the cell surface is proposed to aid T-cell proliferation that is inhibited by excess adenosine (86). The cytoplasmic domain of membrane DPPIV interacts with CD45, a membrane-linked tyrosine phosphatase, and initiates signaling to downstream effectors (87). DPPIV also interacts with the mannose 6-phosphate receptor, a partnership that results in receptor internalization following T-cell activation (87). Interactions between DPPIV and the extracellular matrix protein molecules fibronectin and collagen are thought to increase cell migration (87). Additionally, soluble DPPIV (sDPPIV) can up-regulate CD86 on monocytes through a co-stimulation interaction with caveloin-1 to activate T-cells (75, 88).

Mice lacking DPPIV have been generated (89) and rat strains with spontaneous mutations of DPPIV have been identified (90, 91). There appears to be no defect in blood cell production as DPPIV deficient animals have normal blood levels of most leukocytes (92-94). When DPPIV knockout mice have experimentally induced arthritis, an increased severity is observed with more than a 2-fold increase in the number of cells in the joint (95). DPPIV deficient rats have an increase in neutrophils in ovalbumin-induced lung inflammation (96). Reduced levels of DPPIV correlate with increased inflammation in the joints of rheumatoid arthritis patients (97). The increased

9

inflammation observed in DPPIV deficient situations has been assumed to be due to a persistent chemokine presence, as DPPIV was not present to cleave those chemokines (98).

DPPIV has a complex role in disease. Aggressive lymphomas and gliomas are associated with increased expression of DPPIV (75, 99), while melanoma progression is associated with decreased DPPIV expression (75, 99, 100). The conflicting implications of DPPIV in disease are probably due to misregulation of DPPIV substrates from altered levels of enzymatic activity. DPPIV's role in blood/glucose regulation (diabetes), activation and inactivation of chemokines (cell migration and immune response), neuropeptides, and vascular regulatory peptides (angiogenesis), tissue remolding (wound healing), fibroblast activation (immune response, fibrosis), cell adhesion, gives it a wide range of processes where its misregulation would prove detrimental or beneficial (77, 81, 99).

Acute Respiratory Distress Syndrome

Damage to the lung tissue in Acute Respiratory Distress Syndrome (ARDS) ultimately results in respiratory failure followed by death in 40% of patients respiratory assistance, such as mechanical ventilation, and 90 % of unassisted patients (101-103). ARDS can develop following gas or acid inhalation, sepsis, trauma, pneumonia, or severe burns (104-106). In early stages of ARDS, alveolar epithelial cells are damaged causing a vascular leak (106). Immune cells, primarily neutrophils, infiltrate the alveolar

space (105, 106). Neutrophils release reactive oxygen species and proteases that exacerbate the damage to lung tissue (105, 106). Resolution of the damage, edema, and removal of neutrophils from the lung tissue may all be misregulated in ARDS (102, 103, 107). Although approximately 60% of patients recover from ARDS, their overall quality of life is reduced and includes chronic respiratory problems, fibrosis, and cognitive problems such as depression (104, 108, 109). No treatments to date have been effective (103, 105). Cell based therapies are currently being investigated (103). The best treatment is management of lung integrity until resolution occurs (103).

CHAPTER II

A *DICTYOSTELIUM* SECRETED FACTOR REQUIRES A PTEN-LIKE PHOSPHATASE TO SLOW PROLIFERATION AND INDUCE CHEMOREPULSION[1]

Summary

In *Dictyostelium discoideum*, AprA and CfaD are secreted proteins that inhibit cell proliferation. We found that the proliferation of cells lacking CnrN, a phosphatase and tensin homolog (PTEN)-like phosphatase, is not inhibited by exogenous AprA and is increased by exogenous CfaD. The expression of CnrN in *cnrN⁻* cells partially rescues these altered sensitivities, suggesting that CnrN is necessary for the ability of AprA and CfaD to inhibit proliferation. Cells lacking CnrN accumulate normal levels of AprA and CfaD. Like cells lacking AprA and CfaD, *cnrN⁻* cells proliferate faster and reach a higher maximum cell density than wild type cells, tend to be multinucleate, accumulate normal levels of mass and protein per nucleus, and form less viable spores. When *cnrN⁻* cells expressing myc-tagged CnrN are stimulated with a mixture of rAprA and rCfaD, levels of membrane-associated myc-CnrN increase. AprA also causes chemorepulsion of *Dictyostelium* cells, and CnrN is required for this process. Combined, these results suggest that CnrN functions in a signal transduction pathway downstream of AprA and CfaD mediating some, but not all, of the effects of AprA and CfaD.

Introduction

Much remains to be understood about how tissue size is regulated. A possible way to regulate tissue growth is through secreted autocrine factors that slow the proliferation of cells in that tissue. A variety of observations suggest the presence of such factors (often referred to as chalones) in many different tissues, but little is known about these factors and their signal transduction pathways (8, 9, 45, 46, 110). Two such secreted autocrine factors have been identified in the model organism *Dictyostelium discoideum*. These proteins, AprA and CfaD, inhibit the proliferation of *Dictyostelium* cells as a population becomes dense. Strains lacking AprA or CfaD proliferate rapidly (39, 40, 42). Cell proliferation is slowed by adding recombinant AprA (rAprA) or recombinant CfaD (rCfaD) to cells, or by overexpressing these proteins (40, 41). Both *aprA*⁻ and *cfaD*⁻ cells are multinucleate (39, 40). Although AprA and CfaD affect proliferation, cells lacking these proteins show mass and protein accumulation on a per nucleus basis similar to that of wild type cells, indicating that AprA and CfaD do not affect the growth of cells (39, 40). In addition to inhibiting proliferation, AprA also causes chemorepulsion of cells, suggesting that AprA helps to disperse a colony of cells (48). When starved, *Dictyostelium* cells develop to form fruiting bodies containing spores that can be dispersed to areas with higher nutrient concentrations. The ability to form viable spores is therefore advantageous. Although AprA and CfaD slow proliferation and appear to be deleterious, these proteins help spore development and are thus advantageous for development (39, 40).

During development, *Dictyostelium* cells aggregate using relayed pulses of cAMP as a chemoattractant. The cells move up a gradient of extracellular cAMP by extending pseudopods in the direction of the cAMP source (62, 111, 112). Phosphatidylinositol 3-kinase (PI3K), which phosphorylates the membrane lipid phosphatidylinositol 4,5-bisphosphate (PIP_2) to phosphatidylinositol 3,4,5-trisphosphate (PIP_3), translocates from the cytosol to the membrane at the leading edge of the cell in response to cAMP and mediates actin polymerization and pseudopod formation (38, 58-60). PTEN negatively regulates the effect of PI3K by dephosphorylating PIP_3 to PIP_2 (38, 62, 113). When PTEN is localized to the membrane of cells, it inhibits the formation of pseudopods (38, 58, 62). When PI3K translocates to the leading edge and PTEN localizes to the back edge of the cell, pseudopod formation is inhibited at the back of the cell, enabling movement toward cAMP (58, 111, 114).

CnrN is a PTEN-like protein in *Dictyostelium* that has PTEN-like phosphatase activity (115, 116). In the absence of CnrN, levels of PIP_3 are higher than in wild-type cells (115). Akt, a downstream target in PI3K pathways, usually requires translocation and phosphorylation from the cytosol to the membrane for its activation (117-119). During development, Akt translocation and phosphorylation is increased in the absence of CnrN (115). The increases in Akt translocation, Akt phosphorylation, and levels of PIP_3 in *cnrN⁻* cells suggests that CnrN acts as a negative regulator of PIP_3 and Akt, which are both components of PI3K pathways (115, 119). Like PTEN, CnrN plays a role in *Dictyostelium* development. By antagonizing the PI3K pathway, CnrN negatively regulates the production of cAMP and stream breakup during aggregation (115).

Compared to wild type cells, $cnrN^-$ cells have smaller aggregation territories and fruiting bodies, increased cell motility, number of aggregation territories, cAMP levels, Akt translocation, and actin polymerization, move faster, move further toward cAMP, are insensitive to counting factor, and have shorter streams (115). All of these phenotypes are rescued by the expression of a myc-tagged CnrN in the $cnrN^-$ cells $(cnrN^-/CnrN^{OE})$(115).

In mammalian cells, PI3K signaling leads to cell proliferation (113, 120, 121). PIP_3 binds to downstream effectors such as PDK1 and Akt, which play a role in cell proliferation, growth, and survival (113, 120, 122-124). As PTEN effectively counteracts PI3K, it negatively regulates proliferation in mammalian systems and functions as a tumor suppressor (113, 125-128). Here we report that CnrN is necessary for the inhibition of proliferation by AprA and CfaD as well as AprA-induced chemorepulsion, indicating that CnrN acts as a negative regulator of proliferation in a chalone signal transduction pathway and mediates AprA-induced chemorepulsion.

Materials and Methods

Ax2 wild-type and $cnrN^-$ clone DBS0302655 (115) were grown in HL5 media (Formedium Ltd, Norwich, England) as previously described (129). $cnrN^-/CnrN^{OE}$ clone DBS0302656 and Ax2/$CnrN^{OE}$ clone YT05A cells were cultured in HL5 containing 15µg/ml geneticin (115). Recombinant AprA and CfaD were made following Bakthavatsalam et al. (40). Levels of extracellular AprA and CfaD were compared by starting cultures of cells in axenic shaking culture at 1.25×10^6 cells/ml and collecting

cells by centrifugation at 3000 x g for 4 minutes when cultures were at 2 x 10^6 cells/ml. A sample of the conditioned medium supernatant was mixed with an equal volume of 2X loading buffer and heated to 95°C for 5 minutes. 10 μl of these samples were run on 4-20% polyacrylamide gels, and Western blots were stained for AprA as previously described (39) or for CfaD as previously described (40). DAPI staining of nuclei was done as described (39). Proliferation inhibition, spore viability, mass and protein determination, doubling time calculations, and statistics were done as previously described (46) with the exception that for spore viability assays, 10^7 cells were washed twice in 8 ml PDF (20 mM KCl, 9.2 mM K_2HPO_4, 13.2 mM KH_2PO_4, 1 mM $CaCl_2$, 2.5 mM $MgSO_4$, pH 6.4) prior to resuspension. In addition, proliferation inhibition was measured using a combination of rAprA and rCfaD, both at 300 ng/ml. Fluorescence microscopy was conducted following (130, 131). Briefly, vegetative cells were placed in 8-well chambered glass slides (Nalge Nunc 177402) at a density of 5 x 10^4 cells/well, fixed with 3.7% formaldehyde for 10 minutes, and permeabilized with 0.5% TritonX-100 in PBS (140 mM NaCl, 2.7 mM KCl, 10 mM Na_2HPO_4, 1.8 mM KH_2PO_4, pH 7.4) for 5 minutes. Cells were stained with a 30-minute incubation with anti-Myc antibodies (Bethyl Laboratories) and a subsequent 30-minute incubation with Alexa Fluor 488 conjugated anti-rabbit IgG (Invitrogen) in PBS containing 0.05% NP-40 and 0.5% BSA at room temperature. Images were taken using an Axioplan Fluorescence Microscope (Carl Zeiss). Binding of AprA, CfaD, a mixture of both, or an equal volume of buffer to myc-tagged *cnrN⁻/CnrN^{OE}* cells was done as previously described (41, 43). Membranes were collected as previously described (41, 43), and Western blots of membrane samples

were stained with anti-Myc antibodies. Membranes were re-probed with anti-AprA and anti-CfaD antibodies (Bethyl Laboratories). Chemorepulsion assays were done as previously described (48).

Results

cnrN⁻ cells show aberrant proliferation inhibition by AprA and CfaD

The proliferation of wild-type cells is inhibited by AprA or CfaD (39-41). If AprA and/or CfaD transduce signaling through CnrN, we would expect *cnrN⁻* cells to be insensitive to AprA and/or CfaD. We incubated proliferating cells with rAprA or rCfaD and determined the decrease in cell density compared to a buffer control after a 16-hour incubation. As previously observed, wild-type cells had an approximately 20 percent decrease in proliferation in response to rAprA or rCfaD (Figure 1) (45, 46). *cnrN⁻* cells were essentially insensitive to rAprA, and this phenotype was rescued by expressing CnrN in the mutant background (Figure 1A). Compared to the addition of buffer, the addition of rCfaD to *cnrN⁻* cells significantly increased their proliferation (Figure 1B). Expressing CnrN in the *cnrN⁻* background blocked the ability of rCfaD to increase proliferation, but did not restore the ability of rCfaD to inhibit proliferation (Figure 1B). A combination of rAprA and rCfaD inhibited wild type proliferation similarly to either recombinant protein alone (Figure 1C). The response of *cnrN⁻* cells to the combination of rAprA and rCfaD mimicked their response to rCfaD alone (Figure 1C). The difference in the increase of proliferation of *cnrN⁻* cells between the addition of rCfaD alone and the combination of rCfaD and rAprA is statistically significant (t-test, p <

17

0.05). The proliferation of $cnrN^-/CnrN^{OE}$ cells was inhibited by the combination of rAprA and rCfaD (Figure 1C). Together, these results suggest that CnrN is necessary for AprA and CfaD to inhibit proliferation.

cnrN⁻ cells have fast proliferation

Cells lacking AprA or CfaD proliferate faster and to a higher stationary density then wild-type cells (39, 40). Like aprA⁻ and cfaD⁻ cells, cnrN⁻ cells proliferate faster, have a faster doubling time, and reach a higher maximum cell density than wild type cells (Figure 2A and Table 1). Occasionally, for unknown reasons, we observed this and other clones of cnrN⁻ cells proliferating slower than wild type cells. There are many reasons a mutant might proliferate slower, such as defects in a metabolic pathway, but it is unusual to find clones that proliferate faster than wild type. Therefore, we believe the fast proliferation phenotype is the true phenotype of cnrN⁻ cells. cnrN⁻/CnrNOE and Ax2/CnrNOE cells showed no significant difference in doubling time or maximal cell density compared to wild type (Figure 2A and Table 1). Although cnrN⁻/CnrNOE and Ax2/CnrNOE cells appeared to proliferate slower and to a lower cell density than cnrN⁻ cells, only the differences between the maximum cell densities were statistically significant. Unlike the proliferation in liquid culture, wild type, cnrN⁻, cnrN⁻/CnrNOE, and Ax2/CnrNOE cells showed similar proliferation rates on bacteria (Figure 2B). Together, the data suggest that in shaking liquid culture, CnrN decreases the proliferation of cells.
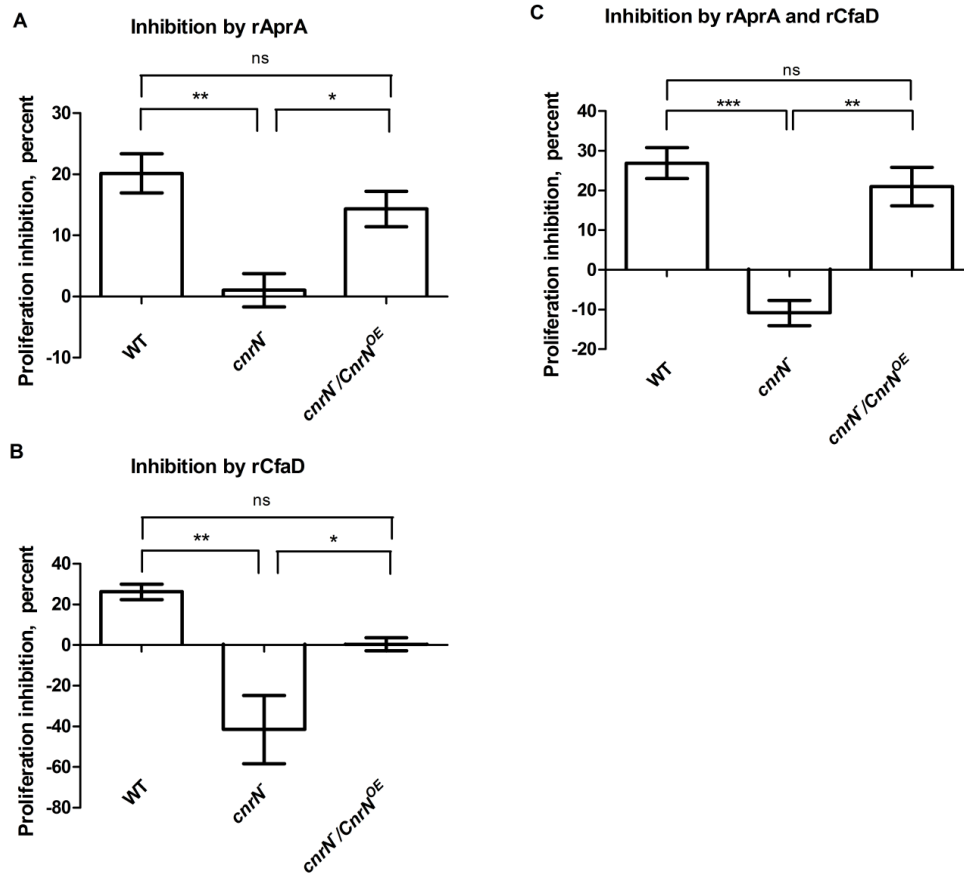
Figure 1: cnrN⁻ cells are insensitive to rAprA and have altered sensitivity to rCfaD. Cell densities were measured after a 16-hour incubation with 300 ng/ml of rAprA or rCfaD, a combination of 300 ng/ml rAprA and 300 ng/ml rCfaD, or an equivalent volume of buffer. The percent of proliferation inhibition by (A) rAprA, (B) rCfaD, or (C) rAprA and rCfaD compared to the proliferation of the buffer control is shown. Values are mean ± SEM from at least three independent experiments. * indicates that the difference is statistically significant at $p < 0.05$, ** indicates $p < 0.01$, *** indicates $p < 0.001$, and ns indicates not significant (one-way ANOVA, Tukey's test). Compared to the addition of an equal volume of buffer, the addition of rCfaD or the combination of rAprA and rCfaD to cnrN⁻ cells significantly increased proliferation (t-test, $p < 0.05$).
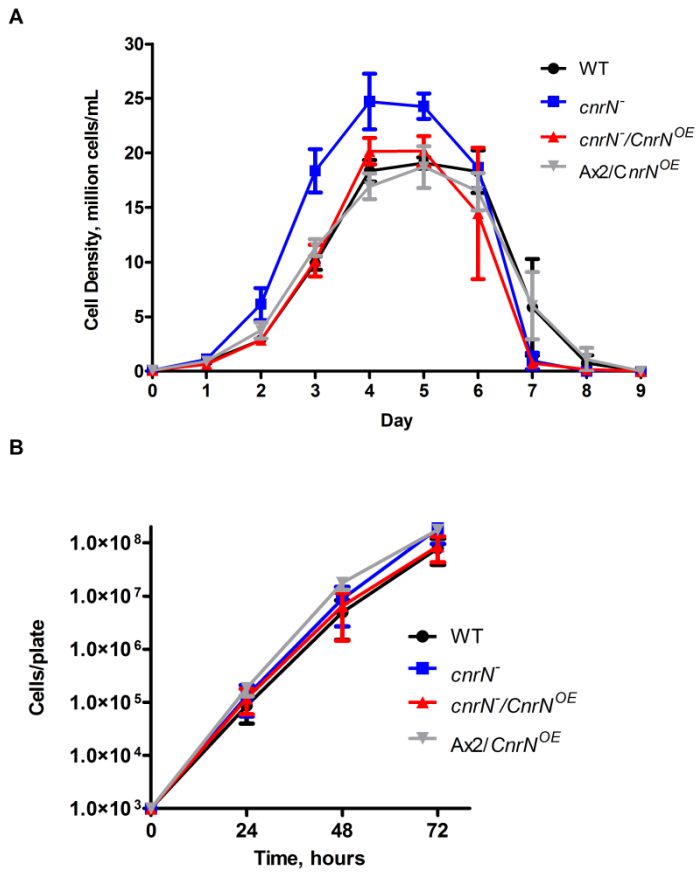
Figure 2: CnrN affects cell proliferation. (A) Log phase cells were inoculated into HL5 media at 1 x 10^5 cells/ml and cell densities were measured daily. Values are mean ± SEM, n = 3 or more for all conditions. WT indicates wild type. **(B)** 1000 cells were plated on SM/5 plates with *K. aerogenes* bacteria and the total number of cells was determined daily. By 72 hours, cells had begun to overgrow the bacteria. Values are mean ± SEM, n=3 for all conditions. The absence of error bars indicates that the error was smaller than the plot symbol. For cells grown on bacteria, there were no statistically significant differences in cell density at any time between the four strains (1-way ANOVA, Tukey's test).

20

Table 1: The effect of CnrN on doubling time and stationary density of cells. Doubling times and stationary densities were measured for the data shown in Figure 2A. Values are mean ± SEM from at least 3 independent experiments. * indicates values are significantly different from wild-type with $p < 0.05$ (one-way ANOVA, Dunnett's test). *** indicates values are significantly different compared to wild type with $p < 0.001$ (one-way ANOVA, Tukey's test). The difference in maximum cell density is statistically significant between $cnrN^-$ and $cnrN^-/CnrN^{OE}$ with $p < 0.01$ and between $cnrN^-$ and Ax2/$CnrN^{OE}$ with $p < 0.001$ (one-way ANOVA, Tukey's test).

Cell Type	Doubling time, hours	Maximum observed cell density, 10^6 cells/ml
Wild-type	13.7 ± 1.1	20.2 ± 0.6
$cnrN^-$	10.9 ± 0.2*	27.9 ± 1.4***
$cnrN^-/CnrN^{OE}$	12.2 ± 0.8	21.6 ± 0.7
Ax2/$CnrN^{OE}$	12.8 ± 0.5	19.8 ± 1.5

cnrN⁻ cells secrete AprA and CfaD

One explanation for the fast proliferation phenotype of *cnrN⁻* cells could be a decrease in extracellular accumulation of AprA or CfaD. To test this hypothesis, we examined the extracellular levels of AprA and CfaD in *cnrN⁻* and *cnrN⁻/CnrN^{OE}* cells. Both AprA and CfaD accumulate in the medium to levels that are comparable to wild-type levels (Figure 3). Although CfaD accumulation appears to be increased in *cnrN⁻* and *cnrN⁻/CnrN^{OE}* cells, this increase is not significant compared to wild type accumulation (Figure 3D). This suggests that the fast proliferation phenotype of *cnrN⁻* cells is not due to a decrease in extracellular levels of AprA or CfaD.

cnrN⁻ cells are multinucleate

Both *aprA⁻* and *cfaD⁻* cells tend to be multinucleate (39, 40). To determine if *cnrN⁻* cells exhibit the same phenotype, the number of nuclei per cell was measured. Compared to wild-type cells, *cnrN⁻* cells have significantly fewer cells with one nucleus per cell and significantly more cells with two nuclei or three or more nuclei per cell (Table 2). Expression of CnrN in the *cnrN⁻* background partially rescued this phenotype. Expression of CnrN in a wild type background caused no significant change in the number of nuclei per cell compared to wild type. These results suggest that like AprA and CfaD, CnrN may be involved in cytokinesis.

22
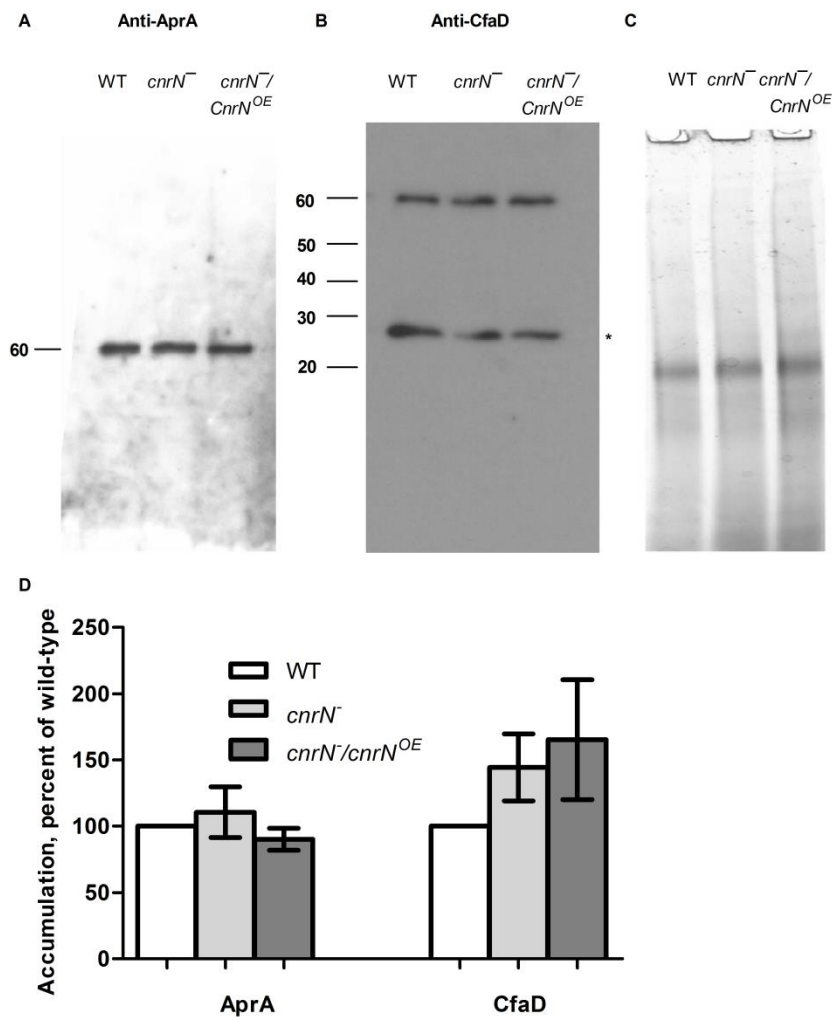
Figure 3: Cells lacking and overexpressing CnrN secrete normal levels of extracellular AprA and CfaD. Conditioned media from the indicated cell lines was assayed by Western blot with anti-AprA (A) or anti-CfaD (B) antibodies. Data is representative of four separate experiments. Molecular weights in kDa are shown at the left of the blots. Asterisk indicates a 27-kDa breakdown product of CfaD whose amount varied somewhat between cell lines and between experiments [5]. (C) Conditioned medium samples were run on a 4-20% PAGE gel and silver stained as a loading control. (D) Quantification of AprA and CfaD accumulation. Autoradiogram densities were normalized to the wild-type value, and are mean $\pm$ SEM. n = 4.

23

Table 2: The effect of CnrN on the number of nuclei per cell. Fluorescence microscopy was used to count the number of nuclei per cell (at least 200 cells for each condition) for log phase cells stained with DAPI. Values are mean ± SEM from at least three independent experiments. * indicates value is significantly different compared to wild-type value at $p < 0.05$, ** indicates $p < 0.01$, and *** indicates $p < 0.001$ (one-way ANOVA, Tukey's test). The difference in the number of cells with 1 nucleus or 3 or more nuclei was significantly different between $cnrN^-$ and $Ax2/CnrN^{OE}$ cells with $p < 0.001$ and between $cnrN^-/CnrN^{OE}$ and $Ax_2/CnrN^{OE}$ cells with $p < 0.01$ (one-way ANOVA, Tukey's test).

Percent of cells with n nuclei

Cell Type	1	2	3+
Wild-type	77.9 ± 1.8	19.0 ± 2.1	3.1 ± 0.3
$cnrN^-$	49.1 ± 4.4***	32.2 ± 3.9*	19.3 ± 2.2***
$cnrN^-/CnrN^{OE}$	55.6 ± 0.8***	30.8 ± 2.1*	13.6 ± 1.9**
$Ax2/CnrN^{OE}$	74.8 ± 1.5	23.3 ± 1.0	1.8 ± 0.5

CfaD decreases the multinucleate phenotype of cnrN⁻ cells

The addition of rCfaD to $cnrN^-$ cells increases their proliferation (Figure 1). One explanation for this increase in proliferation is that rCfaD increases the cytokinesis of $cnrN^-$ cells, which are more multinucleate than wild type cells. To test this possibility, wild type and $cnrN^-$ cells were incubated with and without rCfaD for 16 hours. After verifying that rCfaD decreased the proliferation of wild type cells and increased the proliferation of $cnrN^-$ cells, cells were stained with DAPI, and the nuclei per cell were counted. rCfaD did not cause a significant change in the nuclear phenotype of wild type cells. Adding rCfaD to $cnrN^-$ cells significantly increased the number of cells with a single nucleus and significantly decreased the number of cells with two nuclei and cells

24

with three or more nuclei compared to *cnrN⁻* cells with no rCfaD (Table 3). The addition of rCfaD to either wild type or *cnrN⁻* cells significantly decreased the number of nuclei per 100 cells (Table 3). Together, these data indicate that rCfaD reduces the multinuclearity of *cnrN⁻* cells, presumably by increasing cytokinesis, and this would account for the increase in proliferation during inhibition assays.

Table 3: The effect of rCfaD on the number of nuclei per cell. Following a 16-hour incubation with 300 ng/ml of rCfaD or an equivalent volume of buffer, fluorescence microscopy was used to count the number of DAPI-stained nuclei per cell (at least 200 cells for each condition). Values are mean ± SEM from three independent experiments. * and *** indicate that values are statistically significant between – and + rCfaD for the genotype with $p < 0.05$ and $p < 0.001$, respectively (one-way ANOVA, Tukey's test or one-way paired t-test).

Cell Type	rCfaD	Percent of cells with n nuclei			Nuclei/100 cells
		1	2	3+	
Wild-type	-	85.8 ± 2.1	13.6 ± 2.0	0.6 ± 0.4	115 ± 2
Wild-type	+	87.9 ± 1.5	11.6 ± 1.2	0.6 ± 0.4	112 ± 2*
cnrN⁻	-	50.6 ± 2.8	41.5 ± 1.7	7.9 ± 1.5	164 ± 9
cnrN⁻	+	67.1 ± 5.3*	28.6 ± 3.2*	4.3 ± 2.1*	138 ± 8***

CnrN does not regulate growth on a per nucleus basis

Cell proliferation is defined as an increase in cell number, and cell growth as the accumulation of mass and protein (39, 40, 45, 46). Both *aprA⁻* and *cfaD⁻* cells tend to

25

be more massive than wild type, but do not accumulate mass or protein at an increased rate on a per nucleus basis compared to control (39, 40). This indicates that neither AprA nor CfaD play a role in the regulation of growth. Mass and protein content was analyzed in log phase cells to determine the effect of CnrN on growth. Mass, protein, and nuclei per 100 cells for wild type were similar to previous observations (39, 40, 45, 46). There was no statistically significant difference in mass between wild type, $cnrN^-$, $cnrN^-/CnrN^{OE}$, or Ax2/$CnrN^{OE}$ cells (Table 4). Protein content and nuclei per 100 cells were increased compared to wild type in both $cnrN^-$ and $cnrN^-/CnrN^{OE}$ cells. Protein content and protein content on a per nucleus basis was decreased in Ax2/$CnrN^{OE}$ cells. On a per nucleus basis, $cnrN^-$ cells contained significantly less mass and protein than wild-type. $cnrN^-/CnrN^{OE}$ cells had significantly more protein content per nucleus than $cnrN^-$ cells, rescuing the mutant phenotype.

To estimate mass, protein, and nuclei accumulation per hour, we assumed that a doubling in cell number also results in a doubling of mass, protein, and nuclei. We then divided the mass, protein, and nuclei contents for each genotype by their respective calculated doubling times (Table 1). On a per cell per hour basis, $cnrN^-$, $cnrN^-/CnrN^{OE}$, and Ax2/$CnrN^{OE}$ cells accumulated mass similarly to wild-type (Table 5). Both $cnrN^-$ and $cnrN^-/CnrN^{OE}$ cells accumulated significantly more protein per cell per hour than either wild type or Ax2/$CnrN^{OE}$ cells. $cnrN^-$ and $cnrN^-/CnrN^{OE}$ cells accumulated nuclei at a faster rate than wild-type. $cnrN^-/CnrN^{OE}$ cells accumulated nuclei at a significantly slower rate compared to $cnrN^-$ cells, partially rescuing the fast nuclei accumulation of $cnrN^-$ cells. Ax2/$CnrN^{OE}$ cells accumulated nuclei at a rate similar to

wild type, and this rate was significantly slower than the *cnrN⁻* and *cnrN⁻/CnrN^{OE}*

nuclei accumulation rates (Table 5). On a per nucleus basis, there were no significant

differences in the mass and protein accumulation per hour in wild type, *cnrN⁻*,

cnrN⁻/CnrN^{OE}, and Ax2/*CnrN^{OE}* cells. These results suggest that like AprA and CfaD,

CnrN does not affect growth on a per nucleus basis.

Table 4: The effect of CnrN on the mass and protein content of cells. Mass and protein content was measured, and the data from Table 2 were use to determine the number of nuclei per 100 cells. Values are mean ± SEM from at least three independent experiments. ** indicates value is significantly different compared to wild type at p < 0.01 and *** indicates p < 0.001 (one-way ANOVA, Tukey's test). The difference in protein per 10^7 cells and protein per 10^7 nuclei is significantly different with p < 0.001 between *cnrN⁻* and *cnrN⁻/CnrN^{OE}* and between *cnrN⁻/CnrN^{OE}* and Ax2/*CnrN^{OE}*. The difference in protein per 10^7 cells is significantly different between *cnrN⁻* and Ax2/*CnrN^{OE}* with p < 0.001. Both *cnrN⁻* and *cnrN⁻/CnrN^{OE}* nuclei per 100 cells are significantly different from Ax2/*CnrN^{OE}* with p < 0.001.

Cell type	Per 10^7 cells			Per 10^7 nuclei	
	Mass (mg)	Protein (mg)	Nuclei/100 cells	Mass (mg)	Protein (mg)
Wild-type	10.3 ± 0.4	0.86 ± 0.02	126 ± 1	8.2 ± 0.3	0.68 ± 0.02
cnrN⁻	9.0 ± 0.4	0.97 ± 0.01**	187 ± 7***	4.8 ± 0.2***	0.52 ± 0.02**
cnrN⁻/CnrN^{OE}	11.2 ± 1.0	1.30 ± 0.04***	170 ± 4***	6.6 ± 0.6	0.76 ± 0.03
Ax2/*CnrN^{OE}*	9.4 ± 1.3	0.70 ± 0.02***	131 ± 6	7.1 ± 0.9	0.53 ± 0.02**

Table 5: The effect of CnrN on mass and protein accumulation of cells. Mass, protein, and nuclei values from Table 4 were divided by the doubling time for each respective genotype from Table 1. Values are mean ± SEM from at least three independent experiments. * indicates value is significantly different compared to wild-type value at $p < 0.05$ and *** is significant at $p < 0.001$ (one-way ANOVA, Tukey's test). The difference in protein per cell per hour is significantly different between $cnrN^-$ and Ax2/$CnrN^{OE}$ and between $cnrN^-$/$CnrN^{OE}$ and Ax2/$CnrN^{OE}$ with $p < 0.01$ and $p < 0.001$, respectively. The differences in nuclei per 10^7 cells per hour are significantly different between $cnrN^-$ and $cnrN^-$/$CnrN^{OE}$, $cnrN^-$ and Ax2/$CnrN^{OE}$, and $cnrN^-$/$CnrN^{OE}$ and Ax2/$CnrN^{OE}$ with $p < 0.001$. The difference in protein per 10^7 nuclei per hour is significantly different between $cnrN^-$/$CnrN^{OE}$ and Ax2/$CnrN^{OE}$ with $p < 0.05$.

Cell type	Per 10^7 cells/hour			Per 10^7 nuclei/hour	
	Mass (mg)	Protein (µg)	Nuclei, x 10^{-5}	Mass (mg)	Protein (µg)
Wild-type	0.75 ± 0.07	62.6 ± 5.4	9.2 ± 0.77	0.60 ± 0.05	50 ± 4
$cnrN^-$	0.82 ± 0.04	88.6 ± 2.1*	17 ± 0.47***	0.44 ± 0.02	47 ± 1
$cnrN^-$/$CnrN^{OE}$	0.92 ± 0.10	107 ± 7.4***	14 ± 0.94***	0.54 ± 0.06	63 ± 5
Ax2/$CnrN^{OE}$	0.87 ± 0.08	54.2 ± 2.5	10 ± 0.61	0.67 ± 0.07	41 ± 3

CnrN affects spore viability

Cells lacking AprA and CfaD have reduced spore viability (39, 40). $cnrN^-$ cells were examined for their ability to form detergent-resistant spores. An equivalent number of wild-type, $cnrN^-$, $cnrN^-$/$CnrN^{OE}$, and Ax2/$CnrN^{OE}$ cells were developed, the spores were collected, and dilutions of detergent-treated spores were plated. The numbers of cells with a spore morphology and the numbers of detergent-resistant spores from $cnrN^-$ cells was significantly less compared to those recovered from wild type (Table 6). Expression of CnrN in the $cnrN^-$ background rescued the number of detergent-resistant spores and appeared to partially rescue the number of visible spores. The number of

recovered spores and the number of viable spores from *cnrN⁻/CnrN^{OE}* or Ax2/*CnrN^{OE}*

cells were similar to wild type levels. These data indicate that like AprA and CfaD,

CnrN affects the ability of cells to form viable spores.

Table 6: The effect of CnrN on spore viability. Cells were developed on filter pads for 48 hours and the percent of visible spores was calculated as a percent of input cells. Detergent-treated spores were plated and analyzed for their ability to produce colonies. Values are mean ± SEM from at least three independent experiments. ** and *** indicates differences are significantly different compared to wild-type with $p < 0.01$ and $p < 0.001$, respectively (one-way ANOVA, Tukey's test). The difference in the number of visible spores between *cnrN⁻* and Ax2/*CnrN^{OE}* is significantly different with $p < 0.01$. The difference in the number of detergent-resistant spores between *cnrN⁻* and *cnrN⁻/CnrN^{OE}* is significantly different with $p < 0.05$. The number of detergent-resistant spores in Ax2/*CnrN^{OE}* is significantly different from both *cnrN⁻* ($p < 0.001$) and *cnrN⁻/CnrN^{OE}* ($p < 0.05$).

Cell type	Number of spores after development as a percent of input cell number	Detergent-resistant spores as a percent of total spores
Wild-type	100 ± 12	83.3 ± 6.3
cnrN⁻	41.3 ± 8.0**	37.8 ± 2.5***
cnrN⁻/CnrN^{OE}	59.9 ± 2.6	66.5 ± 15
Ax2/*CnrN^{OE}*	109 ± 11	107 ± 16

AprA and CfaD affect CnrN localization

PTEN can translocate from the cytosol to the inner face of the plasma membrane

in response to extracellular signals (111). We observed CnrN localization at the

periphery of cells, in the interior of cells, and on vesicle-like structures in the interior of

29

cells (132). To test whether CnrN translocates in response to extracellular AprA or CfaD, we examined the localization of myc-tagged CnrN in the *cnrN⁻* mutant background. Since both the ectopically expressed CnrN and our recombinant proteins are myc-tagged, we used immunoblotting of partially purified membranes to specifically examine CnrN levels. Log-phase $cnrN^-/CnrN^{OE}$ cells were stimulated with rAprA, rCfaD, a mix of rAprA and rCfaD, or buffer for 10 and 20 minutes. The cells were then lysed, and Western blots of the membranes were stained with antibodies against the myc tag. At ten minutes after stimulation, all conditions showed similar amounts of membrane-associated myc-CnrN compared to the zero time point (Figure 4). After 20 minutes of stimulation with AprA alone or CfaD alone, there was no significant effect on the amount of membrane-associated myc-CnrN (Figure 4). A significant increase in membrane-associated myc-CnrN was observed at 20 minutes when cells were stimulated with both AprA and CfaD (Figure 4). For unknown reasons, the amount of membrane-associated myc-CnrN decreased at 20 minutes in the buffer control (Figure 4). These results suggest that AprA and CfaD together can induce localization of CnrN to the membrane.
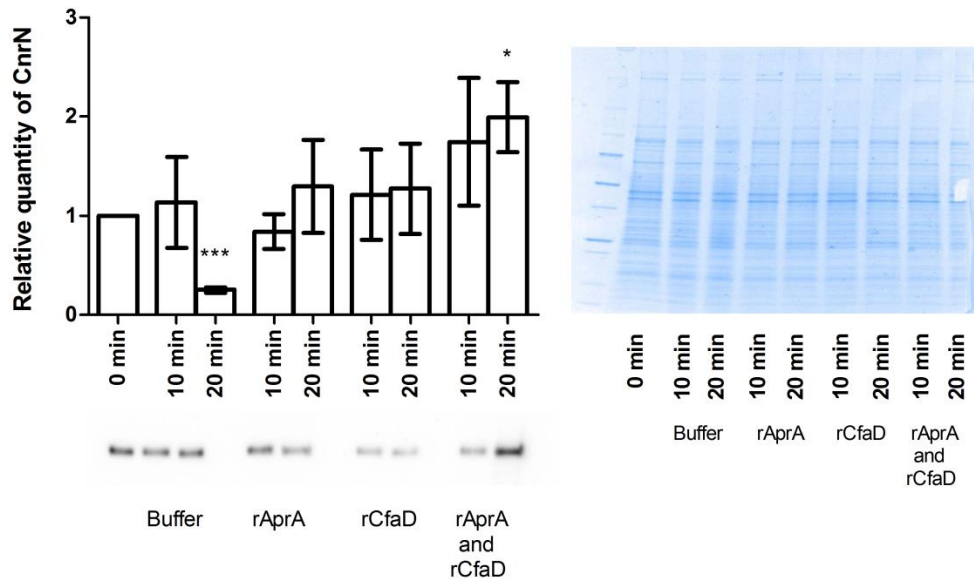
Figure 4: CnrN localization. Myc-tagged *cnrN⁻/CnrN^{OE}* cells were incubated with rAprA, rCfaD, both rAprA and rCfaD, or an equivalent volume of buffer and lysed at the indicated times. Membranes from the lysates were collected by centrifugation and were analyzed for the presence of myc-tagged CnrN by Western blotting and staining for the myc-tag. Band intensities were measured as a ratio of the zero time point. Values are mean ± SEM, n = 3 or more. * and *** indicate a significant difference with $p < 0.05$ or $p < 0.001$, respectively, compared to the zero time point (t-test). Membrane samples were run on a 4-20% PAGE gel and coomassie stained as a loading control.

CnrN is necessary for chemorepulsion by AprA

We previously characterized AprA as a chemorepellent of *Dictyostelium* cells (48). To determine if CnrN is necessary for chemorepulsion by AprA, we used Insall chambers (48, 133) to analyze the response of *cnrN⁻* cells to rAprA. The forward migration index represents the displacement of cells along a gradient as a fraction of the total cell movement. A negative forward migration index indicates displacement away

31

from rAprA. The chemorepulsion of wild type cells away from rAprA was similar to previous observations (48). *cnrN⁻* cells were not chemorepulsed in a gradient of AprA, and expressing CnrN in the mutant background rescued this defect (Figure 5). This indicates that CnrN is required for AprA to act as a chemorepellent of *Dictyostelium* cells.
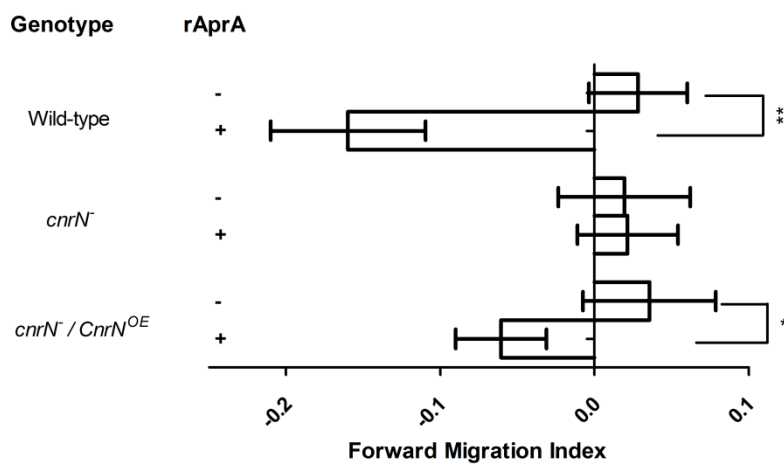
Figure 5: CnrN is necessary for chemorepulsion by AprA. Cells were assayed for chemorepulsion in response to rAprA in an Insall chamber for 1 hour. A negative migration index indicates movement away from the AprA source. Values are mean ± SEM of at least three independent experiments. * ($p < 0.05$) and ** ($p < 0.01$) indicate a significant difference (t-test).

Discussion

Extracellular AprA and CfaD inhibit *Dictyostelium* cell proliferation and extracellular AprA causes cell chemorepulsion (40, 41, 48). *cnrN⁻* cells are insensitive to both the proliferation-inhibiting and chemorepellent effects of rAprA, and these phenotypes are rescued by expressing CnrN in *cnrN⁻* cells. Like *aprA⁻* and *cfaD⁻* cells, *cnrN⁻* cells have a faster doubling time and reach a higher cell density than wild type cells, have similar mass and protein accumulation per nucleus, and form less viable spores. Like *aprA⁻* and *cfaD⁻* cells, *cnrN⁻* cells are also more multinucleate than wild type cells. Interestingly, adding rCfaD to cells lacking CnrN increases proliferation. The increase in proliferation of *cnrN⁻* cells in response to rCfaD appears to be due to an increase in cytokinesis. The significant difference in the increase of *cnrN⁻* cell proliferation between the combination of rAprA and rCfaD, and rCfaD alone, suggests a cooperative role between AprA and CfaD. If AprA and CfaD function independently, *cnrN⁻* cells would respond to the combination of rAprA and rCfaD similarly to rCfaD alone, since *cnrN⁻* cells are insensitive to rAprA signaling. Thus, the presence of AprA decreases the ability of CfaD to increase the proliferation of *cnrN⁻* cells. Together, the data suggest that CnrN is required for AprA and CfaD to inhibit proliferation.

PTEN-like phosphatases are recruited to the plasma membrane to dephosphorylate PIP_3 to PIP_2 (113, 125-128). CnrN is localized in the cytosol, in vesicle-like structures, and at the plasma membrane. PTEN binds to phosphoserine/phosphocholine lipid vesicles via the C2 domain of the protein (134). Since CnrN contains a putative PTEN-like C2 domain (115), CnrN may also bind to

vesicles containing phosphoserine and phosphocholine. We found that CnrN localization is increased on membranes in response to a mixture of rAprA and rCfaD after 20 minutes. AprA and CfaD may recruit CnrN to the membrane to inhibit proliferation-promoting factors. In addition, AprA may also utilize CnrN membrane recruitment to potentiate chemorepulsion of *Dictyostelium* cells. CnrN is a necessary component of the AprA chemorepellent pathway. During chemotaxis, PTEN inhibits the formation of pseudopods at the trailing end of a cell (38, 58, 62). In the AprA chemorepellent system, the PTEN-like phosphatase CnrN may be recruited to the membrane adjacent to the source of AprA. This would then inhibit the formation of pseudopods in the direction of the AprA source, allowing cells to move away from the source of AprA.

Together, our results indicate that CnrN is recruited to the membrane in response to a combination of AprA and CfaD, acts as a negative regulator of proliferation, and mediates AprA-induced chemorepulsion. An intriguing possibility is that in higher eukaryotes, factors that slow proliferation and/or act as chemorepellents may also regulate the localization of PTEN or PTEN-like phosphatases.

CHAPTER III

DIPEPTIDYL-PEPTIDASE IV IS A HUMAN AND MURINE NEUTROPHIL CHEMOREPELLENT[1]

Summary

In *Dictyostelium discoideum*, AprA is a secreted protein that inhibits proliferation and causes chemorepulsion of *Dictyostelium* cells, yet AprA has little sequence similarity to any human proteins. We found that a predicted structure of AprA has similarity to human dipeptidyl-peptidase IV (DPPIV). DPPIV is a serine protease present in extracellular fluids that cleaves peptides with a proline or alanine in the second position. In Insall chambers, DPPIV gradients below, similar to, and above the human serum DPPIV concentration cause movement of human neutrophils away from the higher concentration of DPPIV. A 1% DPPIV concentration difference between the front and back of the cell is sufficient to cause chemorepulsion. Neutrophil speed and viability are unaffected by DPPIV. DPPIV inhibitors block DPPIV-mediated chemorepulsion. In a murine model of acute respiratory distress syndrome (ARDS), aspirated bleomycin induces a significant increase in the number of neutrophils in the lungs after 3 days. These results indicate that DPPIV functions as a chemorepellent of

_____

human and mouse neutrophils, and suggest new mechanisms to inhibit neutrophil accumulation in ARDS.

Introduction

Chemotaxis is the directed movement of cells due to a gradient of an attractant or repellent. Chemotaxis has been observed in both prokaryotes and eukaryotes (56, 135). In humans, neutrophils show chemotaxis towards bacterial products such as N-formyl-methionine-leucine-phenylalanine (fMLP), and towards signals secreted by macrophages and epithelial cells such as interlukin-8 (IL-8) (54, 55). A large number of chemoattractants have been characterized, while relatively few chemorepellents have been identified (64, 67, 68, 136-138).

Dictyostelium cells secrete two proteins, AprA and CfaD, which inhibit *Dictyostelium* cell proliferation (39, 40). Although CfaD has sequence similarity to cathepsin L, AprA shows no significant sequence similarity to eukaryotic proteins (39, 40). We found that AprA also functions as a chemorepellent of *Dictyostelium* cells (48). Wild-type cells in a colony rapidly move away from the dense colony center, while AprA knock-out cells show no directional movement away from the center of a colony (46, 48). When wild-type cells are placed in a gradient of recombinant AprA (rAprA), cells show a biased movement away from rAprA (48).

Protein structure prediction can be highly accurate and reveal new functions of a protein (139-144). The protein prediction server I-TASSER uses a multi-step process to predict protein structure (139, 141). First, initial models of the structure are generated from the amino acid sequence (139, 141). The models are then adjusted using Monte Carlo simulations to identify folds with the lowest free energy (139, 141). Finally, spatial constraints and optimal hydrogen bindings are used to adjust the predicted structure (139, 141). The predicted structure can then be used to search for proteins with similar structures (140, 142-144).

Dipeptidyl-peptidase IV (DPPIV) is a 110 kDa serine protease that cleaves peptides with a proline or alanine in the second position at the N-terminus (145). DPPIV is on the extracellular surface of some lymphocytes and epithelial cells, and a heavily glycosylated soluble form of DPPIV is also found in plasma, serum, cerebrospinal fluid, synovial fluid, semen, and urine (75, 76). DPPIV degrades glucagon-like peptide-1 (GLP-1) (83). Drugs that block DPPIV activity also block this degradation, and are used to treat type 2 diabetes (83). By activating or deactivating peptide signals, DPPIV affects a large variety of signaling molecules regulating chemotaxis, tissue remodeling, cell adhesion, and other processes (81, 146).

Using the I-TASSER program, we identified structural similarity between *Dictyostelium* AprA and human DPPIV. We show that neutrophils are chemorepulsed by DPPIV, and that this chemorepulsion is dependent on the enzyme activity of DPPIV. In an *in vivo* model of neutrophil movement, oropharyngeal aspiration of DPPIV reduces neutrophil accumulation in the lungs of bleomycin-treated mice. In this report, we show

that DPPIV acts as a chemorepellent of human neutrophils and present a new potential method to inhibit neutrophil accumulation in tissues.

Materials and Methods

Structure prediction, alignment, and superimposition

The tertiary structure of AprA was predicted using I-TASSER (139-141). The PDB file of the predicted AprA structure was input into the Dali server to find similar protein structures and calculate structural similarities (147). The structure of AprA and DPPIV were superimposed using pairwise alignment (http://agknapp.chemie.fu-berlin.de/gplus/) (148, 149).

Neutrophil isolation

Blood was collected from healthy volunteers with specific approval from the Institutional Review Board of Texas A&M University. Written consent was received, and all samples were de-identified before analysis. Neutrophils were isolated from the blood using Lympholyte-poly (Cedarlane Laboratories, Hornby, Canada) following the manufacturer's directions and resuspended in 2% BSA (Fraction V, A3059, Sigma) in RPMI-1640 (Lonza).

Neutrophils were further purified using negative selection, as described previously (150). Briefly, neutrophils were depleted of eosinophils, monocytes, and lymphocytes by incubating the cells for 10 minutes at room temperature with 5 µg/ml of anti-human CD244 (Biolegend), and then depleting CD244 positive cells with Pan

Mouse IgG Dynabeads (Invitrogen). Cells were resuspended to a final volume of 1 ml in 2% human-albumin-RPMI.

To determine the purity of CD244-depleted neutrophil preparations, cells were resuspended in PBS containing 2% BSA and cell smears were prepared as described previously (151). Cells smears were air dried overnight, fixed in methanol, stained with hematoxylin and eosin, and cell morphology was determined by microscopy, as described previously (150).

Human albumin was isolated from human serum (Lonza) using Affi-gel Blue Gel beads (BioRad). After washing beads three times with phosphate buffered saline, beads were incubated with serum at room temperature for 2 hours. Beads were collected by centrifugation at 300 x g for 2 minutes and washed with buffer (20 mM Tris, 140 mM NaCl, 2 mM calcium) and the albumin eluted off overnight with 500 mM NaCl. Albumin was then concentrated and buffer exchanged to Earl's balanced salt solution (Sigma) using a 10 kDa centrifugal filter (Millipore) and stored at 4°C.

Insall chamber assays

Recombinant human soluble DPPIV (rDPPIV) was purchased from Enzo Lifesciences. To measure the effect of DPPIV on cell displacement, we used Insall chambers, which allows direct visualization of cell movement, as described previously for melanoma cells, *Dictyostelium*, and neutrophils (48, 133, 152). Briefly, 22 x 22mm glass cover slips were etched with 1 M HCl, rinsed with deionized water, and coated with 20 µg/mL bovine plasma fibronectin (Sigma) for 30 minutes at 37°C. Cover slips

were then washed twice with PBS, and 300 μl of neutrophils at 5 x 10^6 cells/ml were allowed to adhere to the coverslip for 15 minutes at 37°C. We then utilized an Insall chamber slide, a kind gift from Robert Insall (133). Two concentric depressions and the separating bridge were filled with 2%BSA-RPMI. The media was removed from the coverslips, which were then placed face down on the chamber. Media was then removed from the outer chamber and was replaced by DPPIV alone, DPPIV inhibitor alone (Diprotin A, Enzo Lifesciences or DPPI 1c hydrochloride, Tocris), DPPIV plus DPPIV inhibitor (all in 2%BSA-RPMI), or 2%BSA-RPMI. Cells located on the bridge between the square depressions were then filmed as previously described (153), using a 10X objective for 1 hour at 37°C in a humidified 5% CO_2 incubator. Displacement of at least 10 randomly chosen cells per experiment was measured over periods of 10 minutes. Cell tracking and track analysis was done as previously described (48) with the exception that videos of an hour in length were processed into 10 minute segments to yield a TIFF stack of 47 images for analysis (with 13-second intervals between images). Insall chamber assays for pure neutrophils were done with the same procedures expect that coverslips were coated with 20 μg/mL human plasma fibronectin (Trevigen) and 2% human albumin-RPMI was used instead of 2% BSA-RPMI.

For conditioned media assays, neutrophils at 5 x 10^6 cells/ml were incubated with 300 ng/ml DPPIV or an equivalent volume of buffer for 30 minutes at 37°C in tubes that were pre-coated with 4% BSA-RPMI. Where indicated, the DPPIV inhibitor DPPI 1c hydrochloride was added to the conditioned medium to a final concentration of 200 nM. Cells were collected by centrifugation at 500 x g for 5 minutes and the supernatant was

added to the outside chamber of an Insall chamber. Cells were filmed as described above. Samples of conditioned media were separated on 4-20% PAGE gels (BioRad), transferred to Immobilon P membranes (Millipore), and membranes were stained with 100 ng/ml anti-human DPPIV antibodies (R&D Systems).

Effect of DPPIV peptidase activity on albumin stability

2% BSA-RPMI and 2% human albumin-RPMI were incubated with 300 ng/ml rDPPIV or an equivalent volume of buffer for 3 hours. Samples were taken at 0, 15, 30, 45, 60, and 180 minutes, mixed with SDS sample buffer, separated on 4-20% PAGE, and then silver stained.

Neutrophil influx in mice

4-week-old C57/BL6 mice (Jackson, Bar Harbor, ME) were treated with an oropharyngeal aspiration of 50 μl of saline or 3U/kg bleomycin (Calbiochem) (154). The successful aspiration of bleomycin into the lungs was confirmed by listening for the crackling noise heard after the aspiration. 24 hours following bleomycin aspiration (day 1), mice were treated with an oropharyngeal aspiration of 50 μl of 0.9% saline with 0.9 μg rDPPIV (Enzo Lifesciences) or an equal volume of 0.9% saline. Mice were weighed daily and euthanized at day 3 after bleomycin aspiration. Blood was collected by cardiac puncture from the euthanized mice and blood glucose was measured using Accu-check Active (Roche). The lungs were perfused with 300 μl of PBS three times to collect cells by bronchoalveolar lavage (BAL) as described previously (155). The primary BAL cells

were collected by centrifugation at 500 x g for 10 minutes. Primary BAL pellets were resuspended in the secondary and tertiary BAL fluid and the combined cells were collected by centrifugation at 500 x g for 5 minutes. The cells were resuspended in 500 μl of 4% BSA-PBS and counted with a hemocytometer. 100 μl of diluted cells was then aliquoted into cytospin funnels and spun onto glass slides (Superfrost plus white slides, VWR, West Chester, PA) at 400 rpm for 5 minutes using a cytospin centrifuge (Shandon, Cheshire, England). These cells were then air-dried, and stained with Gill's haematoxylin. Greater than 200 cells were counted for total cell number and neutrophils, macrophages, and lymphocytes were identified by morphology. The percent of neutrophils, macrophages, or lymphocytes was then multiplied by the total number of cells recovered from the BAL to obtain the number of each cell type in the BAL. The mice were used in accordance with guidelines published by the National Institutes of Health, and the protocol was approved by the Texas A&M University Animal Use and Care Committee.

Immunohistochemistry

After BAL, lungs were inflated with pre-warmed OCT (VWR) and then embedded in OCT, frozen on dry ice, and stored at -80°C as described previously (156). Lung tissue sections (5 μm) were prepared and immunohistochemistry was done as described previously (156) except slides were incubated with 5 μg/ml primary antibodies in 4% BSA-PBS for 60 minutes. Active caspase-3 staining was done overnight at 4°C. The lung sections were stained for Ly6G (BD Biosciences) to detect neutrophils, CD11b

(BioLegend) to detect infiltrating macrophages and neutrophils, CD11c (MBL) to detect lung resident macrophages and dendritic cells, CD206 (Biolegend) to detect the mannose receptor on macrophages and dendritic cells, and CD107b (Mac3) (Biolegend) to detect alveolar and tissue macrophages and granulocytes, cleaved caspase-3 (Cell Signaling Technologies) to detect activated caspase-3, and isotype-matched mouse or rabbit irrelevant antibodies as controls. Slides were then washed three times with PBS over 30 minutes and incubated with 5 µg/ml biotinylated mouse F(ab')2 anti-rat IgG or 5 µg/ml biotinylated donkey F(ab')2 anti-rabbit IgG in 4% BSA-PBS for 30 minutes. Slides were then washed three times in PBS over 30 minutes and incubated with a 1:500 dilution of streptavidin alkaline phosphatase (Vector Laboratories) in 4% BSA-PBS for 30 minutes. Staining was developed with a VectorRed Alkaline Phosphatase Kit (Vector Laboratories) for 10 minutes. Slides were then mounted as described previously (156). Five or ten 450 µm fields of view were counted for Ly6G-stained or active caspase-3-stained positive cells, respectively. Areas containing large blood vessels and bronchioles were excluded from analysis.

Neutrophil survival

Isolated neutrophils were cultured in RPMI-1640 containing 10% (v:v) fetal bovine serum and 2 mM glutamine in 96-well tissue-culture plates at 37°C for 20 hours, as described previously (157). Neutrophils were cultured in the presence or absence of 25 ng/ml human IL-8 or human TNF-α (both from Peprotech), or 400 ng/ml DPPIV. After 20 hours neutrophils were labeled with annexin V (BioLegend) and propidium

iodide (Sigma) according to the manufacturer's instructions, to identify early and late stages of cell death. In addition, cytospin preparations were used to assess for morphological changes associated with apoptosis, as described previously (157-159).

Statistics

Statistics were done using Prism (GraphPad Software, San Diego, CA). One-way ANOVA was used to compare between multiple groups and Student's t-test was used to compare between two groups.

Results

AprA has structural similarity to the human protein dipeptidyl-peptidase IV

AprA has little sequence similarity to any mammalian protein (39). Using I-TASSER, we generated a predicted structure for AprA (Figure 6). The Dali Server, used to compare protein structures, composes a list of the proteins with the most structural similarity to the query protein. The proteins with the top structural similarities to the predicted structure of AprA were Cephalosporin C deacetylase (a β-lactamase from the fungus *Acremonium*), acetyl xylan esterase (from the bacteria *Bacillis pumilus*, cleaves carboxyl-ester bonds), acylamino-acid-releasing-enzyme (from the Archaea *Aeropyrum pernix* K1, cleaves acylated terminal amino acids), and dipeptidyl-peptidase IV (DPPIV) (human soluble form, cleaves terminal amino acids with proline or alanine in the second position). AprA has an 11% structural identity to the entire structure of soluble human DPPIV (Figure 6, the α/β hydrolase domain of DPPIV is shown). Since DPPIV, like

44

AprA, can be found as an extracellular protein, these results suggested that AprA might

have functional similarity to DPPIV or vice versa.
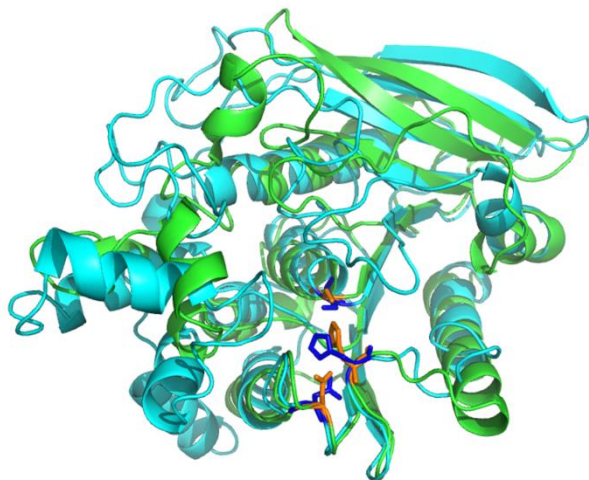
Figure 6: Superimposition of the predicted structure of AprA with the structure of the α/β hydrolase domain of human DPPIV. The catalytic domains of DPPIV (the α/β hydrolase domain of PDB ID 1J2E), and AprA (predicted structure) were superimposed and the catalytic triads highlighted. The α/β hydrolase domain of DPPIV is shown in green and its catalytic triad (Asp708, His740, and Ser630) is orange. The predicted structure of AprA is shown in cyan and its potential catalytic triad (Asp288, His319, and Ser195) is blue. The β-propeller domain of DPPIV was removed for simplicity since the predicted structure of AprA had no overlap with this domain.

Neutrophils show biased movement away from a source of DPPIV

AprA functions as a chemorepellent of *Dictyostelium* cells (48). *Dictyostelium*

and neutrophils share many properties of chemotaxis (160, 161). Therefore, we

hypothesized that DPPIV may regulate human neutrophil motility due to its structural

similarity to AprA. To examine neutrophil chemotaxis in gradients of DPPIV, we used

an Insall chamber. When neutrophil movement was tracked over 10 minute periods, there was no bias of movement in the media control (Figure 7A and Figure 8). A biased movement away from a source of DPPIV was observed (Figure 7B and Figure 8). Cells were tracked and the average center of mass observed for the endpoints of cells in each population was determined. The center of mass of cell endpoints showed displacement away from the source of DPPIV (Figure 7 and Figure 8). The concentration of DPPIV in human blood ranges from 400 to 800 ng/ml, or 4.7 to 9.4 nM (162, 163). Therefore, we tested the ability of DPPIV to affect neutrophil migration above, below, and within this concentration range. Neutrophils showed biased movement away from higher concentrations of rDPPIV in a variety of DPPIV concentration gradients (Table 7). An equal concentration of DPPIV in both wells of the chamber resulted in no biased directional movement of neutrophils (Table 7). The presence of DPPIV affected directionality, although not in any systematic manner (Table 7). Because we used different sets of donors for each gradient concentration, the directionality in the media controls vary somewhat within the different sets of experiments. TNF-α stimulated neutrophils also migrated away from DPPIV (Table 7). For unknown reasons, some of the cells appeared to move towards the higher concentration of DPPIV. In Figure 7B, two such cells can be seen. The fraction of cells exhibiting this anomalous behavior was not obviously affected by the amount of DPPIV in the gradient (Table 7). Combined, these data indicate that a gradient of DPPIV causes chemorepulsion of neutrophils.

46
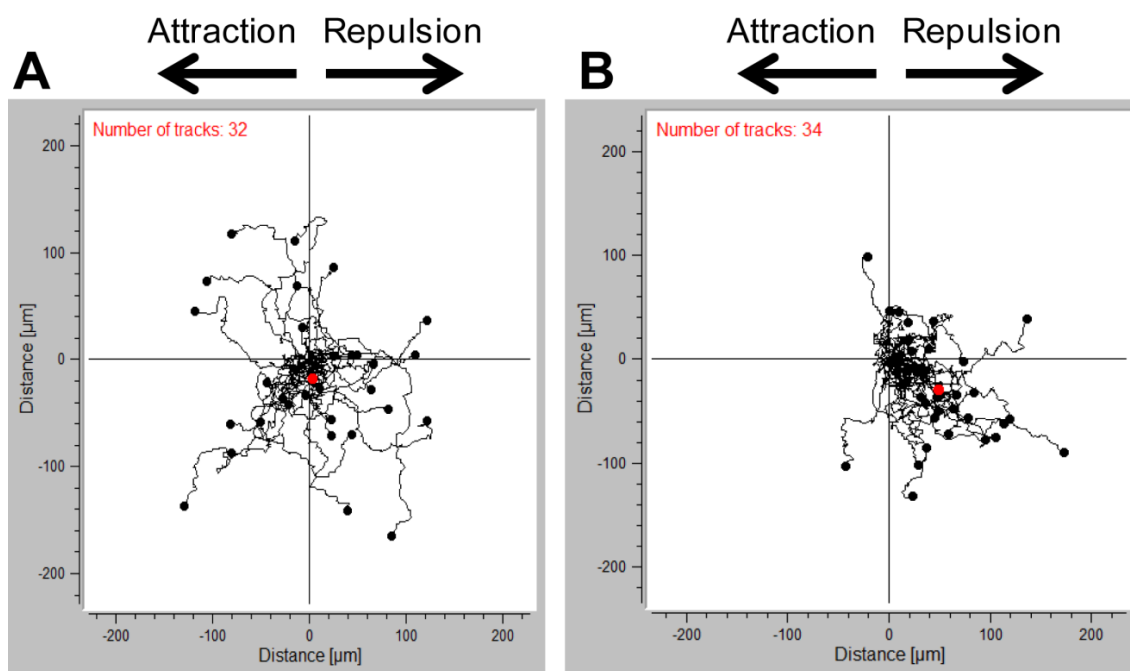
Figure 7: Human neutrophils show biased movement away from rDPPIV. Neutrophil migration was measured in the **A)** absence or **B)** presence of a 0-1.2 nM rDPPIV gradient. Neutrophils were filmed and tracked (see Methods and Materials) over 10-minute periods. Orientation is such that the source of rDPPIV is on the left. Graphs are data from one of three independent experiments (see Figure 8 for the other two experiments). Red dots represent the average center of mass for the ending positions of all cells.
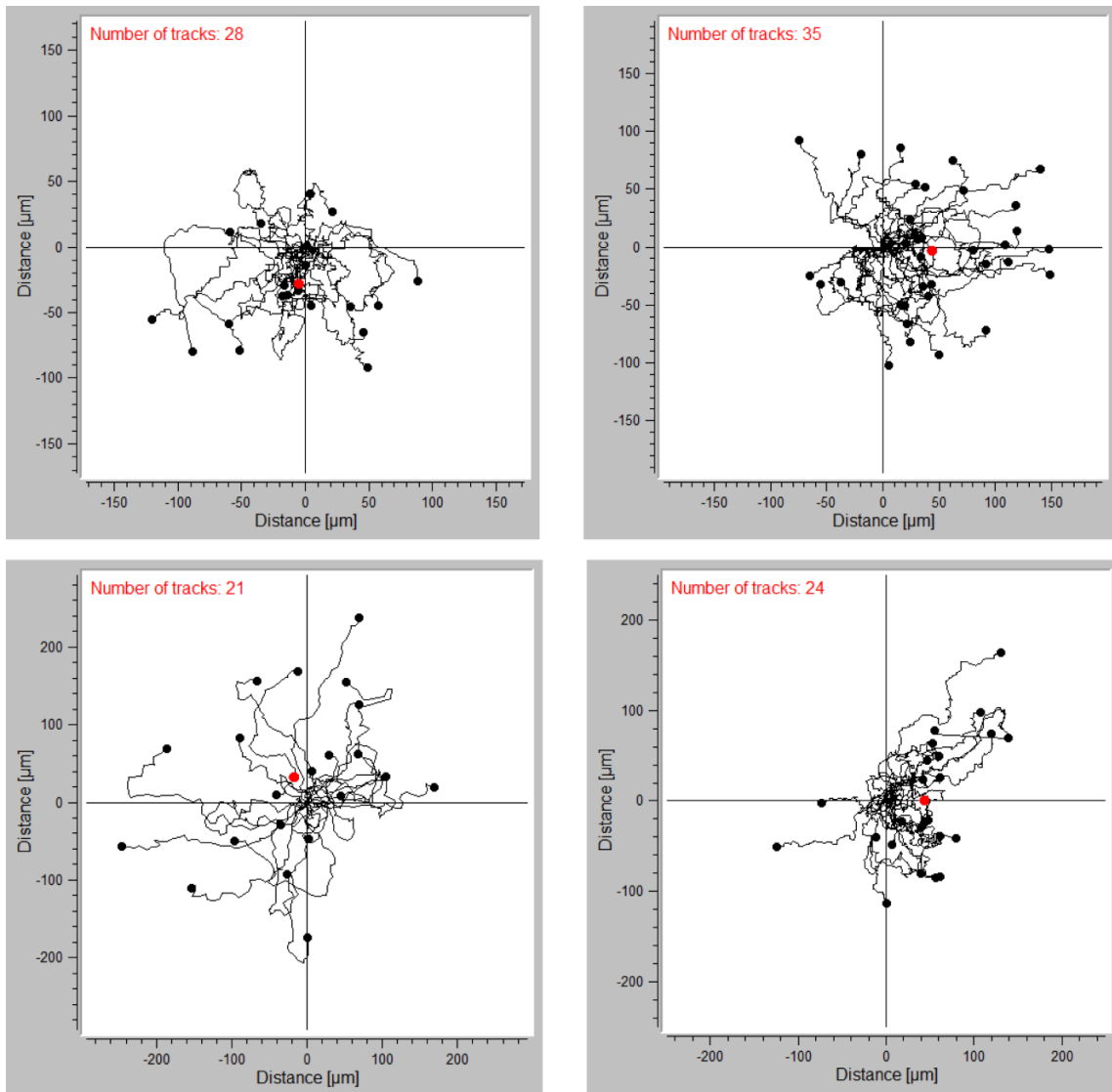
Figure 8: Human neutrophils show biased movement away from rDPPIV. Neutrophil migration was measured in the absence (left two panels) or presence (right two panels) of a 0-1.2 nM rDPPIV gradient. Neutrophils were filmed and tracked over 10-minute periods. Orientation is such that the source of rDPPIV is on the left. Graphs show the remaining two replicates from Figure 3. Red dots represent the average center of mass for all the ending positions of all cells.

Table 7: The effect of DPPIV on forward migration and directness of neutrophil movement. The data from at least three independent sets of cell population tracks (see Figure 7 and 8 as an example) were analyzed to determine the forward migration index (FMI) and directionality. FMI is a measure of migration of cells along the gradient, where zero equals no movement, a positive number equals movement away from the source, and a negative number indicates movement toward the source. Directionality is the ratio of Euclidean distance to accumulated distance. For each gradient, neutrophils from at least three different volunteers were used. * indicates $p < 0.05$, ** indicates $p < 0.01$, and *** indicates $p < 0.001$ compared to the media control (t-test). [TNF] represents a gradient of DPPIV with TNF-α stimulated neutrophils. N/A indicates not applicable.

rDPPIV gradient (nM)	Forward Migration Index		Directionality		Number of cells moving toward DPPIV
	Media control (0 nM rDPPIV)	rDPPIV	Media control (0 nM rDPPIV)	rDPPIV	rDPPIV
0-1.2	0.00 ± 0.03	0.21 ± 0.03***	0.35 ± 0.02	0.39 ± 0.02*	10 / 93
0-3.5	-0.04 ± 0.04	0.21 ± 0.06***	0.26 ± 0.02	0.50 ± 0.03***	9 / 55
0-11.7	0.01 ± 0.06	0.15 ± 0.05*	0.47 ± 0.03	0.47 ± 0.02	6 / 50
4.7-4.7	0.01 ± 0.06	-0.01 ± 0.04	0.47 ± 0.03	0.30 ± 0.02***	N/A
4.7-11.7	-0.02 ± 0.06	0.22 ± 0.06**	0.50 ± 0.03	0.42 ± 0.04*	4 / 32
9.4-23	-0.01 ± 0.05	0.13 ± 0.05*	0.36 ± 0.03	0.50 ± 0.02***	25 / 74
0-3.5[TNF]	-0.02 ± 0.03	0.10 ± 0.03**	0.32 ± 0.02	0.34 ± 0.02	8 / 81

DPPIV gradients affect the probability of directional movement but do not affect cell speed

We also examined the ability of DPPIV to affect cell speed and directional movement using the cell-tracking data. A gradient of DPPIV did not affect cell speed, and speeds were consistent with previous measurements of neutrophil migration (Table

8), and were similar to neutrophil speed observed in gradients on fMLP in an Insall chamber (30.2 ± 3.6) (164, 165). P_A and P_T can be defined as the probability that a cell would move away or toward a source of DPPIV, respectively in a 13-second interval (48). In gradients of DPPIV, with the exception of a 9.4-23 nM gradient, either P_T was significantly less or P_A was significantly more than the control (Table 9). The probability of a cell moving toward or away from DPPIV was similar to the control when equal concentrations were present on either side of the chamber (Table 9). DPPIV did not significantly affect P_0, the probability that a cell did not move in a 13-second interval. These results indicate that although a gradient of DPPIV does not significantly affect cell speed, it does affect the movement of a cell toward or away from the source of DPPIV.

Table 8: The effect of DPPIV on the average speed of neutrophils. The data from at least three independent sets of cell population tracks (see Figure 7 and Figure 8) were used to determine the average speed of neutrophils. Values are mean ± SEM, n = 3 or more.

Average Cell Speed (µm/minute)		
rDPPIV gradient (nM)	Media control (0 nM rDPPIV)	rDPPIV
0-1.2	27 ± 1	26 ± 1
0-3.5	23 ± 1	23 ± 1
0-11.7	24 ± 2	25 ± 2
4.7-4.7	17 ± 1	16 ± 1
4.7-11.7	17 ± 1	18 ± 2
9.4-23	17 ± 1	17 ± 1

Table 9: Percentage of cells in the population moving in a biased direction over 10 min. The data from at least three independent sets of cell population tracks (see Figure 7 and Figure 8 for an example) were used to determine the probability of cell movement toward or away from the source of DPPIV. P_A and P_T are the probabilities that a cell would move away from or toward the source of DPPIV, respectively in a 13-second interval. P_0 is the probability that a cell will not move. P_A and P_T are statistically significantly different in all DPPIV gradients at $p < 0.05$ (t-test), except for 0-11.7 nM DPPIV, which is significant at $p < 0.01$. In the controls, P_A and P_T are statistically significant only in the 4.7-11.7 and 9.4-23 nM controls ($p < 0.05$). ^{TNF} represents a gradient of DPPIV with TNF-α stimulated neutrophils.

rDPPIV concentration gradient (nM)	P_0		P_T		P_A	
	Control	rDPPIV	Control	rDPPIV	Control	rDPPIV
0-1.2	0.39 ± 0.14	0.54 ± 0.02	0.32 ± 0.08	0.16 ± 0.01*	0.29 ± 0.06	0.31 ± 0.02
0-3.5	0.27 ± 0.13	0.28 ± 0.08	0.39 ± 0.08	0.27 ± 0.04	0.34 ± 0.06	0.45 ± 0.06*
0-11.7	0.10 ± 0.03	0.13 ± 0.06	0.46 ± 0.01	0.35 ± 0.02*	0.44 ± 0.03	0.52 ± 0.05
4.7-4.7	0.17 ± 0.07	0.20 ± 0.05	0.44 ± 0.03	0.43 ± 0.03	0.39 ± 0.04	0.37 ± 0.03
4.7-11.7	0.19 ± 0.06	0.22 ± 0.06	0.44 ± 0.03	0.26 ± 0.05*	0.38 ± 0.04	0.53 ± 0.02*
9.4-23	0.29 ± 0.02	0.22 ± 0.06	0.39 ± 0.03	0.38 ± 0.03	0.33 ± 0.02	0.40 ± 0.08
0-3.5^{TNF}	0.26 ± 0.04	0.26 ± 0.03	0.38 ± 0.04	0.31 ± 0.03	0.36 ± 0.01	0.43 ± 0.02*

Neutrophil chemorepulsion is sensitive to DPPIV enzyme inhibitors

DPPIV enzyme activity has been implicated in the chemotaxis of several types of immune cells through cleavage of human chemokines (84, 146, 166, 167). To determine if DPPIV enzyme activity affects DPPIV-induced neutrophil chemorepulsion, we used two enzyme inhibitors of DPPIV, Diprotin A and DPPI 1c hydrochloride (DPPI 1cHCl) (168, 169). The inhibitors alone caused no attraction or repulsion of human neutrophils (Figure 9). When either of the inhibitors was added with DPPIV, the chemorepulsion of neutrophils away from the source of DPPIV was significantly reduced compared to DPPIV alone (Figure 9). This suggests that DPPIV inhibitors block the ability of DPPIV to induce neutrophil chemorepulsion.
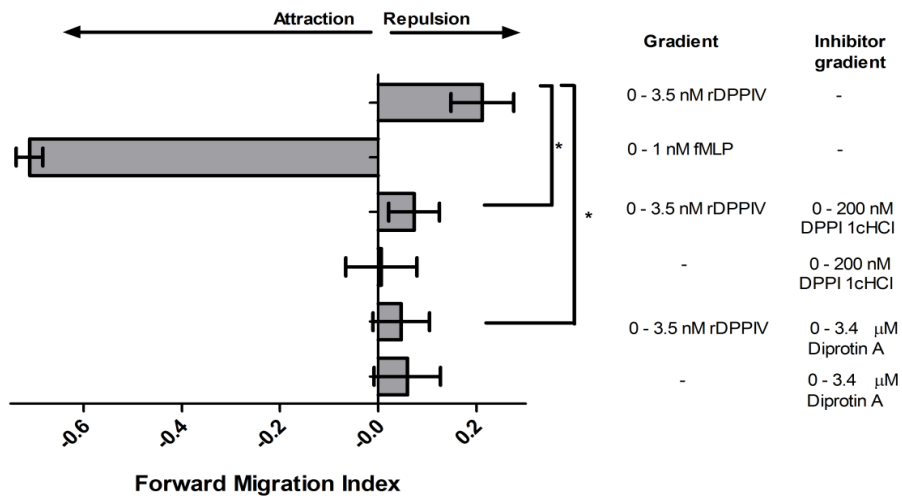
Figure 9: Inhibitors of DPPIV reduce the chemorepulsion of neutrophils away from DPPIV. The forward migration index is shown for a gradient of DPPIV, fMLP, two DPPIV inhibitors, or DPPIV with the inhibitors. Values are mean ± SEM, n = 3. * indicates a significant difference compared to a gradient of DPPIV ($p < 0.05$ by t-test).

DPPIV does not appear to cleave albumin

Several possibilities exist to explain why DPPIV enzymatic activity seems to be required for neutrophil chemorepulsion. In addition to DPPIV directly regulating neutrophil chemorepulsion, DPPIV could cleave a component of the media, such as creating a breakdown component of BSA that acts as a chemorepellent. To determine whether a component of the media was broken down by rDPPIV, BSA-RPMI or human albumin-RPMI were incubated with rDPPIV for 3 hours. While BSA is not pure, the human albumin media appears to contain only human albumin and DPPIV as protein components (Figure 10A and 10B). In both cases, there was no indication of cleavage products accumulating over time, or when time points are compared in the presence and absence of rDPPIV (Figure 10A and 10B).

Purified neutrophils are chemorepulsed by DPPIV

A protein or peptide released by contaminating cells into the media and then cleaved by DPPIV could also act as the chemorepellent. Neutrophils were further purified after isolation, resuspended in pure human albumin, and assayed for chemorepulsion from DPPIV. Both the number of contaminating eosinophils and monocytes in the neutrophil preparation decreased significantly following depletion (Figure 10C). Neutrophils were 97% pure following CD244 depletion, making a gradient of attractant or repellent from remaining contaminating cells unlikely (Figure 10C). Pure neutrophils showed a biased movement away from rDPPIV (Figure 10D). These data

suggest that it is unlikely that DPPIV cleaves a component of the media or from contaminating cells to induce chemorepulsion.
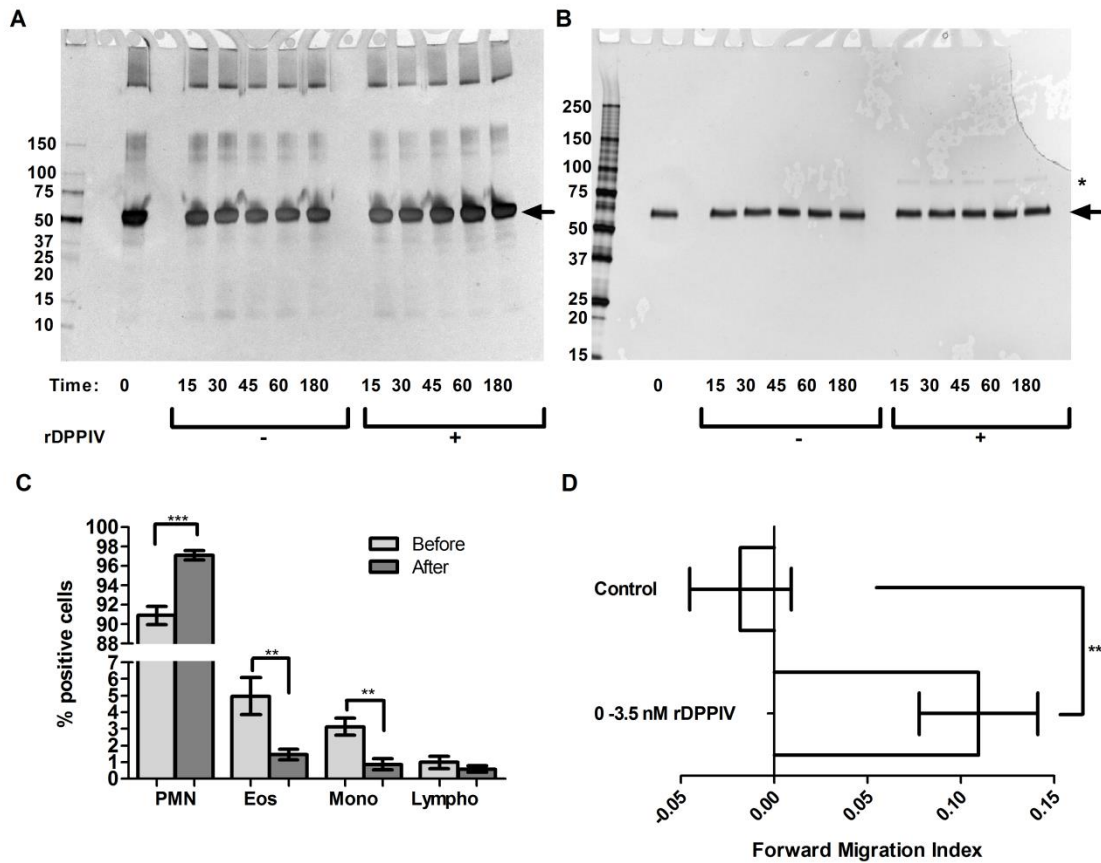
Figure 10: Purified neutrophils are chemorepulsed by DPPIV. A) 2% BSA-RPMI or **B)** 2% human albumin-RPMI was incubated with (+) or without (-) 300 ng/ml rDPPIV for 3 hours. Time at which samples were taken is given in minutes. Gels were silver stained to identify cleavage products. Molecular masses in kDa are indicated at left, and * indicates the position of DPPIV and the arrow indicates the position of albumin. **C)** Isolated neutrophils were further purified by CD244 depletion. Purity was determined by morphology. Values are mean ± SEM. n = 7. ** and *** indicate that percentages after depletion are statistically different from their paired before percentage with $p < 0.01$ and $p < 0.001$, respectively (t-test). PMN indicates neutrophils, Eos indicates eosinophils, Mono indicates monocytes, and Lympho indicates lymphocytes. **D)** The forward migration index is shown for a DPPIV gradient on purified neutrophils in 2% human albumin-RPMI buffer. Values are mean ± SEM. n = 7. ** indicates values are statistically significant from the control with $p < 0.01$ (two-tailed unpaired t-test).

54
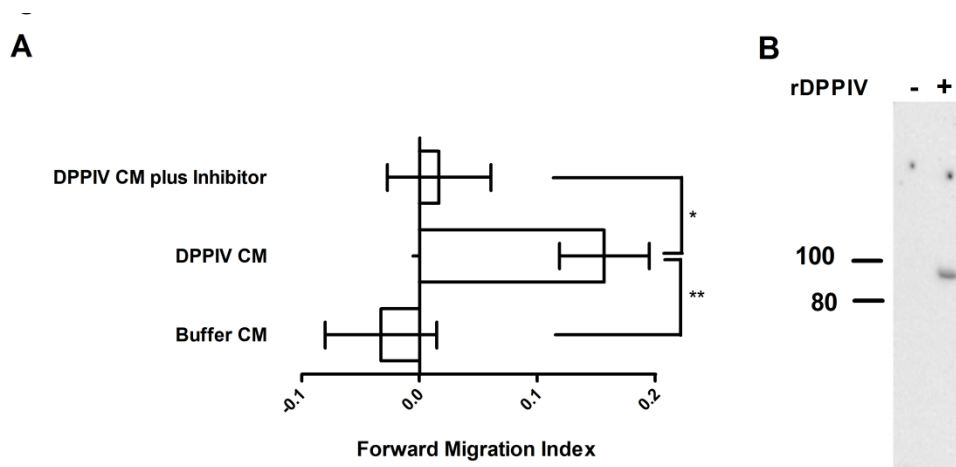
Figure 11: The effect of neutrophil conditioned media on chemorepulsion. A) The forward migration index is shown for gradients of conditioned media from DPPIV-treated neutrophils (DPPIV CM), gradients of this material treated with DPPIV inhibitor, and gradients of conditioned media from buffer-treated neutrophils (Buffer CM). Values are mean ± SEM. n = 4. * and ** indicate values are statistically significant from the control with $p < 0.05$ and $p < 0.01$, respectively (two-tailed unpaired t-test). **B)** A western blot of conditioned media using anti-DPPIV antibodies. The position of molecular mass standards (in kDa) is indicated on the left.

Conditioned medium from neutrophils does not affect chemorepulsion

Proteases on the neutrophil surface could create a neutrophil chemorepellent or cleave a breakdown component of the media that acts as a chemorepellent. Additionally, neutrophils could be releasing a chemorepellent or chemoattractant that is then affected by DPPIV. To determine if neutrophil proteins are responsible for the chemorepulsion effect, neutrophils were incubated with DPPIV or an equivalent volume of buffer for 30 minutes at 37°C. Neutrophils were then collected by centrifugation, the conditioned media recovered, and media from the outer chamber of the Insall chamber was replaced with this conditioned media. Half of the conditioned media from cells pre-incubated with DPPIV was mixed with the DPPIV inhibitor DPPIV 1c hydrochloride immediately

before addition to the Insall chamber. Conditioned media from buffer-treated cells or conditioned media from DPPIV-treated cells that was mixed with the inhibitor failed to promote chemorepulsion of neutrophils (Figure 11A). Conditioned media from DPPIV-treated cells did promote chemorepulsion of neutrophils (Figure 11A). As determined by Western blots stained with anti-DPPIV antibodies, there was no detectable DPPIV present in conditioned media from buffer-treated cells, while there was DPPIV present in the conditioned media from DPPIV-treated cells (Figure 11B). Together, these data suggest that DPPIV promotes neutrophil chemorepulsion, rather than cleaving a component of the media or a substrate secreted from cells.

DPPIV reduces the number of neutrophils in lungs of mice treated with bleomycin

Oropharyngeal aspiration of bleomycin in mice causes neutrophils to accumulate in the lungs within 24 hours of bleomycin administration (170). If DPPIV functions as a neutrophil chemorepellent, then administering DPPIV to a tissue could drive neutrophils out of the tissue or prevent their entry. We examined the ability of DPPIV to affect neutrophil accumulation in the lungs of bleomycin-treated mice. Assuming the volume of liquid in the airways of mouse lungs is no more than 0.1 ml, administering 0.9 µg of DPPIV creates a DPPIV concentration considerably greater than the DPPIV serum concentration of 0.4 µg/ml (89). Mice were treated with bleomycin on day 0 and were treated with aspirated rDPPIV or an equivalent volume of saline on day 1. Bleomycin is metabolized and excreted within 24 hours, so the DPPIV treatment at 24 hours does not block the effect of bleomycin (171, 172). Three days after bleomycin treatment, mice

56

were euthanized and weakly adhered cells from the airways were collected by bronchoalveolar lavage (BAL). Although the BAL from DPPIV-treated mice appeared to have fewer total number of cells than mice given bleomycin alone, this difference was not significant (Figure 12A). BALs from mice given rDPPIV following saline had significantly less cells than mice given saline or bleomycin alone (Figure 12A). Cell morphology was used to determine the total number of neutrophils, macrophages, and lymphocytes in the BAL. Significantly fewer neutrophils were present in the BALs from bleomycin plus rDPPIV and saline plus rDPPIV treated mice compared to mice treated with bleomycin alone (Figure 12B). There was no difference in total macrophage or lymphocyte numbers in the BAL between DPPIV-treated mice and their untreated counterparts (Figure 12B). Following BAL, lungs were sectioned and stained with anti-mouse Ly6G to detect neutrophils. There were significantly fewer Ly6G positive cells in the post-BAL lungs of mice treated with bleomycin and then treated with DPPIV on day 1 than the post-BAL lungs of mice treated with bleomycin alone (Figure 12C and 12D). There was no difference in the numbers of CD11b, CD11c, CD206, or CD107b (Mac3) positive cells in the lungs of mice treated with bleomycin compared to those treated with bleomycin and then treated with DPPIV (Figure 12E), suggesting that the effect of DPPIV is specific to neutrophils.

DPPIV regulates GLP-1, which regulates glucose levels in the blood (173). Inhibiting DPPIV affects glucose levels in mice (174). To determine if oropharyngeal aspiration of DPPIV at day 1 affected weight gain or serum glucose levels, we measured weight change over 3 days and measured glucose levels in the blood of mice euthanized
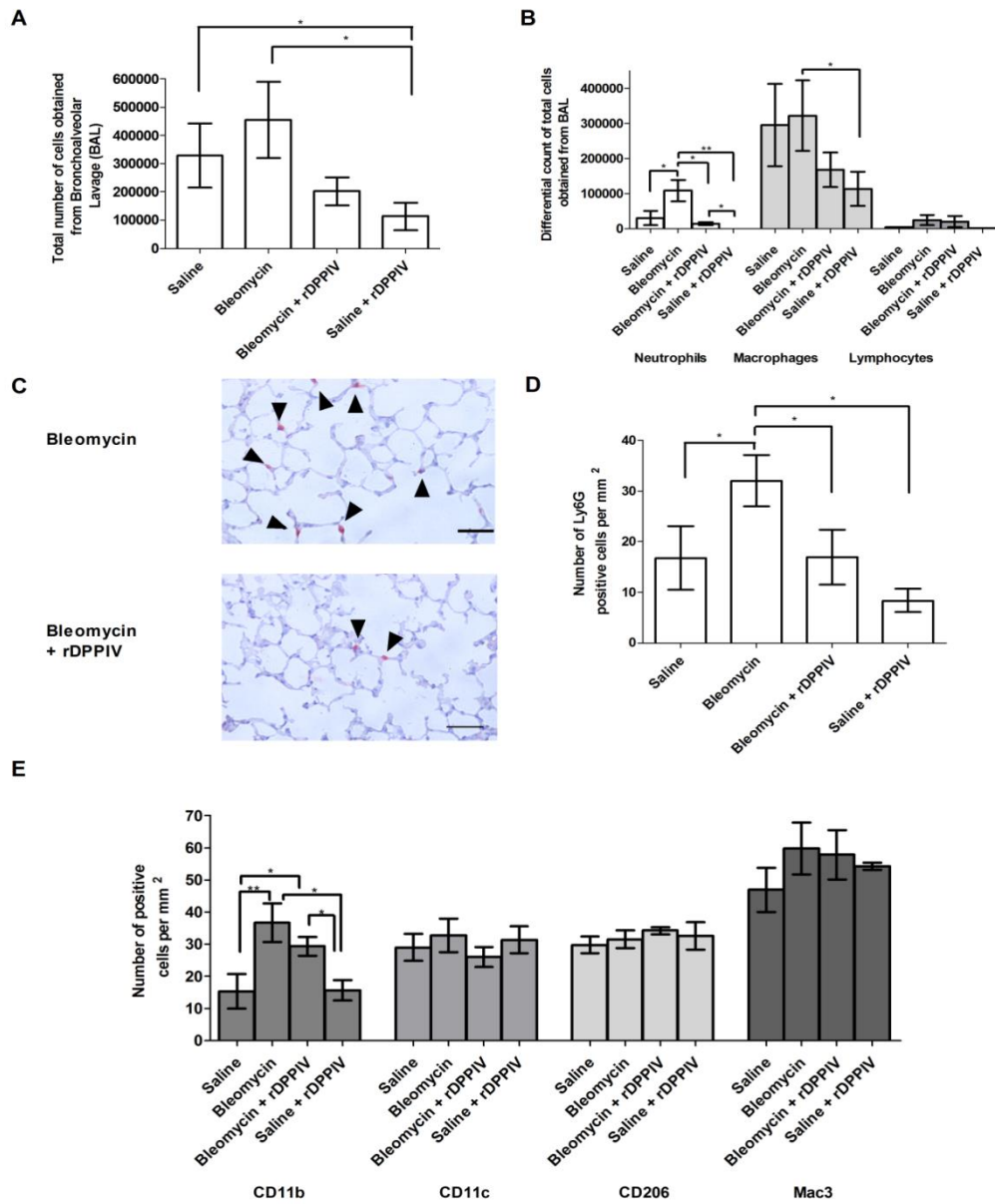
Figure 12: DPPIV reduces the number of neutrophils in bleomycin-treated lungs. Mice were treated with 3 U/kg bleomycin by oropharyngeal aspiration on day 0. On day 1, mice were treated with oropharyngeal aspiration of 0.9 µg of human rDPPIV or an equal volume of buffer. Mice were sacrificed on day 3 and cells were collected by BAL. **A)** The total number of cells collected from the BAL. Values are mean ± SEM (n = 4 bleomycin and bleomycin + DPPIV, n = 3 saline and saline + DPPIV). **B)** The total number of neutrophils, macrophages, and lymphocytes obtained in the BAL for the above experimental groups. Values are mean ± SEM (n = 4 bleomycin and bleomycin + DPPIV, n = 3 saline and saline + DPPIV). * and ** indicate a significant difference with $p < 0.05$ or $p < 0.01$, respectively, as determined by paired one-tailed t-tests. **C)** Lung sections were stained with anti-mouse Ly6G to detect neutrophils. Arrows indicate Ly6G positive cells. Scale bars are 50 µm. **D)** Counts of Ly6G positive cells in lung sections. Values are mean ± SEM (n = 4 for bleomycin and bleomycin + DPPIV, n = 3 for saline and saline + DPPIV). * indicates a significant difference with $p < 0.05$ as determined by paired two-tailed t-test. **E)** Counts of CD11b, CD11c, CD206, or CD107b (Mac3) positive cells in lun. sections. Values are mean ± SEM (n = 3). * and ** indicate a significant difference with $p < 0.05$ or $p < 0.01$, respectively, as determined by paired two-tailed t-test.

58

A
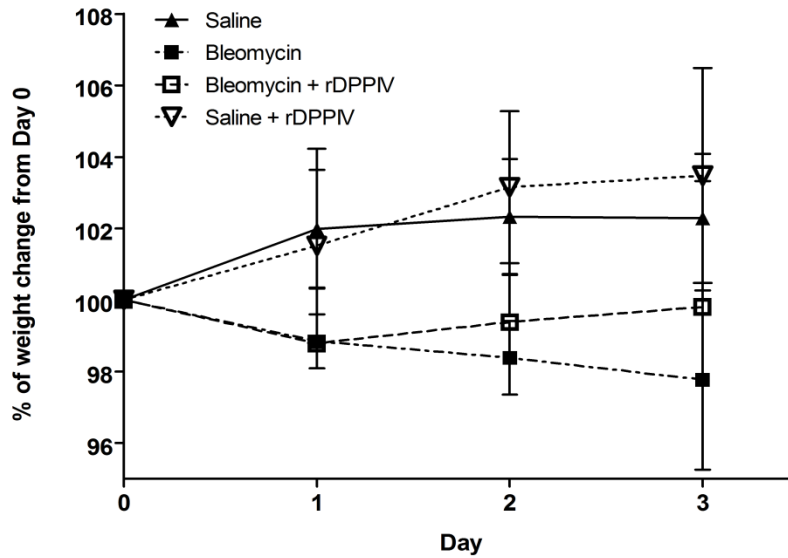
B
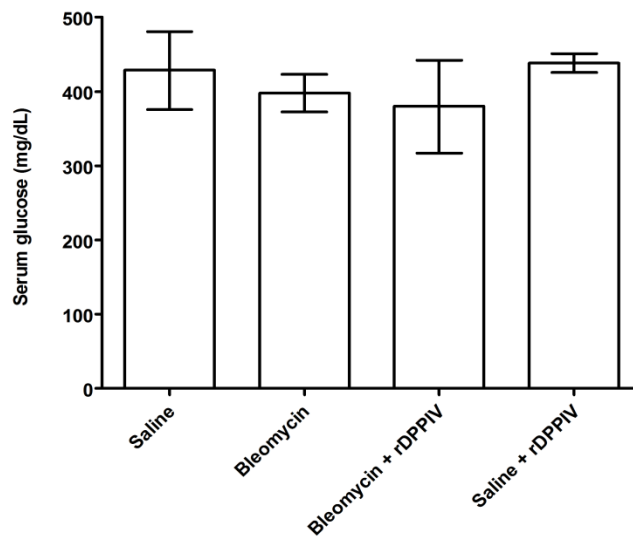
Figure 13: Physiological responses of mice treated with DPPIV. Mice were treated with 3 U/kg bleomycin by oropharyngeal aspiration on day 0. On day 1, mice were treated with oropharyngeal aspiration of 0.9 μg of human rDPPIV or an equal volume of buffer. Mice were sacrificed on day 3. Values are mean ± SEM (n = 4 bleomycin and bleomycin + DPPIV, n = 3 saline and saline + DPPIV). **A)** DPPIV reduces the weight loss caused by bleomycin administration and has no effect on weight gain in control mice. **B)** DPPIV has no effect on blood glucose levels.

on day 3. Although not statistically significant, DPPIV administration appeared to rescue the weight loss caused by bleomycin and had no significant impact on weight gain when administered on day 1 to mice given saline on day 0 (Figure 13A). Additionally, DPPIV administration had no significant effect on serum glucose levels at day 3 (Figure 13B). Together, our results indicate that DPPIV reduces the accumulation of neutrophils in the lungs of mice but does not cause significant changes in weight or serum glucose levels two days after administration.

DPPIV does not promote or inhibit neutrophil survival

The number of cells in any tissue is dependent on four factors; proliferation, death, recruitment, and emigration (175). As neutrophils are terminally differentiated cells, proliferation is not likely to regulate neutrophil numbers in an inflammatory environment. To determine if the reduction in the number of neutrophils in DPPIV-treated lungs was due to altered cell survival, we cultured human neutrophils in the presence or absence of DPPIV for 20 hours. In the absence of exogenous proteins, the majority of neutrophils were apoptotic, as determined by Annexin V staining and morphological changes (Figure 14A and 14B). The addition of DPPIV had no significant effect on neutrophil survival (Figure 14A-C). To determine if DPPIV was regulating neutrophil survival *in vivo*, we stained lung sections with antibodies against active caspase-3. Similar to previous observations in the presence or absence of bleomycin, there was no difference in the number of cells labeled with active caspase-3 antibodies with the addition of DPPIV (Figure 14D) (176). These data indicate that the reduction in
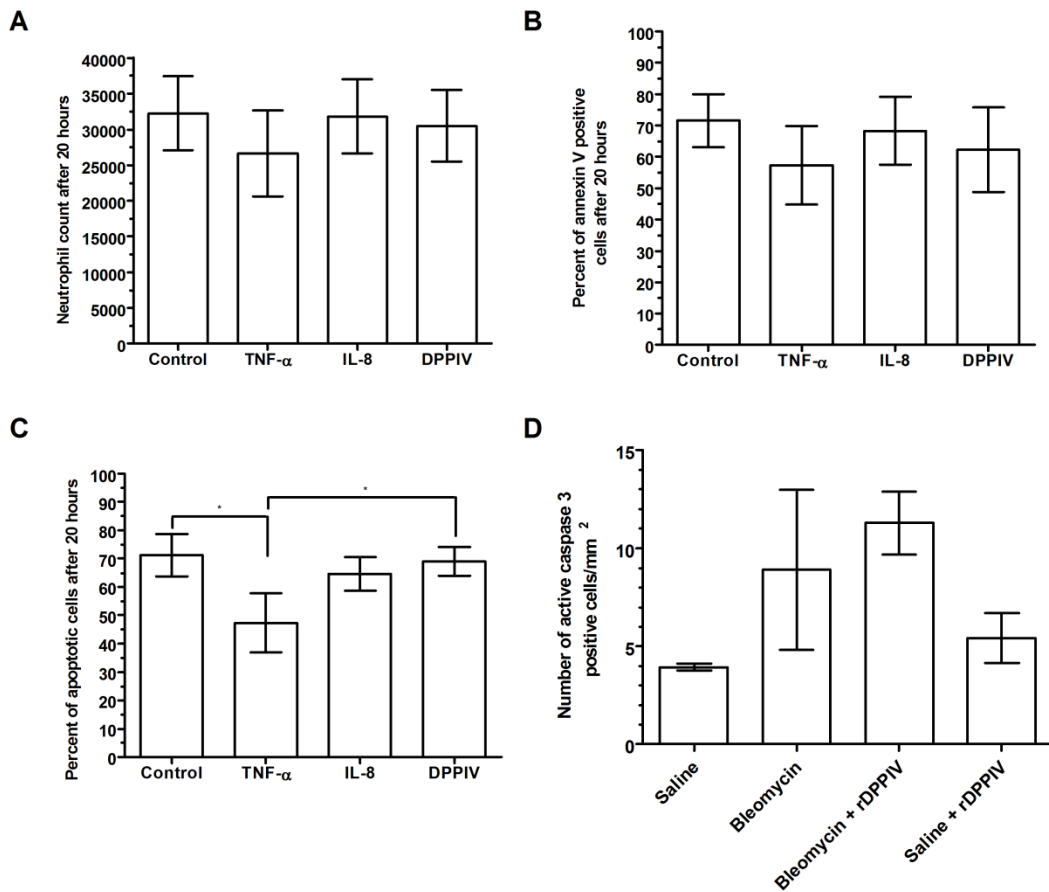
Figure 14: DPPIV does not regulate neutrophil survival. Human neutrophils were incubated for 20 hours in the presence or absence of TNF-a, IL-8, or DPPIV. Values are mean ± SEM. **A)** Neutrophils were identified by their forward and side scatter characteristics and the number of propidium iodide negative cells were counted by flow cytometry. n=4. **B)** The percentage of Annexin V positive neutrophils was determined by flow cytometry. n=3. **C)** The percentage of apoptotic neutrophils was assessed by counting nuclei with apoptotic morphology on cytospin preparations. n=3. **D)** Counts of activated caspase-3 in lung sections. n=3.

the number of neutrophils in the lungs of mice following DPPIV administration is unlikely to be due to increased neutrophil cell death.

Discussion

We previously characterized AprA as an endogenous chemorepellent of *Dictyostelium* cells (48). Here, we identified structural similarities between AprA and human DPPIV, and found that DPPIV appears to act as a neutrophil chemorepellent at physiological concentrations.

In the Insall chambers, we observed a strong DPPIV chemorepellent effect using a 0 to 100 ng/ml (0-1.2 nM) gradient. The gradient in the Insall chamber forms over a 970-µm gap. Making the first-order assumption that the gradient is linear, DPPIV is effective at 0.10 ng/ml/µm, or 0.0012 nM/µm. With an observed average neutrophil length of 10.5 µm (consistent with previous observations) (177), a cell in the middle of the gradient would correspond to a difference of 1.1 ng over the length of the cell at a place where the average DPPIV concentration is 50 ng/ml. This would then represent a 2.2% difference in the DPPIV concentration between the front and the back of the cell. For the 4.7-11.7 nM and the 9.4-23 nM gradients, the difference is 0.9%. This is similar to the 1.25% concentration difference of cAMP that induces chemotaxis for aggregating *Dictyostelium* cells (164), or the 1% fMLP concentration gradient that induces neutrophil chemotaxis (178).

For unknown reasons, we observed that for all of the DPPIV gradients in the Insall chambers, approximately 17% of the neutrophils showed movement toward the

source of DPPIV over 10 minutes. There was no obvious difference in the percentage of cells moving toward DPPIV as a function of the DPPIV concentration gradient. This effect is strikingly similar to the observation that 17% of *Dictyostelium* cells also move toward a source of AprA in the Insall chambers (48). At the lowest gradient concentration used, the DPPIV concentration at the middle of the gradient was 0.6 nM, or ~110 DPPIV molecules per cell volume in the extracellular environment. By Poisson statistics, there could be momentary conditions where the cell does not detect the gradient or detects an 'opposite' gradient. However, over 10 minutes all cells should detect the gradient. As the percentage of non-neutrophils in both isolated and purified neutrophils is below 17% of the total population, some portion of the backwards moving cells must be neutrophils. The existence of cells moving backwards thus indicates an unknown heterogeneity in both *Dictyostelium* cells and human neutrophils.

Inhibitors that block the active site of DPPIV also blocked the ability of DPPIV to act as a chemorepellent. It is possible that the inhibitors disrupt the DPPIV structure, and therefore disturb its ability to act as a ligand for a chemorepellent receptor. However, the crystal structure of human DPPIV in a complex with Diprotin A shows no significant structural difference compared to DPPIV alone (179). This suggests that the inhibitors block chemorepulsion in some other manner, such as blocking the ability to cleave something in the assay medium. In the Insall chamber assays, neutrophils were in RPMI containing BSA or human albumin, on a fibronectin surface. The only known enzymatic activity of DPPIV is cleavage of two amino acids from the N-terminus of a protein if the second amino acid is a proline or alanine (81). RPMI does not contain

63

proteins, and BSA and human albumin do not have a proline or an alanine as the second amino acid. Additionally, no cleavage products of BSA or human albumin were seen following incubation with rDPPIV for 3 hours. DPPIV does not cleave fibronectin (180). Following CD244 depletion, neutrophils were 97% pure and rDPPIV was still able to cause repulsion, indicating that a factor secreted by cells contaminating the neutrophil preparation is not likely responsible for the effect. There are no known neutrophil-secreted neutrophil chemoattractants that are, or could be, affected by DPPIV (146, 181-185). Conditioned media from neutrophils incubated with buffer alone did not cause attraction or repulsion of neutrophils, supporting this idea. Conditioned media from neutrophils incubated with DPPIV caused chemorepulsion of neutrophils. The chemorepulsive activity of the conditioned media was lost with the addition of a DPPIV inhibitor, suggesting the chemorepulsive activity in the conditioned media is due specifically to the presence of DPPIV activity. Although DPPIV-induced neutrophil chemorepulsion appears to require the DPPIV active site, the chemorepulsion does not appear to be caused by DPPIV's enzymatic activity on material in the medium, on chemoattractants or repellents, or components from cells.

DPPIV knockout mice have been generated (89) and rat strains lacking DPPIV have been identified (90, 91). DPPIV deficient animals have normal blood levels of most leukocytes, including neutrophils (92-94). Arthritic joints in mammals contain abnormally high numbers of neutrophils (70). DPPIV knockout mice have increased severity of experimentally induced arthritis, with a 2.4 fold increase in the number of cells in the joint (95). A two-fold increase in neutrophils occurs in ovalbumin-induced

lung inflammation in DPPIV deficient rats compared to normal rats (96). Reduced levels of DPPIV correlate with increased inflammation in the joints of rheumatoid arthritis patients (97). The increased inflammation observed in DPPIV deficient situations has been assumed to be due to a persistent chemokine presence, as DPPIV was not present to cleave those chemokines that have an alanine or proline as the second amino acid (98).

We found that oropharyngeal aspiration of DPPIV caused a reduction in the accumulation of neutrophils, but not other immune cells, in the lungs of mice treated with bleomycin, suggesting that the chemorepulsive effect of DPPIV is specific to neutrophils. In addition, the reduction in neutrophils was not due to increased neutrophil death. Our data suggests an alternative hypothesis to the persistence of chemokines in a tissue. We hypothesize that DPPIV acts directly as a neutrophil chemorepellent. Following neutrophil influx, activated T cells enter a site of inflammation (186). Activated T cells highly express membrane DPPIV, and extracellular DPPIV is thought to be cleaved from the membrane of T cells (75). An increase in extracellular DPPIV could promote neutrophil egress from the inflammatory site. In the resolution of zebrafish wounds, neutrophils are able to move out of the tissue and back into the vasculature (71). An intriguing possibility is that T cell-released DPPIV may help cause the egress of neutrophils out of the lung tissue to resolve lung inflammation. Some lung diseases such as acute respiratory distress syndrome (ARDS) involve an excess number of neutrophils in the lungs (103). The ability of DPPIV to induce neutrophil chemorepulsion suggests the existence of new mechanisms that may be used to treat these diseases.

CHAPTER IV

CONCLUSIONS AND FUTRE DIRECTIONS

Conclusions

Cancer results in half a million deaths per year in the United States, but most deaths occur after removal of the primary tumor when metastases proliferate rapidly (2-7). This suggests a factor is secreted by the primary tumor to keep metastatic cells dormant. The 40% mortality rate in ARDS is attributable to an influx of neutrophils that further damages lung tissue (100-102, 104, 105). Currently, the specific factors that inhibit proliferation of tumor metastases and those that could prevent or slow the influx of neutrophils are unknown. In in the model organism, *Dictyostelium*, we have found a factor named AprA that shows promise as a research target for two separate human diseases, cancer and ARDS. This dissertation explored the mechanism of proliferation inhibition in *Dictyostelium discoideum* through AprA. AprA's dual role as a chemorepellent allowed us to also analyze the mechanisms of chemorepulsion in *Dictyostelium* cells and neutrophils.

The existence of chalones, or factors that inhibit the proliferation of a subset of cells, has long been known. Examples such as liver regrowth and tumor dormancy leave us questioning the identity of the chalones. Members of the TGF-β superfamily, such as myostatin, have been identified as protein chalones. Knowing the identity of the chalone leads us to ask what are the mechanisms of proliferation inhibition. In this dissertation, I

66

have used the known *Dictyostelium* chalone, AprA, to study the mechanism of its inhibition.

Cellular proliferation is initiated by mitogens that activate downstream signaling. Chalones inhibit the proliferation of cells, but it is unclear if they use a reverse of the proliferation pathway or function in novel mechanisms to inhibit cellular proliferation. We found that the *Dictyostelium* chalone AprA functions through the PTEN-like protein CnrN. PTEN proteins inhibit cellular proliferation and are typically negative regulators of proliferation-inducing signaling pathways (113, 125-128). Activating a PTEN would block any proliferation-promoting signals by counteracting the PI3K pathway (113, 125-128). Previous work found that AprA requires a ROCO kinase, a basic leucine zipper transcription factor, and a retinoblastoma tumor suppressor to inhibit *Dictyostelium* cell proliferation (45-47). The work in this dissertation combined with previous work suggests that chalones may function in two ways (1) to block proliferation-promoting pathways and (2) to activate their own set of transcription factors to induce genes to inhibit proliferation. This could identify new methods to inhibit the proliferation of cells such as in cancer. The work in this dissertation suggests that a better way to mediate cell division may be to activate suppressor pathways rather than block proliferative pathways. Activating PTENs to 'naturally' inhibit proliferation pathways may be more beneficial than blocking the signals in the proliferation pathway. This work could also identify ways to block the inhibition of proliferation when regrowth is necessary. The regulation of tissue sizes suggests that progenitor cell division, such as the case with myoblasts, are highly regulated (10). It is tempting to speculate that enhancing

67

progenitor cell division could be used for therapies such as rapid muscle recovery following surgical atrophy or improve blood cell counts following chemotherapy. The dissertation work suggests that cell proliferation is inhibited by activating suppressors of proliferation. Therapies could be developed to reversibly inactivate proliferation inhibitors to allow regrowth when necessary.

ARDS results in 40% mortality and currently has no effective treatment (100-102, 104). Lung tissue damage in ARDS patients is attenuated by the release of proteases and reactive oxygen species from infiltrated neutrophils (104, 105). Other diseases, such as rheumatoid arthritis (RA), are characterized by neutrophil-induced damage (70). A need exists for a mechanism to stop neutrophil damage in these diseases so resolution and repair can occur.

Reverse migration, or movement of cells out of a tissue back into the bloodstream, would serve to remove neutrophils from a damaged environment and allow resolution to begin. Recently, reverse migration has been observed *in vivo* in zebrafish and both *in vitro* and *in vivo* in mice (71, 73). Chemorepellents are molecules that cause cell movement away from the substance. One could induce reverse migration of cells through application of a chemorepellent. A number of chemorepellents including those for *Dictyostelium*, neurons, mast cells, neutrophils, and cancer cells have been identified (49, 63-66).

In this dissertation, a novel neutrophil chemorepellent, DPPIV, was identified based on its structural similarity to the *Dictyostelium* chemorepellent, AprA (187). A number of studies have shown that structural similarities equate to functional similarities

(139-144). We examined whether DPPIV, like AprA, had chemorepellent activity. We found that *in vitro* a gradient of DPPIV could chemorepulse human neutrophils above, below, and within physiological concentrations. Cleavage of substrates by DPPIV enzymatic activity is known to effect chemotaxis (77, 81, 99). Although we found that the enzymatic activity of DPPIV is necessary for chemorepulsion, DPPIV did not cleave another substance to induce a secondary gradient of chemorepellent.

Approximately 17% of cells in any given experiment moved toward the source of DPPIV. Intriguingly, 17% of *Dictyostelium* cells moved toward AprA (187). It would be of interest to determine why these subsets of cells respond differently than most. Using *Dictyostelium*, one could use under agarose assays to isolate the chemoattracted cells. These cells could be enriched for in culture and analyzed for their varying properties. A Boyden chamber assay with DPPIV in the top would isolate chemoattracted or unresponsive neutrophils in the top of the well. All chemorepulsed neutrophils would migrate through the filter to the bottom well. These neutrophils could be analyzed for differences from the neutrophils in the bottom well. One would expect that the cells that are chemoattracted and those that are chemorepulsed would display differing characteristics. These could easily be identified by examining cell surface markers on either *Dictyostelium* cells or neutrophils. Neutrophil activation status could also be determined, observing their ability to adhere to surfaces, produce reactive oxygen species, and chemotax.

Diseases such as ARDS and RA have a misregulation in neutrophil clearance from the injured tissue (70, 102, 103, 107). We examined the ability of DPPIV to repulse

neutrophils from the lungs of a mouse model of ARDS. DPPIV did not affect the number of CD11b, CD11c, CD206, or Mac3 positive cells. DPPIV specifically acted to reduce the accumulation of neutrophils in the lungs of these mice. This was true for neutrophils within the air space and those in the alveolar tissue. Additionally, DPPIV reduced the accumulation of neutrophils in uninjured mice treated with DPPIV. After neutrophils enter a tissue and clear the infection, many undergo apoptosis and are ingested by macrophages (188). One reason DPPIV could reduce the accumulation of neutrophils in a tissue is by promoting apoptosis. DPPIV did not inhibit or promote apoptosis *in vitro* with human neutrophils or *in vivo* on mouse neutrophils in the lungs. This leaves two mechanisms for the reduction of neutrophils in the lungs to be studied in future work. DPPIV may either block the movement of neutrophils into the lungs or promote their reverse migration out of the lungs.

Both tumor dormancy and ARDS are diseases with high mortalities and few effective non-toxic treatments. This dissertation approaches these diseases through the unique link in the model organism *Dictyostelium*. A secreted protein, AprA, in *Dictyostelium* acts as an inhibitor of proliferation and a chemorepellent. A human structural equivalent of AprA, called DPPIV functions as a chemorepellent of human and mouse neutrophils. Future work will help expand the knowledge about the mechanisms of chalone and chemorepellent signaling, with an ultimate goal in identifying novel candidates for therapies of tumor dormancy and ARDS.

Future Work

There are a number of ways the work in this dissertation can be further developed. Several ways are outlined in the following section.

- Identify other components of the AprA chalone and chemorepulsion pathways. Use restriction-enzyme mediated insertion (REMI) screens in *Dictyostelium* to identify new mutants or screen known mutants by their ability to respond to AprA in proliferation inhibition and chemorepulsion assays.

- Are AprA and CfaD conserved enough in structure to act on cancer cells? Add rAprA, rCfaD, or a combination on to various cancer lines and determine if proliferation is inhibited in any of the cancer lines.

- We determined that CnrN is necessary for chemorepulsion by AprA and that AprA can induce CnrN to localize to the membrane. Can CnrN affect the ability of cells to polarize? The localization of CnrN in polarized cells could be determined and mutant lines could be examined for polarization along with work suggested in the next bullet.

- Determine the mechanism and components that are necessary for chemorepulsion. Many GFP lines of *Dictyostelium* are available through the Dicty Stock Center (http://dictybase.org/StockCenter/StockCenter.html). Utilize these and/or use conjugated antibodies to determine if AprA cause polarization of *Dictyostelium* cells. Additionally, live cell imaging could be used with the GFP lines to determine a time course for AprA signaling. Likewise, conjugated

antibodies could be used to identify if DPPIV polarizes neutrophils and a time course for neutrophil signaling may be done using markers and flow cytometry.

- Examine the effect of DPPIV on neutrophil activation. Besides chemotaxing, does DPPIV affect cell adhesion, induction of ROS production, or changes in surface expression (degranulation)?

- Further investigate the role of enzymatic activity of DPPIV. Create mutants that lack enzymatic activity, but do not affect binding properties. Investigate if these mutants have the same or abolished ability to cause chemorepulsion.

- Explore the mechanisms DPPIV uses in mouse models of ARDS.

  o Use a time course after DPPIV treatment to determine whether DPPIV prevents neutrophil influx or promotes their egress after an initial influx. If we find a time point where neutrophils are moving out of the lung, use intravital microscopy to visualize the cells moving between the tissue and blood.

  o Several groups have shown that reverse migrated neutrophils have different expression patterns. Examine neutrophils in mice 3 days after DPPIV treatment (or at a time from time course experiment) to determine if any neutrophils have reverse migrated into the blood.

  o We have shown that collected nebulized rDPPIV (nebulizing DPPIV, collecting it in a tube, and testing this on cells) can act as a chemorepellent *in vitro* on human neutrophils and works through oropharyngeal aspiration in mice. Investigate whether ARDS mice

allowed to freely breathe nebulized rDPPIV have a reduction in neutrophils in the lungs. This would mimic the route to be used for human treatment.

- Examine blood from healthy subjects, patients with ARDS, and patients who have recovered from ARDS for the presence of reverse migrated neutrophils.

REFERENCES

1.   Weiss, P., and J. L. Kavanau. 1957. A model of growth and growth control in mathematical terms. *J Gen Physiol* 41: 1-47.

2.   Elgjo, K., and K. L. Reichelt. 2004. Chalones: from aqueous extracts to oligopeptides. *Cell Cycle* 3: 1208-1211.

3.   Bullough, W. S., C. L. Hewett, and E. B. Laurence. 1964. The epidermal chalone; a preliminary attempt at isolation. *Exp Cell Res* 36: 192-200.

4.   Gianfranceschi, G. L., A. Czerwinski, A. Angiolillo, V. Marsili, E. Castigli, L. Mancinelli, A. Miano, M. Bramucci, and D. Amici. 1994. Molecular models of small phosphorylated chromatin peptides. Structure-function relationship and regulatory activity on in vitro transcription and on cell growth and differentiation. *Peptides* 15: 7-13.

5.   Paulsen, J. E., K. L. Reichelt, and A. K. Petersen. 1987. Purification and characterization of a growth inhibitory hepatic peptide. A preliminary note. *Virchows Arch B Cell Pathol Incl Mol Pathol* 54: 152-154.

6.   Paukovits, W. R., and O. D. Laerum. 1982. Isolation and synthesis of a hemoregulatory peptide. *Z Naturforsch C* 37: 1297-1300.

7.   Elgjo, K., and K. L. Reichelt. 1984. Purification and characterization of a mitosis inhibiting epidermal peptide. *Cell Biol Int Rep* 8: 379-382.

8.   Gamer, L. W., J. Nove, and V. Rosen. 2003. Return of the chalones. *Dev Cell* 4: 143-144.

9.   Lee, S. J. 2004. Regulation of muscle mass by myostatin. *Annu Rev Cell Dev Biol* 20: 61-86.

10.   Lander, A. D., K. K. Gokoffski, F. Y. Wan, Q. Nie, and A. L. Calof. 2009. Cell lineages and the logic of proliferative control. *PLoS Biology* 7: e15.

11.   McPherron, A. C., and S. J. Lee. 1997. Double muscling in cattle due to mutations in the myostatin gene. *Proc. Natl. Acad. Sci. USA* 94: 12457-12461.

12.   McPherron, A. C., A. M. Lawler, and S. J. Lee. 1997. Regulation of skeletal muscle mass in mice by a new TGF-beta superfamily member. *Nature* 387: 83-90.

13.   Zimmers, T. A., M. V. Davies, L. G. Koniaris, P. Haynes, A. F. Esquela, K. N. Tomkinson, A. C. McPherron, N. M. Wolfman, and S. J. Lee. 2002. Induction of cachexia in mice by systemically administered myostatin. *Science* 296: 1486-1488.

14.   Thomas, M., B. Langley, C. Berry, M. Sharma, S. Kirk, J. Bass, and R. Kambadur. 2000. Myostatin, a negative regulator of muscle growth, functions by inhibiting myoblast proliferation. *J Biol Chem* 275: 40235-40243.

15.   Rios, R., I. Carneiro, V. M. Arce, and J. Devesa. 2001. Myostatin regulates cell survival during C2C12 myogenesis. *Biochemical and Biophysical Research Communications* 280: 561-566.

16.   Langley, B., M. Thomas, A. Bishop, M. Sharma, S. Gilmour, and R. Kambadur. 2002. Myostatin inhibits myoblast differentiation by down-regulating MyoD expression. *J Biol Chem* 277: 49831-49840.

17. Langley, B., M. Thomas, C. McFarlane, S. Gilmour, M. Sharma, and R. Kambadur. 2004. Myostatin inhibits rhabdomyosarcoma cell proliferation through an Rb-independent pathway. *Oncogene* 23: 524-534.

18. Bullough, W. S., and E. B. Laurence. 1968. Melanocyte chalone and mitotic control in melanomata. *Nature* 220: 137-138.

19. Bullough, W. S., and E. B. Laurence. 1968. Control of mitosis in mouse and hamster melanomata by means of the melanocyte chalone. *Eur J Cancer* 4: 607-615.

20. Bucher, N. L. 1963. Regeneration of mammalian liver. *Int Rev Cytol* 15: 245-300.

21. Lane, B. P., and F. F. Becker. 1967. Regeneration of the mammalian liver. V. Mitotic division in cytologically differentiated liver cells. *Am J Pathol* 50: 435-445.

22. Metcalf, D. 1964. Restricted growth capacity of multiple spleen grafts. *Transplantation* 2: 387-392.

23. Aguirre-Ghiso, J. A. 2007. Models, mechanisms and clinical evidence for cancer dormancy. *Nat Rev Cancer* 7: 834-846.

24. Ossowski, L., and J. A. Aguirre-Ghiso. 2010. Dormancy of metastatic melanoma. *Pigment Cell Melanoma Res* 23: 41-56.

25. Goss, P. E., and A. F. Chambers. 2010. Does tumour dormancy offer a therapeutic target? *Nat Rev Cancer* 10: 871-877.

26.   Hedley, B. D., and A. F. Chambers. 2009. Tumor dormancy and metastasis. *Adv Cancer Res* 102: 67-101.

27.   Peeters, C. F., R. M. de Waal, T. Wobbes, and T. J. Ruers. 2008. Metastatic dormancy imposed by the primary tumor: does it exist in humans? *Annals of Surgical Oncology* 15: 3308-3315.

28.   Willis, L., T. Alarcon, G. Elia, J. L. Jones, N. A. Wright, I. P. Tomlinson, T. A. Graham, and K. M. Page. 2010. Breast cancer dormancy can be maintained by small numbers of micrometastases. *Cancer Research* 70: 4310-4317.

29.   Kessin, R. H. 2001. *Dictyostelium - Evolution, Cell Biology, and the Development of Multicellularity.* Cambridge Univ. Press, Cambridge, UK.

30.   Eichinger, L., J. A. Pachebat, G. Glockner, M. A. Rajandream, R. Sucgang, M. Berriman, J. Song, R. Olsen, K. Szafranski, Q. Xu, B. Tunggal, S. Kummerfeld, M. Madera, B. A. Konfortov, F. Rivero, A. T. Bankier, R. Lehmann, N. Hamlin, R. Davies, P. Gaudet, P. Fey, K. Pilcher, G. Chen, D. Saunders, E. Sodergren, P. Davis, A. Kerhornou, X. Nie, N. Hall, C. Anjard, L. Hemphill, N. Bason, P. Farbrother, B. Desany, E. Just, T. Morio, R. Rost, C. Churcher, J. Cooper, S. Haydock, N. van Driessche, A. Cronin, I. Goodhead, D. Muzny, T. Mourier, A. Pain, M. Lu, D. Harper, R. Lindsay, H. Hauser, K. James, M. Quiles, M. Madan Babu, T. Saito, C. Buchrieser, A. Wardroper, M. Felder, M. Thangavelu, D. Johnson, A. Knights, H. Loulseged, K. Mungall, K. Oliver, C. Price, M. A. Quail, H. Urushihara, J. Hernandez, E. Rabbinowitsch, D. Steffen, M. Sanders, J. Ma, Y. Kohara, S. Sharp, M. Simmonds, S. Spiegler, A. Tivey, S. Sugano, B.

White, D. Walker, J. Woodward, T. Winckler, Y. Tanaka, G. Shaulsky, M.

Schleicher, G. Weinstock, A. Rosenthal, E. C. Cox, R. L. Chisholm, R. Gibbs,

W. F. Loomis, M. Platzer, R. R. Kay, J. Williams, P. H. Dear, A. A. Noegel, B.

Barrell, and A. Kuspa. 2005. The genome of the social amoeba *Dictyostelium*

discoideum. *Nature* 435: 43-57.

31.   Urushihara, H. 2008. Developmental biology of the social amoeba: history,

current knowledge and prospects. *Dev Growth Differ* 50 Suppl 1: S277-281.

32.   Kuspa, A., and W. F. Loomis. 2006. The genome of *Dictyostelium discoideum*.

Meth. Mol. Biol. 346: 15-30.

33.   Loomis, W. F., and G. Shaulsky. 2011. Developmental changes in transcriptional

profiles. *Dev Growth Differ* 53: 567-575.

34.   Gomer, R. H. 1999. Gene identification by shotgun antisense. *Methods - A*

Companion to Methods in Enzymology 18: 311-315.

35.   Spann, T. P., D. A. Brock, and R. H. Gomer. 1997. Shotgun antisense

mutagenesis. In *Antisense Technoloy a Practical Approach*. C. Lichtenstein, and

W. Nellen, eds. Oxford Univ. Press, New York. 273-279.

36.   Spann, T. P., D. A. Brock, D. F. Lindsey, S. A. Wood, and R. H. Gomer. 1996.

Mutagenesis and gene identification in *Dictyostelium* by shotgun antisense. *Proc.*

Natl. Acad. Sci. USA 93: 5003-5007.

37.   Kuspa, A. 2006. Restriction enzyme-mediated integration (REMI) mutagenesis.

Meth. Mol. Biol. 346: 201-209.

38.   Manahan, C. L., P. A. Iglesias, Y. Long, and P. N. Devreotes. 2004. Chemoattractant signaling in *Dictyostelium discoideum*. *Annu Rev Cell Dev Biol* 20: 223-253.

39.   Brock, D. A., and R. H. Gomer. 2005. A secreted factor represses cell proliferation in *Dictyostelium*. *Development* 132: 4553-4562.

40.   Bakthavatsalam, D., D. A. Brock, N. N. Nikravan, K. D. Houston, R. D. Hatton, and R. H. Gomer. 2008. The secreted *Dictyostelium* protein CfaD is a chalone. *J Cell Sci* 121: 2473-2480.

41.   Choe, J. M., D. Bakthavatsalam, J. E. Phillips, and R. H. Gomer. 2009. *Dictyostelium* cells bind a secreted autocrine factor that represses cell proliferation. *BMC Biochem* 10: 4.

42.   Bowman, R. L., Y. Xiong, J. H. Kirsten, and C. K. Singleton. 2011. eIF2alpha kinases control chalone production in *Dictyostelium discoideum*. *Eukaryot Cell* 10: 494-501.

43.   Bakthavatsalam, D., J. M. Choe, N. E. Hanson, and R. H. Gomer. 2009. A *Dictyostelium* chalone uses G proteins to regulate proliferation. *BMC Biol* 7: 44.

44.   Laerum, O. D., S. Frostad, H. I. Ton, and D. Kamp. 1990. The sequence of the hemoregulatory peptide is present in Gi alpha proteins. *FEBS Letters* 269: 11-14.

45.   Phillips, J. E., E. Huang, G. Shaulsky, and R. H. Gomer. 2011. The putative bZIP transcripton factor BzpN slows proliferation and functions in the regulation of cell density by autocrine signals in *Dictyostelium*. *PLoS One* 6: e21765.

46.   Phillips, J. E., and R. H. Gomer. 2010. The ROCO kinase QkgA is necessary for proliferation inhibition by autocrine signals in *Dictyostelium discoideum*. *Eukaryot Cell* 9: 1557-1565.

47.   Bakthavatsalam, D., M. J. White, S. E. Herlihy, J. E. Phillips, and R. H. Gomer. 2014. A retinoblastoma orthologue is required for the sensing of a chalone in *Dictyostelium discoideum. Eukaryotic Cell* 13: 376-382.

48.   Phillips, J. E., and R. H. Gomer. 2012. A secreted protein is an endogenous chemorepellant in *Dictyostelium discoideum. Proc Natl Acad Sci U S A* 109: 10990-10995.

49.   Werbowetski, T., R. Bjerkvig, and R. F. Del Maestro. 2004. Evidence for a secreted chemorepellent that directs glioma cell invasion. *J Neurobiol* 60: 71-88.

50.   Willard, S. S., and P. N. Devreotes. 2006. Signaling pathways mediating chemotaxis in the social amoeba, *Dictyostelium discoideum. European Journal of Cell Biology* 85: 897-904.

51.   Gambardella, L., and S. Vermeren. 2013. Molecular players in neutrophil chemotaxis--focus on PI3K and small GTPases. *Journal of Leukocyte Biology* 94: 603-612.

52.   King, J. S., and R. H. Insall. 2009. Chemotaxis: finding the way forward with *Dictyostelium. Trends Cell Biol* 19: 523-530.

53.   Devreotes, P. N., and S. H. Zigmond. 1988. Chemotaxis in eukaryotic cells: a focus on leukocytes and *Dictyostelium. Annu Rev Cell Biol* 4: 649-686.

54.   Leonard, E. J., and T. Yoshimura. 1990. Neutrophil attractant/activation protein-1 (NAP-1 [interleukin-8]). *Am J Respir Cell Mol Biol* 2: 479-486.

55.   Crossley, L. J. 2003. Neutrophil activation by fMLP regulates FOXO (forkhead) transcription factors by multiple pathways, one of which includes the binding of FOXO to the survival factor Mcl-1. *Journal of Leukoctye Biology* 74: 583-592.

56.   Swaney, K. F., C. H. Huang, and P. N. Devreotes. 2010. Eukaryotic chemotaxis: a network of signaling pathways controls motility, directional sensing, and polarity. *Annu Rev Biophys* 39: 265-289.

57.   Jin, T., N. Zhang, Y. Long, C. A. Parent, and P. N. Devreotes. 2000. Localization of the G protein betagamma complex in living cells during chemotaxis. *Science* 287: 1034-1036.

58.   Iijima, M., Y. E. Huang, H. R. Luo, F. Vazquez, and P. N. Devreotes. 2004. Novel mechanism of PTEN regulation by its phosphatidylinositol 4,5-bisphosphate binding motif is critical for chemotaxis. *J Biol Chem* 279: 16606-16613.

59.   Funamoto, S., K. Milan, R. Meili, and R. A. Firtel. 2001. Role of phosphatidylinositol 3' kinase and a downstream pleckstrin homology domain-containing protein in controlling chemotaxis in *Dictyostelium*. *J Cell Biol* 153: 795-810.

60.   Sasaki, A. T., C. Chun, K. Takeda, and R. A. Firtel. 2004. Localized Ras signaling at the leading edge regulates PI3K, cell polarity, and directional cell movement. *J Cell Biol* 167: 505-518.

61.   Devreotes, P., and C. Janetopoulos. 2003. Eukaryotic chemotaxis: distinctions between directional sensing and polarization. *The Journal of Biological Chemistry* 278: 20445-20448.

62.   Wessels, D., D. F. Lusche, S. Kuhl, P. Heid, and D. R. Soll. 2007. PTEN plays a role in the suppression of lateral pseudopod formation during *Dictyostelium* motility and chemotaxis. *J Cell Sci* 120: 2517-2531.

63.   Shamloo, A., M. Manchandia, M. Ferreira, M. Mani, C. Nguyen, T. Jahn, K. Weinberg, and S. Heilshorn. 2013. Complex chemoattractive and chemorepellent Kit signals revealed by direct imaging of murine mast cells in microfluidic gradient chambers. *Integrative Biology : Quantitative Biosciences from Nano to Macro* 5: 1076-1085.

64.   Tharp, W. G., R. Yadav, D. Irimia, A. Upadhyaya, A. Samadani, O. Hurtado, S. Y. Liu, S. Munisamy, D. M. Brainard, M. J. Mahon, S. Nourshargh, A. van Oudenaarden, M. G. Toner, and M. C. Poznansky. 2006. Neutrophil chemorepulsion in defined interleukin-8 gradients in vitro and in vivo. *Journal of Leukocyte Biology* 79: 539-554.

65.   Keizer-Gunnink, I., A. Kortholt, and P. J. Van Haastert. 2007. Chemoattractants and chemorepellents act by inducing opposite polarity in phospholipase C and PI3-kinase signaling. *The Journal of Cell Biology* 177: 579-585.

66.   Hu, H. 1999. Chemorepulsion of neuronal migration by Slit2 in the developing mammalian forebrain. *Neuron* 23: 703-711.

67.   Masuda, T., K. Watanabe, C. Sakuma, K. Ikenaka, K. Ono, and H. Yaginuma. 2008. Netrin-1 acts as a repulsive guidance cue for sensory axonal projections toward the spinal cord. *J Neurosci* 28: 10380-10385.

68.   Messersmith, E. K., E. D. Leonardo, C. J. Shatz, M. Tessier-Lavigne, C. S. Goodman, and A. L. Kolodkin. 1995. Semaphorin III can function as a selective chemorepellent to pattern sensory projections in the spinal cord. *Neuron* 14: 949-959.

69.   Henle, S. J., L. P. Carlstrom, T. R. Cheever, and J. R. Henley. 2013. Differential role of PTEN phosphatase in chemotactic growth cone guidance. *The Journal of Biological Chemistry* 288: 20837-20842.

70.   Wright, H. L., R. J. Moots, R. C. Bucknall, and S. W. Edwards. 2010. Neutrophil function in inflammation and inflammatory diseases. *Rheumatology (Oxford)* 49: 1618-1631.

71.   Mathias, J. R., B. J. Perrin, T. X. Liu, J. Kanki, A. T. Look, and A. Huttenlocher. 2006. Resolution of inflammation by retrograde chemotaxis of neutrophils in transgenic zebrafish. *Journal of Leukocyte Biology* 80: 1281-1288.

72.   Woodfin, A., M. B. Voisin, M. Beyrau, B. Colom, D. Caille, F. M. Diapouli, G. B. Nash, T. Chavakis, S. M. Albelda, G. E. Rainger, P. Meda, B. A. Imhof, and S. Nourshargh. 2011. The junctional adhesion molecule JAM-C regulates polarized transendothelial migration of neutrophils in vivo. *Nature Immunology* 12: 761-769.

73. Buckley, C. D., E. A. Ross, H. M. McGettrick, C. E. Osborne, O. Haworth, C. Schmutz, P. C. Stone, M. Salmon, N. M. Matharu, R. K. Vohra, G. B. Nash, and G. E. Rainger. 2006. Identification of a phenotypically and functionally distinct population of long-lived neutrophils in a model of reverse endothelial migration. *Journal of Leukocyte Biology* 79: 303-311.

74. Busek, P., R. Malik, and A. Sedo. 2004. Dipeptidyl peptidase IV activity and/or structure homologues (DASH) and their substrates in cancer. *Int J Biochem Cell Biol* 36: 408-421.

75. Cordero, O. J., F. J. Salgado, and M. Nogueira. 2009. On the origin of serum CD26 and its altered concentration in cancer patients. *Cancer Immunol Immunother* 58: 1723-1747.

76. Kotackova, L., E. Balaziova, and A. Sedo. 2009. Expression pattern of dipeptidyl peptidase IV activity and/or structure homologues in cancer. *Folia Biol (Praha)* 55: 77-84.

77. Matteucci, E., and O. Giampietro. 2009. Dipeptidyl peptidase-4 (CD26): knowing the function before inhibiting the enzyme. *Curr Med Chem* 16: 2943-2951.

78. Bakthavatsalam, D., D. Brazill, R. H. Gomer, L. Eichinger, F. Rivero, and A. A. Noegel. 2007. A G protein-coupled receptor with a lipid kinase domain is involved in cell-density sensing. *Curr Biol* 17: 892-897.

79.   Sedo, A., J. S. Duke-Cohan, E. Balaziova, and L. R. Sedova. 2005. Dipeptidyl peptidase IV activity and/or structure homologs: contributing factors in the pathogenesis of rheumatoid arthritis? *Arthritis Res Ther* 7: 253-269.

80.   Abbott, C. A., E. Baker, G. R. Sutherland, and G. W. McCaughan. 1994. Genomic organization, exact localization, and tissue expression of the human CD26 (dipeptidyl peptidase IV) gene. *Immunogenetics* 40: 331-338.

81.   Chen, W. T., T. Kelly, and G. Ghersi. 2003. DPPIV, seprase, and related serine peptidases in multiple cellular functions. *Curr Top Dev Biol* 54: 207-232.

82.   Sedo, A., and R. Malik. 2001. Dipeptidyl peptidase IV-like molecules: homologous proteins or homologous activities? *Biochim Biophys Acta* 1550: 107-116.

83.   Nauck, M. A., I. Vardarli, C. F. Deacon, J. J. Holst, and J. J. Meier. 2011. Secretion of glucagon-like peptide-1 (GLP-1) in type 2 diabetes: what is up, what is down? *Diabetologia* 54: 10-18.

84.   Christopherson, K. W., 2nd, G. Hangoc, and H. E. Broxmeyer. 2002. Cell surface peptidase CD26/dipeptidylpeptidase IV regulates CXCL12/stromal cell-derived factor-1 alpha-mediated chemotaxis of human cord blood CD34+ progenitor cells. *J Immunol* 169: 7000-7008.

85.   Aiuti, A., I. J. Webb, C. Bleul, T. Springer, and J. C. Gutierrez-Ramos. 1997. The chemokine SDF-1 is a chemoattractant for human CD34+ hematopoietic progenitor cells and provides a new mechanism to explain the mobilization of

CD34+ progenitors to peripheral blood. *The Journal of Experimental Medicine* 185: 111-120.

86.   Yu, D. M., L. Slaitini, V. Gysbers, A. G. Riekhoff, T. Kahne, H. M. Knott, I. De Meester, C. A. Abbott, G. W. McCaughan, and M. D. Gorrell. 2011. Soluble CD26 / dipeptidyl peptidase IV enhances human lymphocyte proliferation in vitro independent of dipeptidyl peptidase enzyme activity and adenosine deaminase binding. *Scand J Immunol* 73: 102-111.

87.   Ohnuma, K., O. Hosono, N. H. Dang, and C. Morimoto. 2011. Dipeptidyl peptidase in autoimmune pathophysiology. *Adv Clin Chem* 53: 51-84.

88.   Ohnuma, K., T. Yamochi, M. Uchiyama, K. Nishibashi, N. Yoshikawa, N. Shimizu, S. Iwata, H. Tanaka, N. H. Dang, and C. Morimoto. 2004. CD26 up-regulates expression of CD86 on antigen-presenting cells by means of caveolin-1. *Proc Natl Acad Sci U S A* 101: 14186-14191.

89.   Marguet, D., L. Baggio, T. Kobayashi, A. M. Bernard, M. Pierres, P. F. Nielsen, U. Ribel, T. Watanabe, D. J. Drucker, and N. Wagtmann. 2000. Enhanced insulin secretion and improved glucose tolerance in mice lacking CD26. *Proc Natl Acad Sci U S A* 97: 6874-6879.

90.   Karl, T., W. T. Chwalisz, D. Wedekind, H. J. Hedrich, T. Hoffmann, R. Jacobs, R. Pabst, and S. von Horsten. 2003. Localization, transmission, spontaneous mutations, and variation of function of the DPP4 (Dipeptidyl-peptidase IV; CD26) gene in rats. *Regul Pept* 115: 81-90.

91.   Shibayama, K., T. Nakamura, I. Kinoshita, Y. Ueki, H. Nakao, K. Eguchi, M. Tsujihata, and S. Nagataki. 1992. Remarkable increase in CD26-positive T cells in patients with human T lymphotropic virus type I (HTLV-I) associated myelopathy. *Intern Med* 31: 1081-1083.

92.   Christopherson, K. W., S. Cooper, G. Hangoc, and H. E. Broxmeyer. 2003. CD26 is essential for normal G-CSF-induced progenitor cell mobilization as determined by CD26-/- mice. *Exp Hematol* 31: 1126-1134.

93.   Kidd, S., C. Bueso-Ramos, S. Jagan, L. A. Paganessi, L. N. Boggio, H. C. Fung, S. A. Gregory, and K. W. Christopherson, 2nd. 2011. In vivo expansion of the megakaryocyte progenitor cell population in adult CD26-deficient mice. *Exp Hematol* 39: 580-590 e581.

94.   Frerker, N., K. Raber, F. Bode, T. Skripuletz, H. Nave, C. Klemann, R. Pabst, M. Stephan, J. Schade, G. Brabant, D. Wedekind, R. Jacobs, A. Jorns, U. Forssmann, R. H. Straub, S. Johannes, T. Hoffmann, L. Wagner, H. U. Demuth, and S. von Horsten. 2009. Phenotyping of congenic dipeptidyl peptidase 4 (DP4) deficient Dark Agouti (DA) rats suggests involvement of DP4 in neuro-, endocrine, and immune functions. *Clin Chem Lab Med* 47: 275-287.

95.   Busso, N., N. Wagtmann, C. Herling, V. Chobaz-Peclat, A. Bischof-Delaloye, A. So, and E. Grouzmann. 2005. Circulating CD26 is negatively associated with inflammation in human and experimental arthritis. *Am J Pathol* 166: 433-442.

96.   Schmiedl, A., J. Krainski, F. Schwichtenhovel, J. Schade, C. Klemann, K. A. Raber, K. Zscheppang, T. Beekmann, C. Acevedo, T. Glaab, D. Wedekind, R.

Pabst, S. von Horsten, and M. Stephan. 2010. Reduced airway inflammation in CD26/DPP4-deficient F344 rats is associated with altered recruitment patterns of regulatory T cells and expression of pulmonary surfactant proteins. *Clin Exp Allergy* 40: 1794-1808.

97.   Kamori, M., M. Hagihara, T. Nagatsu, H. Iwata, and T. Miura. 1991. Activities of dipeptidyl peptidase II, dipeptidyl peptidase IV, prolyl endopeptidase, and collagenase-like peptidase in synovial membrane from patients with rheumatoid arthritis and osteoarthritis. *Biochem Med Metab Biol* 45: 154-160.

98.   Yazbeck, R., G. S. Howarth, and C. A. Abbott. 2009. Dipeptidyl peptidase inhibitors, an emerging drug class for inflammatory disease? *Trends Pharmacol Sci* 30: 600-607.

99.   Boonacker, E. P., E. A. Wierenga, H. H. Smits, and C. J. Van Noorden. 2002. CD26/DPPIV signal transduction function, but not proteolytic activity, is directly related to its expression level on human Th1 and Th2 cell lines as detected with living cell cytochemistry. *J Histochem Cytochem* 50: 1169-1177.

100.   Pro, B., and N. H. Dang. 2004. CD26/dipeptidyl peptidase IV and its role in cancer. *Histol Histopathol* 19: 1345-1351.

101.   Grommes, J., and O. Soehnlein. 2011. Contribution of neutrophils to acute lung injury. *Mol Med* 17: 293-307.

102.   Lee, C. M., and L. D. Hudson. 2001. Long-term outcomes after ARDS. *Semin Respir Crit Care Med* 22: 327-336.

103. Matthay, M. A., and R. L. Zemans. 2011. The acute respiratory distress syndrome: pathogenesis and treatment. *Annu Rev Pathol* 6: 147-163.

104. Wilcox, M. E., and M. S. Herridge. 2010. Long-term outcomes in patients surviving acute respiratory distress syndrome. *Seminars in Respiratory and Critical Care Medicine* 31: 55-65.

105. Segel, G. B., M. W. Halterman, and M. A. Lichtman. 2011. The paradox of the neutrophil's role in tissue injury. *Journal of Leukocyte Biology* 89: 359-372.

106. Bastarache, J. A., and T. S. Blackwell. 2009. Development of animal models for the acute respiratory distress syndrome. *Dis Model Mech* 2: 218-223.

107. Lee, W. L., and G. P. Downey. 2001. Neutrophil activation and acute lung injury. *Current Opinion in Critical Care* 7: 1-7.

108. Penuelas, O., J. A. Aramburu, F. Frutos-Vivar, and A. Esteban. 2006. Pathology of acute lung injury and acute respiratory distress syndrome: a clinical-pathological correlation. *Clinics in Chest Medicine* 27: 571-578; abstract vii-viii.

109. Patel, B. V., M. R. Wilson, and M. Takata. 2012. Resolution of acute lung injury and inflammation: a translational mouse model. *The European Respiratory Journal* 39: 1162-1170.

110. Gomer, R. H. 2001. Not being the wrong size. *Nat Rev Mol Cell Biol* 2: 48-54.

111. Iijima, M., and P. Devreotes. 2002. Tumor suppressor PTEN mediates sensing of chemoattractant gradients. *Cell* 109: 599-610.

112. Hoeller, O., and R. R. Kay. 2007. Chemotaxis in the absence of PIP3 gradients. *Curr Biol* 17: 813-817.

113. Leslie, N. R., I. H. Batty, H. Maccario, L. Davidson, and C. P. Downes. 2008. Understanding PTEN regulation: PIP2, polarity and protein stability. *Oncogene* 27: 5464-5476.

114. Huang, Y. E., M. Iijima, C. A. Parent, S. Funamoto, R. A. Firtel, and P. Devreotes. 2003. Receptor-mediated regulation of PI3Ks confines PI(3,4,5)P3 to the leading edge of chemotaxing cells. *Mol Biol Cell* 14: 1913-1922.

115. Tang, Y., and R. H. Gomer. 2008. A protein with similarity to PTEN regulates aggregation territory size by decreasing cyclic AMP pulse size during *Dictyostelium discoideum* development. *Eukaryot Cell* 7: 1758-1770.

116. Tang, Y., and R. H. Gomer. 2008. CnrN regulates *Dictyostelium* group size using a counting factor-independent mechanism. *Commun Integr Biol* 1: 185-187.

117. Sen, P., S. Mukherjee, D. Ray, and S. Raha. 2003. Involvement of the Akt/PKB signaling pathway with disease processes. *Mol Cell Biochem* 253: 241-246.

118. Andjelkovic, M., D. R. Alessi, R. Meier, A. Fernandez, N. J. Lamb, M. Frech, P. Cron, P. Cohen, J. M. Lucocq, and B. A. Hemmings. 1997. Role of translocation in the activation and function of protein kinase B. *J Biol Chem* 272: 31515-31524.

119. Franke, T. F., S. I. Yang, T. O. Chan, K. Datta, A. Kazlauskas, D. K. Morrison, D. R. Kaplan, and P. N. Tsichlis. 1995. The protein kinase encoded by the Akt proto-oncogene is a target of the PDGF-activated phosphatidylinositol 3-kinase. *Cell* 81: 727-736.

120.   Stiles, B., M. Groszer, S. Wang, J. Jiao, and H. Wu. 2004. PTENless means more. *Dev Biol* 273: 175-184.

121.   Klippel, A., M. A. Escobedo, M. S. Wachowicz, G. Apell, T. W. Brown, M. A. Giedlin, W. M. Kavanaugh, and L. T. Williams. 1998. Activation of phosphatidylinositol 3-kinase is sufficient for cell cycle entry and promotes cellular changes characteristic of oncogenic transformation. *Mol Cell Biol* 18: 5699-5711.

122.   Newton, A. C. 2009. Lipid activation of protein kinases. *J Lipid Res* 50 Suppl: S266-271.

123.   Kunkel, M. T., Q. Ni, R. Y. Tsien, J. Zhang, and A. C. Newton. 2005. Spatio-temporal dynamics of protein kinase B/Akt signaling revealed by a genetically encoded fluorescent reporter. *J Biol Chem* 280: 5581-5587.

124.   Alessi, D. R., S. R. James, C. P. Downes, A. B. Holmes, P. R. Gaffney, C. B. Reese, and P. Cohen. 1997. Characterization of a 3-phosphoinositide-dependent protein kinase which phosphorylates and activates protein kinase Balpha. *Curr Biol* 7: 261-269.

125.   Cantley, L. C., and B. G. Neel. 1999. New insights into tumor suppression: PTEN suppresses tumor formation by restraining the phosphoinositide 3-kinase/AKT pathway. *Proc Natl Acad Sci U S A* 96: 4240-4245.

126.   Paramio, J. M., M. Navarro, C. Segrelles, E. Gomez-Casero, and J. L. Jorcano. 1999. PTEN tumour suppressor is linked to the cell cycle control through the retinoblastoma protein. *Oncogene* 18: 7462-7468.

127.   Furnari, F. B., H. J. Huang, and W. K. Cavenee. 1998. The phosphoinositol phosphatase activity of PTEN mediates a serum-sensitive G1 growth arrest in glioma cells. *Cancer Res* 58: 5002-5008.

128.   Weng, L. P., W. M. Smith, P. L. Dahia, U. Ziebold, E. Gil, J. A. Lees, and C. Eng. 1999. PTEN suppresses breast cancer cell growth by phosphatase activity-dependent G1 arrest followed by cell death. *Cancer Res* 59: 5808-5814.

129.   Brock, D. A., and R. H. Gomer. 1999. A cell-counting factor regulating structure size in *Dictyostelium*. *Genes Dev* 13: 1960-1969.

130.   Gomer, R., T. Gao, Y. Tang, D. Knecht, and M. A. Titus. 2002. Cell motility mediates tissue size regulation in *Dictyostelium*. *J. Muscle Res. Cell Motil.* 23: 809-815.

131.   Novak, K. D., and M. A. Titus. 1997. Myosin I overexpression impairs cell migration. *J. Cell Biol.* 136: 633-647.

132.   Herlihy, S. E., Y. Tang, and R. H. Gomer. 2013. A *Dictyostelium* secreted factor requires a PTEN-Like phosphatase to slow proliferation and induce chemorepulsion. *PLoS One* 8: e59365.

133.   Muinonen-Martin, A. J., D. M. Veltman, G. Kalna, and R. H. Insall. 2010. An improved chamber for direct visualisation of chemotaxis. *PLoS One* 5: e15309.

134.   Das, S., J. E. Dixon, and W. Cho. 2003. Membrane-binding and activation mechanism of PTEN. *Proc Natl Acad Sci U S A* 100: 7491-7496.

135.   Baker, M. D., P. M. Wolanin, and J. B. Stock. 2006. Signal transduction in bacterial chemotaxis. *Bioessays* 28: 9-22.

136.   Colamarino, S. A., and M. Tessier-Lavigne. 1995. The axonal chemoattractant netrin-1 is also a chemorepellent for trochlear motor axons. *Cell* 81: 621-629.

137.   Zaki, M., N. Andrew, and R. H. Insall. 2006. Entamoeba histolytica cell movement: a central role for self-generated chemokines and chemorepellents. *Proc Natl Acad Sci U S A* 103: 18751-18756.

138.   Vianello, F., I. T. Olszak, and M. C. Poznansky. 2005. Fugetaxis: active movement of leukocytes away from a chemokinetic agent. *J Mol Med (Berl)* 83: 752-763.

139.   Roy, A., A. Kucukural, and Y. Zhang. 2010. I-TASSER: a unified platform for automated protein structure and function prediction. *Nat Protoc* 5: 725-738.

140.   Roy, A., J. Yang, and Y. Zhang. 2012. COFACTOR: an accurate comparative algorithm for structure-based protein function annotation. *Nucleic Acids Res* 40: W471-477.

141.   Zhang, Y. 2008. I-TASSER server for protein 3D structure prediction. *BMC Bioinformatics* 9: 40.

142.   Whisstock, J. C., and A. M. Lesk. 2003. Prediction of protein function from protein sequence and structure. *Q Rev Biophys* 36: 307-340.

143.   Lee, D., O. Redfern, and C. Orengo. 2007. Predicting protein function from sequence and structure. *Nat Rev Mol Cell Biol* 8: 995-1005.

144.   Kim, S. H., D. H. Shin, I. G. Choi, U. Schulze-Gahmen, S. Chen, and R. Kim. 2003. Structure-based functional inference in structural genomics. *J Struct Funct Genomics* 4: 129-135.

145. Walborg, E. F., Jr., S. Tsuchida, D. S. Weeden, M. W. Thomas, A. Barrick, K. D. McEntire, J. P. Allison, and D. C. Hixson. 1985. Identification of dipeptidyl peptidase IV as a protein shared by the plasma membrane of hepatocytes and liver biomatrix. *Exp Cell Res* 158: 509-518.

146. Struyf, S., P. Proost, and J. Van Damme. 2003. Regulation of the immune response by the interaction of chemokines and proteases. *Adv Immunol* 81: 1-44.

147. Holm, L., and P. Rosenstrom. 2010. Dali server: conservation mapping in 3D. *Nucleic Acids Res* 38: W545-549.

148. Kolbeck, B., P. May, T. Schmidt-Goenner, T. Steinke, and E. W. Knapp. 2006. Connectivity independent protein-structure alignment: a hierarchical approach. *BMC Bioinformatics* 7: 510.

149. Guerler, A., and E. W. Knapp. 2008. Novel protein folds and their nonsequential structural analogs. *Protein Sci* 17: 1374-1382.

150. Hansel, T. T., J. D. Pound, D. Pilling, G. D. Kitas, M. Salmon, T. A. Gentle, S. S. Lee, and R. A. Thompson. 1989. Purification of human blood eosinophils by negative selection using immunomagnetic beads. *J Immunol Methods* 122: 97-103.

151. Pilling, D., G. D. Kitas, M. Salmon, and P. A. Bacon. 1989. The kinetics of interaction between lymphocytes and magnetic polymer particles. *J Immunol Methods* 122: 235-241.

152.   Itakura, A., N. G. Verbout, K. G. Phillips, R. H. Insall, D. Gailani, E. I. Tucker, A. Gruber, and O. J. McCarty. 2011. Activated factor XI inhibits chemotaxis of polymorphonuclear leukocytes. *Journal of Leukocyte Biology* 90: 923-927.

153.   Ochsner, S. A., A. J. Day, M. S. Rugg, R. M. Breyer, R. H. Gomer, and J. S. Richards. 2003. Disrupted function of tumor necrosis factor-alpha-stimulated gene 6 blocks cumulus cell-oocyte complex expansion. *Endocrinology* 144: 4376-4384.

154.   Lakatos, H. F., H. A. Burgess, T. H. Thatcher, M. R. Redonnet, E. Hernady, J. P. Williams, and P. J. Sime. 2006. Oropharyngeal aspiration of a silica suspension produces a superior model of silicosis in the mouse when compared to intratracheal instillation. *Exp Lung Res* 32: 181-199.

155.   Corteling, R., D. Wyss, and A. Trifilieff. 2002. In vivo models of lung neutrophil activation. Comparison of mice and hamsters. *BMC Pharmacol* 2: 1.

156.   Pilling, D., D. Roife, M. Wang, S. D. Ronkainen, J. R. Crawford, E. L. Travis, and R. H. Gomer. 2007. Reduction of bleomycin-induced pulmonary fibrosis by serum amyloid P. *J Immunol* 179: 4035-4044.

157.   Scheel-Toellner, D., K. Wang, N. V. Henriquez, P. R. Webb, R. Craddock, D. Pilling, A. N. Akbar, M. Salmon, and J. M. Lord. 2002. Cytokine-mediated inhibition of apoptosis in non-transformed T cells and neutrophils can be dissociated from protein kinase B activation. *Eur.J.Immunol.* 32: 486-493.

158.   Pilling, D., A. N. Akbar, J. Girdlestone, C. H. Orteu, N. J. Borthwick, N. Amft, D. Scheel-Toellner, C. D. Buckley, and M. Salmon. 1999. Interferon-β mediates

stromal cell rescue of T cells from apoptosis. *European Journal Of Immunology* 29: 1041-1050.

159.   Buckley, C. D., D. Pilling, N. V. Henriquez, G. Parsonage, K. Threlfall, D. Scheel-Toellner, D. L. Simmons, A. N. Akbar, J. M. Lord, and M. Salmon. 1999. RGD peptides induce apoptosis by direct caspase-3 activation. *Nature* 397: 534-539.

160.   Wang, Y., C. L. Chen, and M. Iijima. 2011. Signaling mechanisms for chemotaxis. *Dev Growth Differ* 53: 495-502.

161.   Wang, F. 2009. The signaling mechanisms underlying cell polarity and chemotaxis. *Cold Spring Harb Perspect Biol* 1: a002980.

162.   Aso, Y., N. Ozeki, T. Terasawa, R. Naruse, K. Hara, M. Suetsugu, K. Takebayashi, M. Shibazaki, K. Haruki, K. Morita, and T. Inukai. 2012. Serum level of soluble CD26/dipeptidyl peptidase-4 (DPP-4) predicts the response to sitagliptin, a DPP-4 inhibitor, in patients with type 2 diabetes controlled inadequately by metformin and/or sulfonylurea. *Transl Res* 159: 25-31.

163.   Cordero, O. J., D. Ayude, M. Nogueira, F. J. Rodriguez-Berrocal, and M. P. de la Cadena. 2000. Preoperative serum CD26 levels: diagnostic efficiency and predictive value for colorectal cancer. *Br J Cancer* 83: 1139-1146.

164.   Zigmond, S. H. 1977. Ability of polymorphonuclear leukocytes to orient in gradients of chemotactic factors. *J Cell Biol* 75: 606-616.

165.   Liu, X., B. Ma, A. B. Malik, H. Tang, T. Yang, B. Sun, G. Wang, R. D. Minshall, Y. Li, Y. Zhao, R. D. Ye, and J. Xu. 2012. Bidirectional regulation of

neutrophil migration by mitogen-activated protein kinases. *Nat Immunol* 13: 457-464.

166.   Lambeir, A. M., P. Proost, C. Durinx, G. Bal, K. Senten, K. Augustyns, S. Scharpe, J. Van Damme, and I. De Meester. 2001. Kinetic investigation of chemokine truncation by CD26/dipeptidyl peptidase IV reveals a striking selectivity within the chemokine family. *J Biol Chem* 276: 29839-29845.

167.   Proost, P., P. Menten, S. Struyf, E. Schutyser, I. De Meester, and J. Van Damme. 2000. Cleavage by CD26/dipeptidyl peptidase IV converts the chemokine LD78beta into a most efficient monocyte attractant and CCR1 agonist. *Blood* 96: 1674-1680.

168.   Wright, S. W., M. J. Ammirati, K. M. Andrews, A. M. Brodeur, D. E. Danley, S. D. Doran, J. S. Lillquist, L. D. McClure, R. K. McPherson, S. J. Orena, J. C. Parker, J. Polivkova, X. Qiu, W. C. Soeller, C. B. Soglia, J. L. Treadway, M. A. VanVolkenburg, H. Wang, D. C. Wilder, and T. V. Olson. 2006. cis-2,5-dicyanopyrrolidine inhibitors of dipeptidyl peptidase IV: synthesis and in vitro, in vivo, and X-ray crystallographic characterization. *J Med Chem* 49: 3068-3076.

169.   Rahfeld, J., M. Schierhorn, B. Hartrodt, K. Neubert, and J. Heins. 1991. Are diprotin A (Ile-Pro-Ile) and diprotin B (Val-Pro-Leu) inhibitors or substrates of dipeptidyl peptidase IV? *Biochim Biophys Acta* 1076: 314-316.

170.   Moore, B. B., and C. M. Hogaboam. 2008. Murine models of pulmonary fibrosis. *Am J Physiol Lung Cell Mol Physiol* 294: L152-160.

171. Lazo, J. S., and E. T. Pham. 1984. Pulmonary fate of [3H]bleomycin A2 in mice. *J Pharmacol Exp Ther* 228: 13-18.

172. Giri, S. N. 1986. Pharmacokinetics, subcellular distribution, and covalent binding of [3H]bleomycin in hamsters after intratracheal administration. *Exp Mol Pathol* 45: 207-220.

173. Kieffer, T. J., C. H. McIntosh, and R. A. Pederson. 1995. Degradation of glucose-dependent insulinotropic polypeptide and truncated glucagon-like peptide 1 in vitro and in vivo by dipeptidyl peptidase IV. *Endocrinology* 136: 3585-3596.

174. Reimer, M. K., J. J. Holst, and B. Ahren. 2002. Long-term inhibition of dipeptidyl peptidase IV improves glucose tolerance and preserves islet function in mice. *Eur J Endocrinol* 146: 717-727.

175. Buckley, C. D., D. Pilling, J. M. Lord, A. N. Akbar, D. Scheel-Toellner, and M. Salmon. 2001. Fibroblasts regulate the switch from acute resolving to chronic persistent inflammation. *Trends Immunol.* 22: 199-204.

176. Goto, H., J. G. Ledford, S. Mukherjee, P. W. Noble, K. L. Williams, and J. R. Wright. 2010. The role of surfactant protein A in bleomycin-induced acute lung injury. *Am J Respir Crit Care Med* 181: 1336-1344.

177. Li, Z., X. Dong, Z. Wang, W. Liu, N. Deng, Y. Ding, L. Tang, T. Hla, R. Zeng, L. Li, and D. Wu. 2005. Regulation of PTEN by Rho small GTPases. *Nat Cell Biol* 7: 399-404.

178. Skoge, M., M. Adler, A. Groisman, H. Levine, W. F. Loomis, and W. J. Rappel. 2010. Gradient sensing in defined chemotactic fields. *Integr Biol (Camb)* 2: 659-668.

179. Hiramatsu, H., A. Yamamoto, K. Kyono, Y. Higashiyama, C. Fukushima, H. Shima, S. Sugiyama, K. Inaka, and R. Shimizu. 2004. The crystal structure of human dipeptidyl peptidase IV (DPPIV) complex with diprotin A. *Biol Chem* 385: 561-564.

180. Bermpohl, F., K. Loster, W. Reutter, and O. Baum. 1998. Rat dipeptidyl peptidase IV (DPP IV) exhibits endopeptidase activity with specificity for denatured fibrillar collagens. *FEBS Lett* 428: 152-156.

181. Tomazella, G. G., I. da Silva, H. J. Laure, J. C. Rosa, R. Chammas, H. G. Wiker, G. A. de Souza, and L. J. Greene. 2009. Proteomic analysis of total cellular proteins of human neutrophils. *Proteome Sci* 7: 32.

182. Lominadze, G., D. W. Powell, G. C. Luerman, A. J. Link, R. A. Ward, and K. R. McLeish. 2005. Proteomic analysis of human neutrophil granules. *Mol Cell Proteomics* 4: 1503-1521.

183. de Souza Castro, M., N. M. de Sa, R. P. Gadelha, M. V. de Sousa, C. A. Ricart, B. Fontes, and W. Fontes. 2006. Proteome analysis of resting human neutrophils. *Protein Pept Lett* 13: 481-487.

184. Jethwaney, D., M. R. Islam, K. G. Leidal, D. B. de Bernabe, K. P. Campbell, W. M. Nauseef, and B. W. Gibson. 2007. Proteomic analysis of plasma membrane and secretory vesicles from human neutrophils. *Proteome Sci* 5: 12.

185.   Uriarte, S. M., D. W. Powell, G. C. Luerman, M. L. Merchant, T. D. Cummins, N. R. Jog, R. A. Ward, and K. R. McLeish. 2008. Comparison of proteins expressed on secretory vesicle membranes and plasma membranes of human neutrophils. *J Immunol* 180: 5575-5581.

186.   Barbul, A., R. J. Breslin, J. P. Woodyard, H. L. Wasserkrug, and G. Efron. 1989. The effect of in vivo T helper and T suppressor lymphocyte depletion on wound healing. *Ann Surg* 209: 479-483.

187.   Herlihy, S. E., D. Pilling, A. S. Maharjan, and R. H. Gomer. 2013. Dipeptidyl peptidase IV is a human and murine neutrophil chemorepellent. *J Immunol* 190: 6468-6477.

188.   Kolaczkowska, E., and P. Kubes. 2013. Neutrophil recruitment and function in health and inflammation. *Nat Rev Immunol* 13: 159-175.

189.   Holm, L., and C. Sander. 1996. Mapping the protein universe. *Science* 273: 595-603.

190.   Chandra, N. R., M. M. Prabu, K. Suguna, and M. Vijayan. 2001. Structural similarity and functional diversity in proteins containing the legume lectin fold. *Protein Engineering* 14: 857-866.

191.   Basha, E., H. O'Neill, and E. Vierling. 2012. Small heat shock proteins and alpha-crystallins: dynamic proteins with flexible functions. *Trends Biochem Sci* 37: 106-117.

192.   Brock, D. A., and R. H. Gomer. 1999. A cell-counting factor regulating structure size in *Dictyostelium*. *Genes & Development* 13: 1960-1969.

193. Malumbres, M., and M. Barbacid. 2007. Cell cycle kinases in cancer. *Curr Opin Genet Dev* 17: 60-65.

194. Dhanasekaran, N., and M. V. Prasad. 1998. G protein subunits and cell proliferation. *Biol Signals Recept* 7: 109-117.

195. Strader, C. D., T. M. Fong, M. R. Tota, D. Underwood, and R. A. Dixon. 1994. Structure and function of G protein-coupled receptors. *Annual Review of Biochemistry* 63: 101-132.

196. Gilman, A. G. 1987. G proteins: transducers of receptor-generated signals. *Annu Rev Biochem* 56: 615-649.

197. Rozengurt, E. 2007. Mitogenic signaling pathways induced by G protein-coupled receptors. *Journal of Cellular Physiology* 213: 589-602.

198. Wu, Y., and C. Janetopoulos. 2013. The G alpha subunit Galpha8 inhibits proliferation, promotes adhesion and regulates cell differentiation. *Developmental Biology* 380: 58-72.

199. Kumagai, A., M. Pupillo, R. Gundersen, R. Miake-Lye, P. N. Devreotes, and R. A. Firtel. 1989. Regulation and function of G alpha protein subunits in *Dictyostelium*. *Cell* 57: 265-275.

200. Parikh, A., E. R. Miranda, M. Katoh-Kurasawa, D. Fuller, G. Rot, L. Zagar, T. Curk, R. Sucgang, R. Chen, B. Zupan, W. F. Loomis, A. Kuspa, and G. Shaulsky. 2010. Conserved developmental transcriptomes in evolutionarily divergent species. *Genome Biol* 11: R35.

201.   Wu, L., C. Gaskins, K. Zhou, R. A. Firtel, and P. N. Devreotes. 1994. Cloning and targeted mutations of G alpha 7 and G alpha 8, two developmentally regulated G protein alpha-subunit genes in *Dictyostelium*. *Molecular Biology of the Cell* 5: 691-702.

202.   Brzostowski, J. A., C. Johnson, and A. R. Kimmel. 2002. Galpha-mediated inhibition of developmental signal response. *Current Biology : CB* 12: 1199-1208.

203.   Brzostowski, J. A., C. A. Parent, and A. R. Kimmel. 2004. A G alpha-dependent pathway that antagonizes multiple chemoattractant responses that regulate directional cell movement. *Genes & Development* 18: 805-815.

204.   Anjard, C., Y. Su, and W. F. Loomis. 2009. Steroids initiate a signaling cascade that triggers rapid sporulation in *Dictyostelium*. *Development* 136: 803-812.

205.   Kuwayama, H., Y. Miyanaga, H. Urushihara, and M. Ueda. 2013. A RabGAP regulates life-cycle duration via trimeric G-protein cascades in *Dictyostelium discoideum*. *PLoS One* 8: e81811.

206.   O'Hayre, M., M. S. Degese, and J. S. Gutkind. 2014. Novel insights into G protein and G protein-coupled receptor signaling in cancer. *Curr Opin Cell Biol* 27C: 126-135.

207.   Heptinstall, R. H. 1968. Pathology of end-stage kidney disease. *Am J Med* 44: 656-663.

208.   Krediet, R. T., and D. G. Struijk. 2013. Peritoneal changes in patients on long-term peritoneal dialysis. *Nat Rev Nephrol* 9: 419-429.

209. Bargman, J. M. 2012. Advances in peritoneal dialysis: a review. *Semin Dial* 25: 545-549.

210. Chan, T. M., and S. Yung. 2007. Studying the effects of new peritoneal dialysis solutions on the peritoneum. *Perit Dial Int* 27 Suppl 2: S87-93.

211. de Lima, S. M., A. Otoni, P. Sabino Ade, L. M. Dusse, K. B. Gomes, S. W. Pinto, M. A. Marinho, and D. R. Rios. 2013. Inflammation, neoangiogenesis and fibrosis in peritoneal dialysis. *Clin Chim Acta* 421: 46-50.

212. Schilte, M. N., J. W. Celie, P. M. Wee, R. H. Beelen, and J. van den Born. 2009. Factors contributing to peritoneal tissue remodeling in peritoneal dialysis. *Peritoneal Dialysis International : Journal of the International Society for Peritoneal Dialysis* 29: 605-617.

213. Tomino, Y. 2012. Mechanisms and interventions in peritoneal fibrosis. *Clin Exp Nephrol* 16: 109-114.

214. Fielding, C. A., and N. Topley. 2008. Piece by piece: solving the puzzle of peritoneal fibrosis. *Peritoneal Dialysis International : Journal of the International Society for Peritoneal Dialysis* 28: 477-479.

215. Abe, R., S. C. Donnelly, T. Peng, R. Bucala, and C. N. Metz. 2001. Peripheral blood fibrocytes: differentiation pathway and migration to wound sites. *Journal of Immunology* 166: 7556-7562.

216. Pilling, D., C. D. Buckley, M. Salmon, and R. H. Gomer. 2003. Inhibition of fibrocyte differentiation by serum amyloid P. *Journal of Immunology* 171: 5537-5546.

217.   Reilkoff, R. A., R. Bucala, and E. L. Herzog. 2011. Fibrocytes: emerging effector cells in chronic inflammation. *Nat Rev Immunol* 11: 427-435.

218.   Pilling, D., T. Fan, D. Huang, B. Kaul, and R. H. Gomer. 2009. Identification of markers that distinguish monocyte-derived fibrocytes from monocytes, macrophages, and fibroblasts. *PLoS One* 4: e7475.

219.   Bucala, R., L. A. Spiegel, J. Chesney, M. Hogan, and A. Cerami. 1994. Circulating fibrocytes define a new leukocyte subpopulation that mediates tissue repair. *Molecular Medicine* 1: 71-81.

220.   Chesney, J., C. Metz, A. B. Stavitsky, M. Bacher, and R. Bucala. 1998. Regulated production of type I collagen and inflammatory cytokines by peripheral blood fibrocytes. *Journal of Immunology* 160: 419-425.

221.   Iwano, M., D. Plieth, T. M. Danoff, C. Xue, H. Okada, and E. G. Neilson. 2002. Evidence that fibroblasts derive from epithelium during tissue fibrosis. *The Journal of Clinical Investigation* 110: 341-350.

222.   Okada, H., T. Inoue, Y. Kanno, T. Kobayashi, Y. Watanabe, S. Ban, E. G. Neilson, and H. Suzuki. 2003. Selective depletion of fibroblasts preserves morphology and the functional integrity of peritoneum in transgenic mice with peritoneal fibrosing syndrome. *Kidney International* 64: 1722-1732.

223.   Jimenez-Heffernan, J. A., A. Aguilera, L. S. Aroeira, E. Lara-Pezzi, M. A. Bajo, G. del Peso, M. Ramirez, C. Gamallo, J. A. Sanchez-Tomero, V. Alvarez, M. Lopez-Cabrera, and R. Selgas. 2004. Immunohistochemical characterization of

fibroblast subpopulations in normal peritoneal tissue and in peritoneal dialysis-induced fibrosis. *Virchows Arch* 444: 247-256.

224.	Aroeira, L. S., A. Aguilera, J. A. Sanchez-Tomero, M. A. Bajo, G. del Peso, J. A. Jimenez-Heffernan, R. Selgas, and M. Lopez-Cabrera. 2007. Epithelial to mesenchymal transition and peritoneal membrane failure in peritoneal dialysis patients: pathologic significance and potential therapeutic interventions. *Journal of the American Society of Nephrology : JASN* 18: 2004-2013.

225.	McAnulty, R. J. 2007. Fibroblasts and myofibroblasts: their source, function and role in disease. *The International Journal of Biochemistry & Cell Biology* 39: 666-671.

226.	Cox, N., D. Pilling, and R. H. Gomer. 2012. NaCl potentiates human fibrocyte differentiation. *PLoS One* 7: e45674.

227.	Pilling, D., V. Vakil, and R. H. Gomer. 2009. Improved serum-free culture conditions for the differentiation of human and murine fibrocytes. *Journal of Immunological Methods* 351: 62-70.

228.	White, M. J., M. Glenn, and R. H. Gomer. 2013. Trypsin potentiates human fibrocyte differentiation. *PLoS One* 8: e70795.

229.	Carpenter, A. E., T. R. Jones, M. R. Lamprecht, C. Clarke, I. H. Kang, O. Friman, D. A. Guertin, J. H. Chang, R. A. Lindquist, J. Moffat, P. Golland, and D. M. Sabatini. 2006. CellProfiler: image analysis software for identifying and quantifying cell phenotypes. *Genome Biol* 7: R100.

230. Crawford, J. R., D. Pilling, and R. H. Gomer. 2010. Improved serum-free culture conditions for spleen-derived murine fibrocytes. *J Immunol Methods* 363: 9-20.

231. Haudek, S. B., Y. Xia, P. Huebener, J. M. Lee, S. Carlson, J. R. Crawford, D. Pilling, R. H. Gomer, J. Trial, N. G. Frangogiannis, and M. L. Entman. 2006. Bone marrow-derived fibroblast precursors mediate ischemic cardiomyopathy in mice. *Proc. Natl. Acad. Sci. USA* 103: 18284-18289.

232. Sakai, N., T. Wada, H. Yokoyama, M. Lipp, S. Ueha, K. Matsushima, and S. Kaneko. 2006. Secondary lymphoid tissue chemokine (SLC/CCL21)/CCR7 signaling regulates fibrocytes in renal fibrosis. *Proc. Natl. Acad. Sci. USA* 103: 14098-14103.

233. Wynn, T. A. 2004. Fibrotic disease and the T(H)1/T(H)2 paradigm. *Nat Rev Immunol* 4: 583-594.

234. Shao, D. D., R. Suresh, V. Vakil, R. H. Gomer, and D. Pilling. 2008. Pivotal advance: Th-1 cytokines inhibit, and Th-2 cytokines promote fibrocyte differentiation. *Journal of Leukocyte Biology* 83: 1323-1333.

235. Rippe, B., D. Venturoli, O. Simonsen, and J. de Arteaga. 2004. Fluid and electrolyte transport across the peritoneal membrane during CAPD according to the three-pore model. *Peritoneal Dialysis International : Journal of the International Society for Peritoneal Dialysis* 24: 10-27.

236. Crawford, J. R., D. Pilling, and R. H. Gomer. 2012. FcgammaRI mediates Serum Amyloid P inhibition of fibrocyte differentiation. *Journal of Leukocyte Biology* 92: 699-711.

237.   Dick, F. A., and S. M. Rubin. 2013. Molecular mechanisms underlying RB
       protein function. *Nature Reviews. Molecular Cell Biology* 14: 297-306.

238.   Henley, S. A., and F. A. Dick. 2012. The retinoblastoma family of proteins and
       their regulatory functions in the mammalian cell division cycle. *Cell Div* 7: 10.

239.   Moll, A. C., S. M. Imhof, A. Y. Schouten-Van Meeteren, D. J. Kuik, P. Hofman,
       and M. Boers. 2001. Second primary tumors in hereditary retinoblastoma: a
       register-based study, 1945-1997: is there an age effect on radiation-related risk?
       Ophthalmology 108: 1109-1114.

240.   Strasser, K., G. Bloomfield, A. MacWilliams, A. Ceccarelli, H. MacWilliams,
       and A. Tsang. 2012. A retinoblastoma orthologue is a major regulator of S-phase,
       mitotic, and developmental gene expression in *Dictyostelium*. *PLoS One* 7:
       e39914.

241.   Ohnuma, K., H. Inoue, M. Uchiyama, T. Yamochi, O. Hosono, N. H. Dang, and
       C. Morimoto. 2006. T-cell activation via CD26 and caveolin-1 in rheumatoid
       synovium. *Mod Rheumatol* 16: 3-13.

APPENDIX A

STRUCTURAL SIMILARITIES BETWEEN THE *DICTYOSTELIUM* PROTEIN APRA AND THE HUMAN PROTEIN DIPEPTIDYL-PEPTIDASE IV INFER FUNCTIONAL SIMILARITIES

Summary

While sequence similarity often signifies similar function, proteins with structural similarities may also indicate convergent function. We were working with the *Dictyostelium* secreted protein, AprA, which had no sequence similarity to any human proteins. We found that a predicted structure of AprA had structural similarity to the human protein dipeptidyl peptidase IV (DPPIV). Additionally, we found that both AprA and DPPIV were able to function as chemorepellents of cells. This led us to investigate the idea that structural similarities, like sequence similarities, could equate to functional similarities. The work in this appendix takes the functional attributes of one protein and examines if the protein structure similarity allows for similar functional properties in the other. For example, can the ability of AprA to inhibit the proliferation of cells translate into DPPIV being able to inhibit the proliferation of cells? We found that AprA and DPPIV share many of the same functional properties.

Introduction

AprA is a secreted *Dictyostelium* protein that both inhibits the proliferation and causes chemorepulsion of *Dictyostelium* cells (39, 48). AprA functions in conjunction with another secreted protein called CfaD, which also inhibits the proliferation of *Dictyostelium* cells (40). Loss of the AprA or CfaD proteins results in cells that proliferate faster and reach a higher density than wild type cells (39, 40). The addition of recombinant AprA (rAprA) or CfaD (rCfaD) to wild type cells causes a significant reduction in cell proliferation (40, 41). rAprA reduces the proliferation of *aprA¯* cells, but not *cfaD¯* cells (41). Likewise, rCfaD can inhibit the proliferation of *cfaD¯* cells, but not *aprA¯* cells indicating the two proteins are necessary for each other's function (40). In addition to its ability to inhibit *Dictyostelium* cell proliferation, AprA chemorepulses *Dictyostelium* cells (48). Cells at the edge of wild type colonies move away from the dense colony center while cells at the edge of an *aprA¯* colony form a tight edge with little movement outward (46). Additionally, both wild type and *aprA¯* cells move away from a source of rAprA (48).

DPPIV is a 110 kDa protein that can be found in a transmembrane or soluble form (145). The membrane form is found on some lymphocytes and epithelial cells and has a number of binding partners including adenosine deaminase, fibronectin, and collagen (75, 76, 86, 87). Additionally, the cytoplasmic portion of the membrane form can bind CD45 (87). The heavily glycosylated form is found in most bodily fluids (75, 76). Both the membrane and soluble forms have serine protease activity. They cleave proteins or peptides with a proline or alanine at the second position of the N-terminus

(145). One of the major functions of DPPIV is the cleavage of glucagon-like peptide-1 (GLP-1), which normally increases the secretion of insulin to promote glucose uptake (83). DPPIV cleavage of GLP-1 inhibits this process. Inhibitors of DPPIV are used as treatment for type 2 diabetes (83).

Protein structure prediction can reveal protein function that was not obvious from sequence analysis. Structure prediction can be extremely accurate (139-144). Structure based classification can help identify related proteins that have low sequence similarities (189, 190). Lectins, which bind carbohydrates, contain a characteristic structural fold (190). Although the fold is present in many different protein families with proteins that bind carbohydrates, there is little or no sequence similarity within the fold (190). Heat shock proteins and α-crystallins share a common structure of anti-parallel β-strands where distinct sequence similarity is not present (191). These studies are evidence that structural and functional properties may be comparable even when sequence similarities are lacking.

The AprA protein has no amino acid sequence similarity to human proteins. Previously we found that the predicted structure of AprA has structural similarity to the crystal structure of DPPIV (187). AprA chemorepulses *Dictyostelium* cells, and as *Dictyostelium* cells paved the way for neutrophil chemotaxis, we found that DPPIV can chemorepulse human and mouse neutrophils (48, 187). In this report, we sought to identify other functional similarities between AprA and DPPIV. We show that besides their ability to chemorepulse cells, AprA and DPPIV have a number of functional

similarities. This suggests that protein structure similarity may be a good predictor of protein function where sequence similarities are absent.

Methods

Wild-type, *aprA⁻*, and *cfaD⁻* cells were grown as previously described (192). Proliferation inhibition and chemorepulsion assays were done as previously described (132). rDPPIV (Enzo) was used at 300 ng/ml or at various concentrations in proliferation inhibition assays. An equivalent volume of buffer (10 mM Tris, 100 mM NaCl) was used as a control. For rAprA binding, 10% serum or 100 μg/ml of collagen I, Collagen IV, plasma fibronectin, cellular fibronectin, fibronectin 110, fibronectin 45, or adenosine demainase was added to appropriate wells and incubated overnight at 4°C. Wells were washed with PBST and blocked with 4% BSA/PBS. Positive wells were labeled with 10 μg/ml rAprA. rAprA was detected with rabbit anti-AprA antibodies (Bethyl Laboratories) and read with Synergy Mx (BioTek). Conditioned media from log phase cells was collected as previously described (132). DPPIV-like enzymatic activity of conditioned media was measured using various concentrations of pNA substrate (H-Gly-Pro-pNA · p-tosylate) for 60 minutes at room temperature and read at 410nm. Prism (Graphpad Software) was used to perform all statistical analyses.

Results

*Like AprA, DPPIV can inhibit the proliferation of Dictyostelium cells*

rAprA inhibits the proliferation of wild type *Dictyostelium* cells (41). To determine if rDPPIV functions similarly to rAprA and inhibits the proliferation of *Dictyostelium* cells, 300 ng/ml rDPPIV was added to wild type cells. rDPPIV inhibits the proliferation of wild type cells (Figure 15A). Various concentrations of rDPPIV were added to wild type cells and rDPPIV was able to inhibit cellular proliferation of wild type cells within a certain concentration range (Figure 15B). rDPPIV was unable to inhibit the proliferation of *Dictyostelium* cells at 0.3 ng/ml as indicated by a statistical difference compared to rAprA inhibition from Figure 15A (Figure 15B). To determine if rDPPIV could function to inhibit proliferation in the absence of endogenous AprA or its counterpart CfaD, rDPPIV was added to AprA or CfaD mutant cells. rDPPIV was able to inhibit the proliferation of *aprA⁻* and *cfaD⁻* cells in the absence of these endogenous proteins (Figure 16). Together, these data indicate that DPPIV can function similarly to AprA by inhibiting the proliferation of *Dictyostelium* cells. Moreover, DPPIV does not require the endogenous AprA or CfaD proteins to exert its effect.
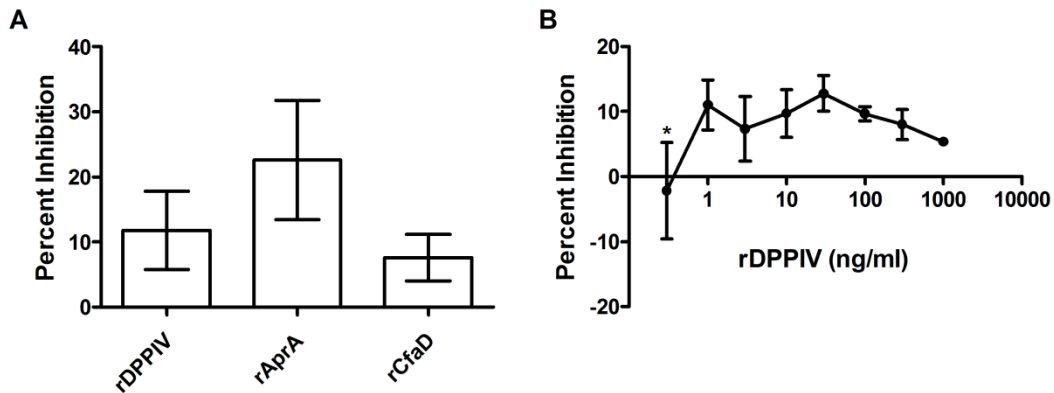
Figure 15: rDPPIV inhibits proliferation of wild-type *Dictyostelium* cells. A) rDPPIV, rAprA, or rCfaD was added to wild-type cells at 300ng/ml. **B)** Various concentrations of rDPPIV were added to wild-type cells and proliferation counted after 16 hours. The percent of proliferation inhibition compared to control cell density is shown. Values are mean ± SEM. * indicates $p < 0.05$ from rAprA percent inhibition from **(A)**.

Like DPPIV, rAprA can bind fibronectin

DPPIV is known to have a number of binding partners including fibronectin, adenosine deaminase, and collagen (86). Fibronectin, collagen, adenosine deaminase, or 10% serum were coated on a plate and the ability of rAprA to bind them was accessed. rAprA was able to bind both cellular and plasma fibronectin but not the 110 kDa or 45 kDa fragments of fibronectin (Figure 17). Additionally, rAprA appears to weakly bind collagen although binding is not statistically different from BSA control (Figure 17). This indicates that like DPPIV, AprA can bind fibronectin, but not any of the other DPPIV-binding partners.
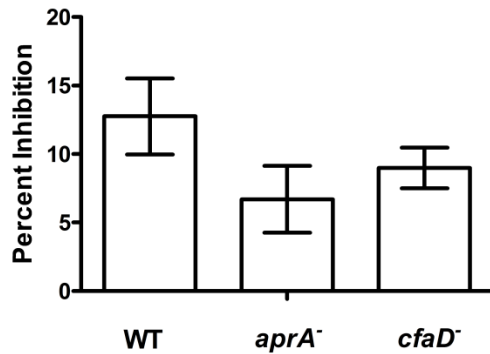
Figure 16: rDPPIV inhibits proliferation of *aprA⁻* and *cfaD⁻* *Dictyostelium* cells.
rDPPIV was added to cells at 300ng/ml and proliferation counted after 16 hours. The percent of
proliferation inhibition compared to control cells is shown. Values are mean ± SEM, n=3.
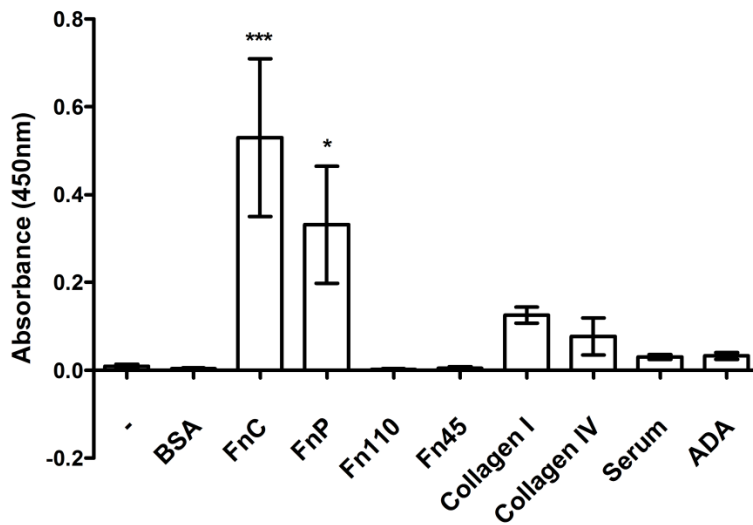

**Figure 17: rAprA binds fibronectin, but not collagen, serum proteins, or adenosine
deaminase.** Plates were coated with bovine serum albumin (BSA), cellular fibronectin (FnC),
plasma fibronectin (FnP), the 110 –kDa fibronectin fragment (Fn110), the 45-kDa fibronectin
fragment (Fn45), collagen I, collagen IV, 10% serum, or adenosine deaminase and anti-AprA
was used to determine if rAprA bound the substances. Values are mean ± SEM, n=3. **, $p <
0.01$; ***, $p < 0.001$ (one-way ANOVA).

*Dictyostelium conditioned media has DPPIV-like enzymatic activity*

DPPIV has serine protease activity, cleaving peptides or proteins with a proline or alanine in the second position at the N-terminus (77, 167). Conditioned media was collected from log-phase wild type or *aprA*⁻ cells and tested for its ability to cleave the substrate H-Gly-Pro-pNA p-tosylate. Wild type conditioned media had statistically significantly more DPPIV-like enzymatic activity than conditioned media from cells lacking AprA (Figure 18). This suggests that AprA in the conditioned media may be responsible for the DPPIV-like activity.
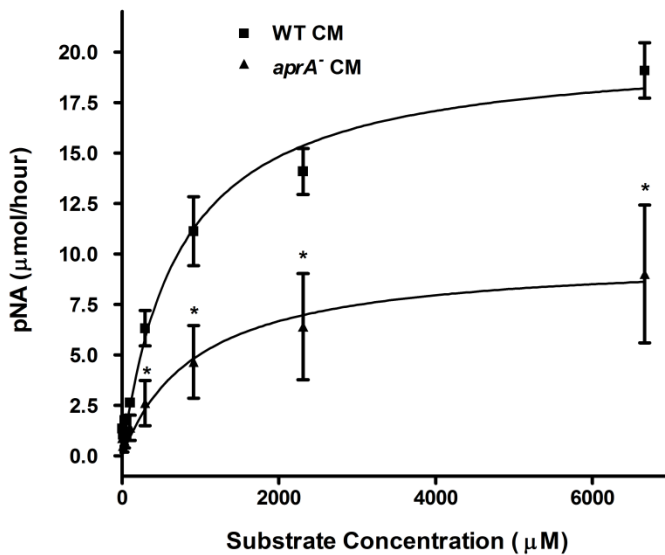
Figure 18: *Dictyostelium* **conditioned media (CM) lacking AprA has reduced DPPIV-like enzyme activity.** Wild-type or *aprA*⁻ CM was incubated with various concentrations of H-Gly-Pro-pNA p-tosylate. Values are mean ± SEM, n=3. * indicates $p < 0.05$.

Like AprA, rDPPIV can chemorepulse Dictyostelium cells

In addition to its ability to inhibit proliferation, AprA causes chemorepulsion of *Dictyostelium* cells (48). Buffer solutions of recombinant AprA, recombinant DPPIV, or buffer alone were analyzed for their ability to cause chemorepulsion of wild type cells. DPPIV can also chemorepulse *Dictyostelium* cells with a similar strength to AprA (Figure 19). These data indicate that AprA and DPPIV both possess the ability to chemorepulse *Dictyostelium* cells.
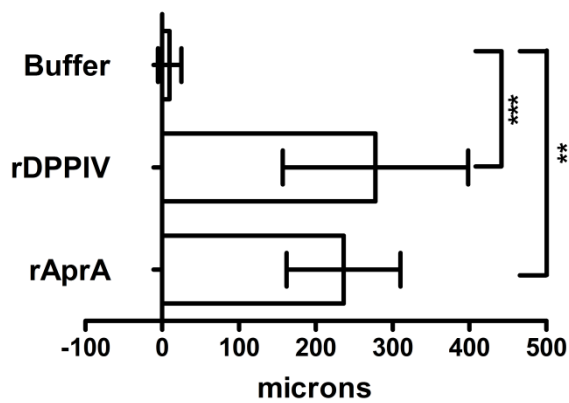
Figure 19: rDPPIV induces chemorepulsion of *Dictyostelium* cells. 2000 ng/ml of rDPPIV or rAprA was added to one side of an Insall chamber. Movement of cells was observed by videomicroscopy and displacement on the x-axis was plotted in microns. Values are mean ± SEM, n=3. ** and *** indicate statistical significance from buffer with p <0.01 and p < 0.001, respectively.

Discussion

A number of recent studies suggest that using protein structure to predict or identify protein function is accurate and may be better than using protein sequences (139-144). The *Dictyostelium* protein AprA and the human protein DPPIV share structural similarity, but lack much sequence similarity. Here we show that AprA and DPPIV also have functional similarity. Like AprA, DPPIV is able to inhibit the proliferation and chemorepulse *Dictyostelium* cells. Like DPPIV, AprA can bind fibronectin and weakly to collagen. Additionally, AprA may be responsible for DPPIV-like enzymatic activity in *Dictyostelium* conditioned media. It is clear from this work that structural similarity can be used to determine functional similarities in cases where sequence similarity is lacking. Although AprA and DPPIV do not share sequence similarity, they display a number of functional similarities and DPPIV can even substitute for AprA on *Dictyostelium* cells. Future work will determine if AprA can substitute for DPPIV in the chemorepulsion of human neutrophils.

APPENDIX B

THE *DICTYOSTELIUM* CHALONE CFAD REQUIRES G PROTEINS TO
INHIBIT PROLIFERATION

Summary

The *Dictyostelium* chalone AprA signals through the G protein, Gα8. CfaD is a second *Dictyostelium* chalone. AprA and CfaD require each other to function, but may activate different signaling effectors. In this part of the dissertation, I sought to identify if CfaD also signals with a Gα protein.

A previous experiment by Deen Bakthavatsalam found that $ga1^-$, $ga8^-$, $ga9^-$, and $g\beta^-$ cells were insensitive to CfaD signals. This indicated that CfaD could signal using a G protein. Gα8 and Gα9 have been characterized in previous work by our lab. Therefore, this appendix focuses mainly on the properties of Gα1 and CfaD binding to *Dictyostelium* cells.

I found that $ga1^-$ cells proliferate faster than wild type cells and share some, but not all of the phenotypes of CfaD mutant cells. Additionally, $ga1^-$, $ga8^-$, $ga9^-$, and $g\beta^-$ all appear to be necessary for CfaD to bind to cells. CfaD may signal through Gα1, as binding of CfaD is reduced in $ga1^-$ cells. Together, these data indicate that Gα1 is a good candidate for a component of CfaD signaling.

Introduction

The ability to regulate tissue size is an essential process. Tissue size is maintained with tight control over cellular proliferation (110). Misregulation in proliferation is seen in diseases such as cancer (193). A lack of proliferation control in cancer leads to tumor growth, and often death (193). As evidenced from rapid metastatic proliferation following primary tumor removal, primary tumors secrete factors to inhibit cancer cell proliferation (23-28). Factors that inhibit cell proliferation are termed chalones (1, 2).

Two secreted *Dictyostelium* chalones have been identified (39, 40). As vegetative *Dictyostelium* populations become dense, these proteins, AprA and CfaD, are enriched in the extracellular space (39, 40). AprA and CfaD inhibit proliferation to maintain a specific sized population of cells. Cells lacking AprA or CfaD proliferate rapidly (39, 40). Rapid proliferation is rescued by restoring AprA and CfaD (39, 40). A basic leucine zipper transcription factor, a ROCO kinase, and a PTEN-like protein are known signaling components in AprA and CfaD proliferation inhibition pathway(s) (45, 46, 132). Additionally, the Gα protein, Gα8 and a tumor suppressor are necessary for AprA signaling (43, 47).

Gα proteins are part of heterotrimeric complex (194, 195). The G-protein complex is composed of Gα, Gβ, and Gγ (194, 195). Typically, G proteins are associated with G protein-coupled receptors (194, 195). In its resting state, Gα is associated with guanosine diphosphate (GDP) (194, 195). When the receptor is activated, the GDP on the Gα is exchanged for guanosine-5'-triphosphate (GTP) (194, 195). Activated Gα is

dissociated from Gβγ and both subunits can relay the signal to downstream effectors (194, 195). G protein signaling is involved in many signaling cascades including proliferation, survival, and chemotaxis (194, 196, 197).

Here we show that CfaD appears to use the Gα proteins Gα1, Gα8, and Gα9 and Gβ to signal *Dictyostelium* cells to stop proliferating. Additionally, *gα1¯* cells have proliferation faster than wild type cells and mediate some, but not all of CfaD-induced effects.

Methods

Wild type, *gα1¯*, *gα8¯*, *gα9¯*, and *gβ¯* cells were grown as previously described (40). Proliferation, spore viability, mass, protein, and nuclei were done as previously described (132). Colony expansion, binding assays, GTPγS was done as previously described (43, 46). Statistics were done using Prism Graphpad software.

Results

gα1¯ cells exhibit a fast proliferation phenotype

cfaD¯, *gα8¯*, *gα9¯*, and *gβ¯* cells have faster proliferation than wild type cells (40, 43). *gα1¯* cells have faster proliferation (Figure 20A and 20B). *gα1¯* cells have a significantly faster doubling time than wild type cells (Table 10). Full proliferation curves show that although *gα1¯* cells proliferate faster than wild type, they do not reach a higher maximum cell density (Table 10). *gα1¯* cells proliferate at a rate similar to wild type cells on bacterial lawns (Figure 20C) and colonies of *gα1¯* cells expand more

slowly on bacterial lawns than wild type colonies (Figure 20D). This suggests that like CfaD, Gα1 may help inhibit cell proliferation.
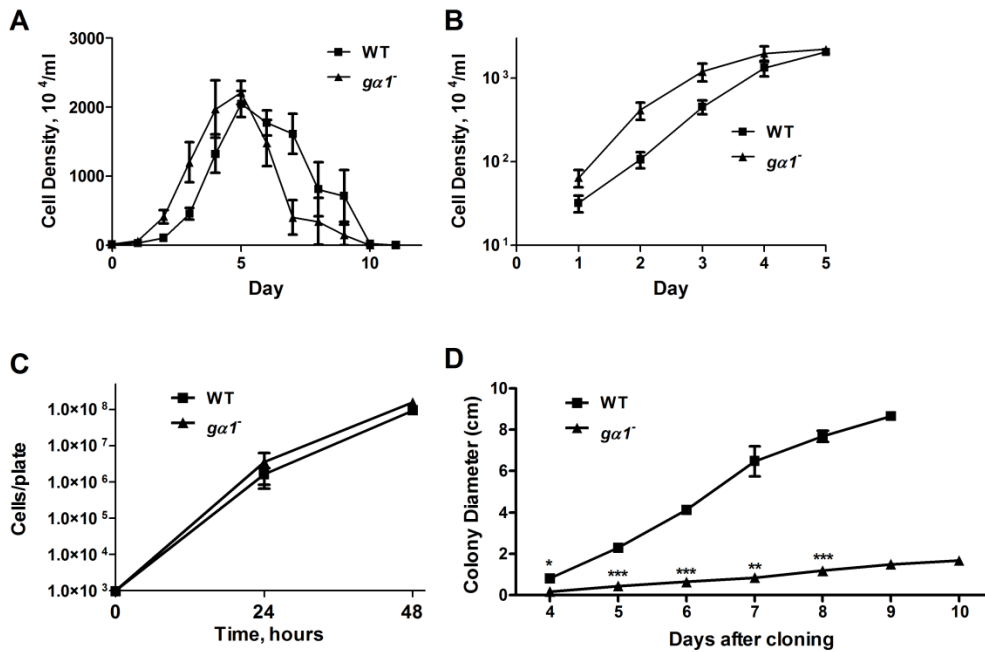
Figure 20: The effect of Gα1 on proliferation. Values are mean ± SEM, $n \geq 3$. Absence of error bars indicates error was smaller than the plot symbol. *, **, and *** indicate values with $p < 0.05$, $p < 0.01$, and $p < 0.001$, respectively. **(A)** Cells in shaking culture were started at 1×10^5 cells/ml and counted daily. **(B)** A Log plot of the first 5 days from A. **(C)** 1×10^3 cells were plated and counted daily, after 48 hours, WT cells cleared the plate. **(D)** Cells were plated at low density to form individual colonies. At least 3 colony diameters per plate were measured daily. After day 8, wild type colonies were indistinguishable from each other.

Table 10. The effect of Gα1 on doubling time and stationary density. Doubling times and maximum densities were calculated from the data in Figure 20. Values are mean ± SEM, n ≥ 3. Values are statistically different from wild type with p < 0.01 (t-test).

Cell Type	Doubling time, hours	Maximum observed cell density, 10^6 cells/ml
Wild-type	14.9 ± 1.0	24 ± 1
$g\alpha 1^-$	9.7 ± 1.3**	26 ± 2

$g\alpha 1^-$ cells are multinucleate

Cells lacking CfaD are multinucleate (40). Previous work has shown that overexpressing Gα1 leads to a multinucleate phenotype (198, 199). DAPI stained cells were counted for their number of nuclei to determine if $g\alpha 1^-$ cells are multinucleate. We found that $g\alpha 1^-$ have less with one nucleus and more cells with 3 or more nuclei (Table 11). Together, these data indicate that loss or gain of Gα1 causes disruption in normal nuclei phenotypes.

Table 11. The effect of Gα1 on nuclei per cell. DAPI stained cells were counted for the presence of 1, 2, or 3 or more nuclei. Values are mean ± SEM (n=4). * and ** indicate $p < 0.05$ and $p < 0.01$, respectively.

Percent of cells with n nuclei

Cell Type	1	2	3+
Wild-type	60 ± 3	36 ± 4	3 ± 2
gα1‾	48 ± 5*	37 ± 4	15 ±1**

Gα1 has no effect on cell growth

Proliferation, an increase in the number of cells, and growth, an increase in the mass of a cell, are processes that can be regulated together or independently of each other (43, 110). Gα1 regulates cell proliferation. To determine if Gα1 regulates growth, mass and protein content were measured. There was no difference in mass content compared to wild type cells (Table 12). *gα1*‾ cells had significantly more protein content than wild type cells (Table 12). However, when the protein content was corrected for the multinucleate phenotype of *gα1*‾ cells, there was no difference in protein content.

Doubling times were used to calculate the accumulation of mass, protein, and nuclei per hour. We would expect an increase in cell number would result in an increase of mass, protein, and nuclei. There were no differences in mass or protein accumulation between *gα1*‾ cells and wild type cells (Table 13). *gα1*‾ cells accumulated more nuclei

per hour than wild type cells (Table 13). Together, this data indicates that Gα1 does not control cell growth.

Table 12. The effect of Gα1 on the mass and protein content of cells. Mass and protein content was measured. Data from Table 11 was used to calculate the nuclei per 100 cells. Nuclei per 100 cells was used to calculate the mass and protein content per 10^7 nuclei. * and ** indicate values are statistically significant from wild type with $p < 0.05$ and $p < 0.01$, respectively. Values are mean ± SEM, $n \geq 3$.

Cell type	Per 10^7 cells			Per 10^7 nuclei	
	Mass (mg)	Protein (mg)	Nuclei/100 cells	Mass	Protein
Wild-type	12.0 ± 0.05	0.93 ± 0.17	145 ± 4	8.3 ± 0.4	0.71 ± 0.19
gα1⁻	12.1 ± 1.1	1.19 ± 0.08*	173 ± 4**	7.0 ± 0.6	0.69 ± 0.05

Table 13. The effect of Gα1 on mass and protein accumulation of cells. Doubling times from Table 10 were used to determine mass, protein, and nuclei accumulation per hour. Mean ± SEM, $n \geq 3$. Values are statistically significant from wild type at ** with $p < 0.01$ (t-test).

Cell type	Per 10^7 cells/hour			Per 10^7 nuclei/hour	
	Mass (µg)	Protein (µg)	Nuclei, x 10^{-5}	Mass (mg)	Protein (µg)
Wild-type	80 ± 12	78 ± 5	6.2 ± 0.2	63 ± 10	65 ± 4
gα1⁻	111 ± 16	109 ± 15	15.9 ± 2.0**	64 ± 10	63 ± 9

Gα1 is not important for spore development

The cost of lacking CfaD is a decrease in the viability of cells (40). *gα1¯* cells were examined for their ability to develop spores. *gα1¯* cells developed a similar number of spores to wild type cells (Table 14). Additionally, detergent treated spores from *gα1¯* cells were as viable as wild type spores (Table 14). This indicates that unlike *cfaD¯* cells, *gα1¯* cells do not have a defect in spore development or viability and that Gα1 does not play a role in spore sustainability.

Table 14. The effect of Gα1 on spore viability. Cells were developed and spores counted. Spores were treated with detergent, plated, and colony formation analyzed to determine viable spores. Values are mean ± SEM (n ≥ 3).

Cell Type	Viable spores after development as a percent of input cell number	Detergent resistant spores as a percent of total spores
Wild-type	100 ± 12	68 ± 4
gα1¯	71 ± 32	74 ± 5

Gα1 is important for CfaD binding to cells

Previous work found that rAprA had saturable binding to *Dictyostelium* cells (41, 43). rCfaD was incubated with wild type cells to determine if it also had saturatable

125

binding. We found that rCfaD has saturatable binding to wild type cells (Figure 21). *gα1*¯ cells were analyzed for their ability to bind rCfaD, as the cells are insensitive to rCfaD proliferation inhibition (data not shown). *gα1*¯ cells had similar binding of rCfaD compared to wild type cells with no difference in K_D or Bmax (Figure 21). Together, these data indicate that rCfaD can bind to *Dictyostelium* cells and that *gα1*¯ cells have similar binding properties to wild type cells.
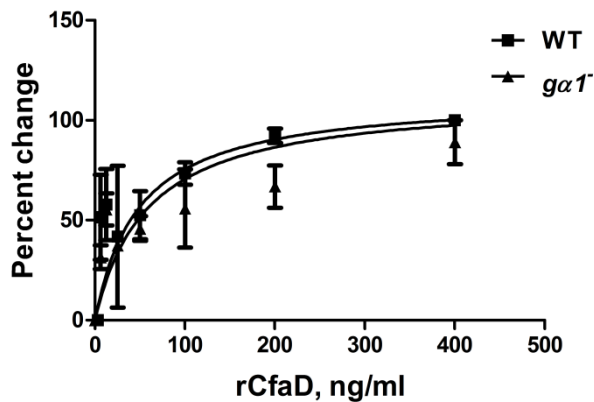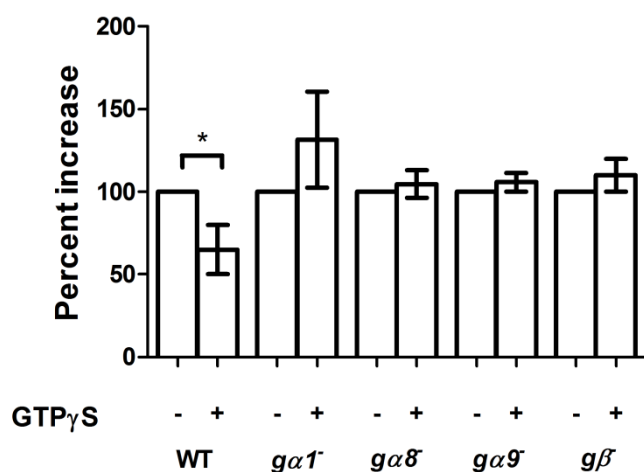

Figure 21: The effect of Gα1 on CfaD binding. Cells were incubated with various concentrations of rCfaD for 10 minutes, collected, and analyzed for bound rCfaD with anti-myc antibodies. Values are mean ± SEM. Curves are fit to one-site specific binding.

Gα1, Gα8, Gα9, and Gβ are required for GTPγS inhibition of CfaD binding

The addition of non-hydrolyzable GTPγS to membranes can affect ligand binding (196). When GTPγS is used Gα subunits remain bound to GTP in the active state (196). Wild type membranes were incubated with rCfaD in the presence or absence

of GTPγS. Wild type membranes bound rCfaD and binding was reduced by ~40% in the presence of GTPγS (Figure 22). The same assay was repeated with *gα1⁻*, *gα8⁻*, *gα9⁻*, and *gβ⁻* cells to determine which of these are necessary for CfaD signaling through G proteins. The addition of GTPγS had no effect on any of the mutant cell lines (Figure 22). Together, the data suggest that Gα1, Gα8, Gα9, and Gβ are required for CfaD signaling through G proteins.

Figure 22: The effect of GTPγS on CfaD binding. Cell membranes were incubated with rCfaD in the presence or absence of GTPγS. Values shown are percentage change compared to no added GTPγS. Values are mean ± SEM (n ≥ 3). * indicates $p < 0.05$ (t-test).

Discussion

Here, the chalone CfaD has been found to bind *Dictyostelium* cells to saturation. *gα1¯* cells have faster proliferation, but no role in the growth of cells. *gα1¯* cells are also multinucleate, have normal proliferation on bacterial lawns, slow colony expansion, and develop normal, viable spores. rCfaD sensitivity is lost in *gα1¯* cells, although *gα1¯* cells have normal cell binding of rCfaD. GTPγS reduces the binding of rCfaD to cell membranes, and this requires Gα1, Gα8, Gα9, and Gβ. Together, this indicates that CfaD uses G proteins to induce signaling and Gα1, Gα8, Gα9, and Gβ are necessary for this process.

Gα1 is expressed a low levels in vegetative *Dictyostelium* cells and increased throughout development (200). Overexpression of Gα1 in wild type cells results in a multinuclear phenotype and did not result in inhibition of proliferation (198). This is a phenotype we have seen with other AprA/CfaD signaling components (132). Gα1 mutants do not affect spore viability, unlike CfaD mutant cells. Gα1 is insensitive to rCfaD proliferation inhibition, but has normal rCfaD binding. GTPγS did not reduce the ability of rCfaD to bind cells in *gα1¯* cells. This suggests that Gα1 is involved in CfaD signaling as the reduction in GTPγS binding is lost with the loss of Ga1. Together, these data indicate that Gα1 in required for rCfaD signaling and mediates some, but not all of CfaD effects.

Gα8 is expressed throughout *Dictyostelium* cell vegetation and development (201). *gα8¯* cells have rapid proliferation and overexpression of Gα8 inhibits cell proliferation (43, 198). Gβ is essential for Gα8-induced proliferation inhibition (198).

Ga8 is required for AprA signaling (43). Gα8 mediates some, but not all of the phenotypes of AprA, many of which are shared by CfaD (43). This indicates that Gα8 also mediates some of the CfaD phenotypes. Gα8 appears to be required for CfaD signaling as reduction in GTPγS binding is lost in cells lacking Gα8. Together, this indicates that both AprA and CfaD signal through Gα8.

Gα9 is also expressed during *Dictyostelium* vegetation and development (202). Gα9 is known to inhibit chemotaxis and couple to the G protein-coupled receptor, GrlE (202-204). Conflicting evidence for the role of Gα9 has been presented. Gα9 is not involved in the proliferation inhibition of AprA (43). Gα9 has been suggested to be involved in regulation of proliferation through an interaction with Rgb-3, in which mutants display fast proliferation (205). Gα9 appears to be necessary for CfaD signaling. The requirement of AprA for CfaD signaling may explain the previous observation that Gα9 was not needed for AprA signaling, but insensitive to proliferation inhibition by AprA. Gα9's role in AprA signaling could be indirect through CfaD signaling. Together, these data indicate that Gα9 is required for CfaD-induced proliferation inhibition.

Gβ, which is expressed in vegetative and developing cells, is necessary for AprA signaling (43). We observed that Gβ is also necessary for CfaD signaling increasing the evidence that CfaD signals through G proteins.

Conclusions and future directions

We observed that CfaD requires three Gα proteins, Gα1, Gα8, and Gα9 and Gβ to induce proliferation inhibition in *Dictyostelium* cells. Combined with previous work,

this provides evidence for convergent and divergent signaling in the AprA and CfaD signaling pathways. Both AprA and CfaD require Gα8 and Gβ for signaling, while CfaD additionally needs Gα1 and Gα9. This strengthens the evidence for multiple branched pathways of AprA and CfaD signaling. Future work will look at additional properties of Gα1, examine the rescue of $g\alpha1^-$ cells, and determine the effect of CfaD binding on [H^{3+}] GTP recruitment to the membrane of *Dictyostelium* cells.

APPENDIX C

THE *DICTYOSTELIUM* CHALONES APRA AND CFAD USE G PROTEIN-COUPLED RECEPTORS TO SIGNAL PROLIFERATION INHIBITION

Summary

Previous work in our lab had found that AprA functions through the $G\alpha8$ protein. Work in the previous appendix suggests that CfaD also signals through a $G\alpha$ protein, $G\alpha1$. The receptor(s) for AprA and CfaD signaling are unknown. This previous data suggests that AprA and CfaD may signal using G protein-coupled receptors (GPCRs). Eight mutant GPCR strains were a gift from Dr. Janetopoulos. These eight GPCR mutants were analyzed to determine their role in AprA and/or CfaD signaling of proliferation inhibition and additionally their role in AprA chemorepulsion signaling. The work in this appendix focuses on identifying if any of the GPCR mutants are the receptor(s) for AprA and CfaD signaling. GrlB, GrlE, and GrlH are candidates for proliferation inhibition signaling while GrlB and GrlH are candidates for chemorepulsion signaling.

Two undergrads, Francisco Brito and Jose Ting, have helped with the analysis of these GPCR mutants.

Introduction

Chalones are secreted factors that inhibit the proliferation of the cells that secrete them (1, 2). Melanocyte proliferation can be inhibited by an unknown secreted factor (18, 19). When the chalone is injected under the skin of melanomas, the proliferation ceases (18, 19). Despite its action, the chalone and the signaling pathway used to inhibit proliferation remain a mystery. In fact, the identity of most predicted chalones and their signaling pathways are unknown.

We have previously identified two *Dictyostelium* chalones, AprA and CfaD. Both are secreted proteins that inhibit *Dictyostelium* cell proliferation (39, 40). Lacking AprA or CfaD results in faster proliferation, which returns to wild-type levels by either rescuing the mutant or the addition of recombinant proteins to the mutant strains (39-41). Both AprA and CfaD are necessary for proliferation inhibition as recombinant AprA (rAprA) cannot rescue the *cfaD*⁻ phenotype and recombinant CfaD (rCfaD) cannot rescue the *aprA*⁻ phenotype (41, 43). Several components of the AprA and/or CfaD signaling pathway have been identified including the transcription factor BzpN, the ROCO kinase QkgA, the PTEN-like protein CnrN, and the tumor suppressor RblA (45-47, 132). Additionally, AprA functions to chemorepulse *Dictyostelium* cells (48). Wild type cells move in a biased direction away from a source of AprA (48). AprA proliferation and chemorepulsion signaling require the Gα protein Gα8, suggesting that AprA functions through a G protein-coupled receptor (GPCR) (43, 48).

GPCRs are comprised of 7 transmembrane α-helicies that interact with heterotrimeric G proteins upon stimulation from a ligand (197). G proteins have three

subunits, Gα, Gβ, and Gγ that relay the initial signal to numerous downstream effectors (206). GPCR signaling is important for many cellular processes including proliferation and chemotaxis. When a signal activates a GPCR, the Gα subunit dissociates from the Gβγ subunit and each can initiate signaling cascades (206). Gβγ subunits are known to activate phosphatidylinositol 3-kinase (PI3K) (206). PI3K phosphorylation of the membrane lipid phosphatidylinositol 4,5-bisphosphate (PIP_2) to phosphatidylinositol 3,4,5-trisphosphate (PIP_3) recruits proteins such as Akt which regulates cell proliferation (113, 120, 122-124). Additionally, activation of PI3K, and subsequently PIP_3, leads to promotion of actin remodeling (38, 51, 58-60). Polarization of PIP_3 and actin remodeling at one end of the cell induces pseudopodia formation and chemotaxis (38, 58-60).

Here we have examined eight GPCR mutants in *Dictyostelium*. We have analyzed the mutants for sensitivity to AprA and CfaD. We have identified that GrlB, GrlE, and GrlH are candidates for proliferation inhibition signaling and GrlB and GrlH are candidates for chemorepulsion signaling.

Methods

$grlB^-$, $grlD^-$, $grlE^-$, $grlH^-$, $fslA^-$, $fslB^-$, $fslK^-$, and $fscE^-$ cells were a gift from Dr. Janetopelous. Wild-type and mutants were grown as previously described (192). Proliferation in shaking culture and on bacterial plates, proliferation inhibition, chemotaxis, nuclei, mass and protein, colony expansion, and spore viability were all done as previously described (46, 132). Colony edge assays were done as previously described except that 200 µl of HL5 media without bacteria was added to each well (46).

Quantification of movement at the colony edge was determined by measuring the distance traveled of 30 randomly chosen cells per strain. All statistics were done with significance determined as $p < 0.05$ using Prism Graphpad software (San Diego, CA).

Results

Several GPCR mutants exhibit fast proliferation phenotypes

AprA and Cfad mutant cells exhibit faster proliferation compared to wild type cells, resulting in a faster doubling time and a higher maximum density (39, 40). We examined GPCR mutants for a faster proliferation phenotype. Two mutants, $grlE^-$ and $grlH^-$, had a significantly faster doubling time when compared to wild type (Figure 23). Two mutants, $grlB^-$ and $fslA^-$, has slightly higher maximum densities compared to wild type, although these values were not significant (Table 15). One mutant, $grlD^-$, had a significantly lower maximum cell density compared to wild type cells. The remaining mutants were similar to wild type in both doubling time and maximum cell density. This suggests that some GPCR mutants exhibit the fast proliferation phenotype we would expect to see when a component of the AprA and/or CfaD pathways is eliminated or defective.
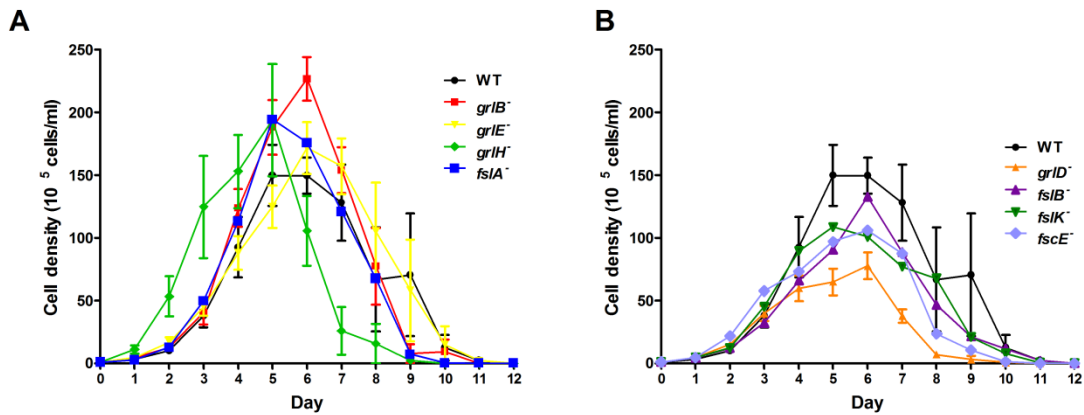
Figure 23: The effect of GPCR mutants on proliferation. Log phase cells were started at 1 x 105 cells.ml and counted daily. Data from (A) fast proliferation mutants and (B) normal or slow proliferation mutants was taken simultaneously. Values are mean ± SEM, n ≥ 3.
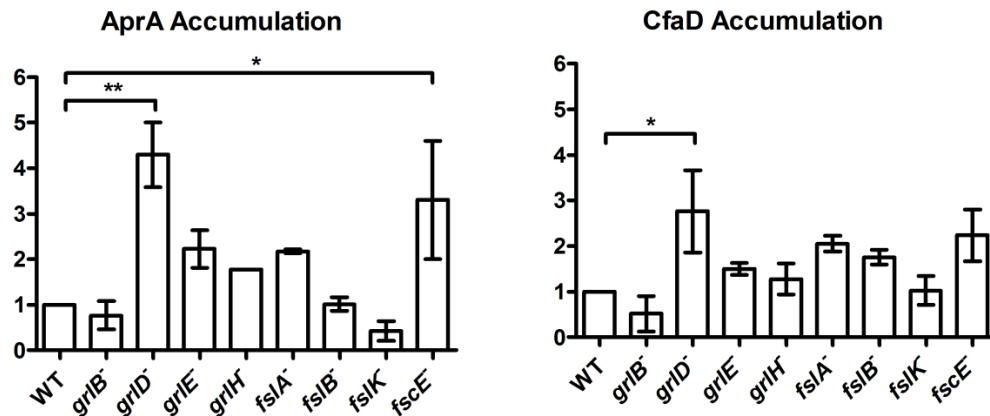
Accumulation of AprA and CfaD in GPCR mutant media

One reason a mutant *Dictyostelium* strain would have varied proliferation from wild type cells is a change in the accumulation of AprA or CfaD. An increase in AprA or CfaD accumulation would result in slower proliferation as these proteins both inhibit cell proliferation. A decrease in AprA or CfaD accumulation would result in faster proliferation. The conditioned media from GPCR mutants were analyzed for the concentrations of extracellular AprA and CfaD. All but two strains had normal accumulation of AprA and CfaD (Figure 24). *fscE*⁻ cells had a higher accumulation of AprA. *grlD*⁻ cells had higher accumulation of both AprA and CfaD. None of mutants accumulated less AprA or CfaD. Together these data indicate that the faster proliferation observed in several of the mutant strains is not due to less accumulation of AprA or

135

CfaD and that the slower proliferation of some mutants may be explained by an increase

in AprA and/or CfaD accumulation.

Table 15. The effect of GPCRs on doubling time and stationary density. Doubling times and maximum cell densities were calculated using the data in Figure 23A and B. Values are mean $\pm$ SEM, n $\geq$ 3. Statistical significance compared to wild type is shown as * (p < 0.05) and ** (p < 0.01) (one-way ANOVA).

| Cell Type	Doubling time, hours	Maximum observed cell density, 10^5 cells/ml
Wild-type	14.1 $\pm$ 0.8	186 $\pm$ 20.6
grlB$^-$	12.1 $\pm$ 1.2	234 $\pm$ 15.3
grlD$^-$	14.3 $\pm$ 1.3	89.8 $\pm$ 6.3**
grlE$^-$	10.8 $\pm$ 0.9*	188 $\pm$ 16.5
grlH$^-$	8.9 $\pm$ 1.7*	198 $\pm$ 22.4
fslA$^-$	13.7 $\pm$ 1.2	221 $\pm$ 41.9
fslB$^-$	15.4 $\pm$ 1.0	136 $\pm$ 12.8
fslK$^-$	14.8 $\pm$ 1.4	137 $\pm$ 11.8
fscE$^-$	11.4 $\pm$ 0.7	120 $\pm$ 8.41

Figure 24: Accumulation of AprA and CfaD in GPCRs mutants. Conditioned media from mid-log phase cells was analyzed for accumulated **(A)** AprA and **(B)** CfaD using anti-AprA and anti-CfaD antibodies. Quantifications (n=3, mean ± SEM) of western blot bands are shown. * and ** indicate statistical significance from wild type accumulation with $p < 0.05$ and $p < 0.01$, respectively (one-way ANOVA).

Several GPCR mutants are insensitive to AprA and CfaD

We would expect when components of the AprA and CfaD pathways are knocked out, the mutant strains would be insensitive to AprA and/or CfaD. Thus, the addition of AprA and CfaD should not be able to slow the proliferation of cells. No difference in cell proliferation was observed for *grlH⁻* cells in response to CfaD, *fslB⁻* and *fscE⁻* cells in response to AprA, or *fslA⁻* and *fslK⁻* cells in response to either AprA or CfaD (Figure 25). *fslB⁻* and *fscE⁻* cells were insensitive to only CfaD and *grlH⁻* cells were insensitive to only AprA. *grlB⁻*, *grlD⁻*, and *grlE⁻* cells were insensitive to both AprA and CfaD. Together, with the data from previous sections, these data indicate that

GrlB and GrlE may be candidates for AprA and CfaD signaling and GrlH for AprA

signaling only.

A

Inhibition by rAprA

B

Inhibition by rCfaD
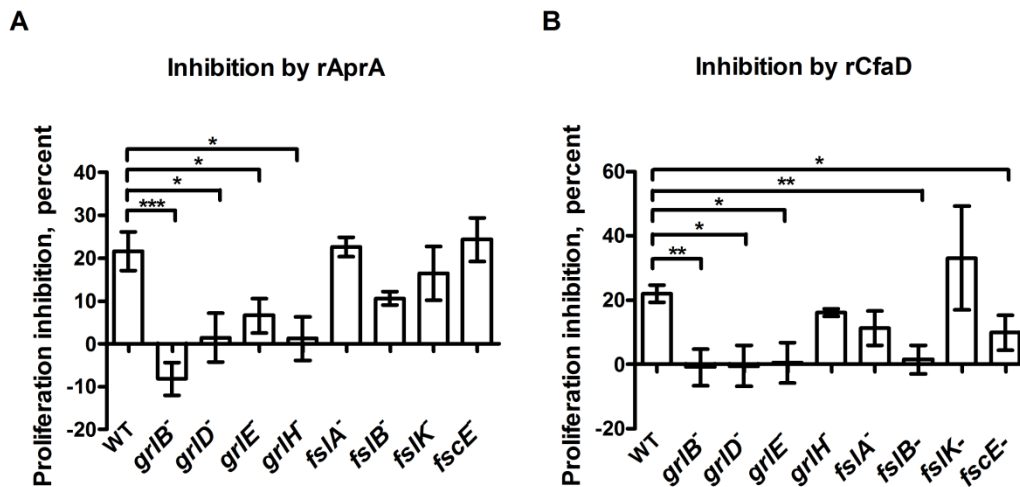
Figure 25: Sensitivity of GPCRs to rAprA and rCfaD. 300 ng/ml rAprA or rCfaD or an equivalent volume of buffer was added to cell cultures which were left for 16 hours before cell densities were determined. Percent inhibition of proliferation in **(A)** rAprA or **(B)** rCfaD compared to the buffer control proliferation is shown. Mean ± SEM, n ≥ 3. *, **, and *** indicate p < 0.05, p < 0.01, and p < 0.001, respectively (one-way ANOVA).

grlD⁻, grlH⁻, and fslK⁻ cells are multinucleate

Both AprA and CfaD mutants are more multinucleate than wild type cells (39, 40). To determine if any of the mutants exhibited this phenotype, cells were stained with DAPI and their nuclei counted. *grlD⁻, grlH⁻,* and *fslK⁻* cells had significantly less cells with a single nucleus than wild type cells (Table 16). Both *grlH⁻* and *fslK⁻* cells had significantly more cells with two nuclei and *fslK⁻* cells had significantly more cells with

138

three or more nuclei. These data indicate that like AprA and CfaD, several GPCR mutants are more multinucleate than wild type.

The screened GPCRs have no effect on cell growth

AprA and CfaD affect the proliferation of cells, but not cell growth, which is defined as an increase in mass and protein (39, 40). Mutant GPCR strains were analyzed for their mass and protein content. $grlD^-$, $fslA^-$, $fslB^-$, $fslK^-$, and $fscE^-$ cells had increased amounts of protein compared to wild type cells (Table 17). $grlH^-$ cells had significantly less protein than wild type cells (Table 17). $grlD^-$, $grlH^-$, and $fslK^-$ had more nuclei per 100 cells than wild type cells (Table 17). Mass and protein contents were adjusted for the number of nuclei per 100 cells for each strain. When protein content was adjusted, all mutant strains had a similar amount of protein as wild type cells (Table 17). There were no differences in cell mass.

The accumulation of mass, protein, and nuclei are a function of their proliferation rate. A doubling of cell number should then result in a doubling of mass, protein, and

Table 16. The effect of GPCR on nuclei per cell. Cells with one, two, or three or more nuclei were counted. *, **, *** indicate statistical significance compared to wild type with $p < 0.05$, $p < 0.01$, and $p < 0.001$, respectively (one-way ANOVA). Values are mean ± SEM, n=3.

Percent of cells with n nuclei

Cell Type	1	2	3+
Wild-type	79 ± 3.5	20 ± 3.6	0.6 ± 0.2
$grlB^-$	76 ± 2.6	22 ± 1.8	1.8 ± 0.6
$grlD^-$	62 ± 3.1**	34 ± 1.7*	3.7 ± 1.9
$grlE^-$	79 ± 4.3	20 ± 3.9	0.8 ± 0.6
$grlH^-$	55 ± 4.1***	40 ± 3.4***	4.3 ± 0.8
$fslA^-$	69 ± 3.7	27 ± 2.6	4.1 ± 2.2
$fslB^-$	71 ± 2.3	27 ± 1.7	2.4 ± 0.6
$fslK^-$	49 ± 3.8***	41 ± 3.1***	9.4 ± 1.6***
$fscE^-$	71 ± 1.3	29 ± 1.2	0.9 ± 0.3

nuclei. The doubling times from Table 15 were used to calculate the accumulation of mass, protein, and nuclei. Compared to wild type cells, none of the mutant strains had differences in mass accumulation. $fscE^-$ cells accumulated significantly more protein per hour than wild type cells, but there was no difference in protein accumulation per nuclei per hour between wild type and $fscE^-$ cells (Table 18). There were no other differences

140

Table 17. The effect of GPCRs on the mass and protein content of cells. Mass and protein content of GPCR mutants was measured. Data from Table 16 was used to calculate the nuclei per 100 cells. Nuclei per 100 cells was used to calculate the mass and protein content per 10^7 nuclei. *, **, and *** indicate values are statistically significant from wild type with $p < 0.05$, $p < 0.01$, and $p < 0.001$, respectively. Values are mean ± SEM, $n \geq 3$.

Cell	Per 10^7 cells			Per 10^7 nuclei	
	Mass	Protein (mg)	Nuclei/100	Mass	Protein
Wild-	15.4 ± 2.9	1.10 ± 0.02	121 ± 3	12.6 ± 2.3	0.91 ± 0.21
grlB⁻	20.8 ± 5.0	1.21 ± 0.02	126 ± 3	16.4 ± 4.0	0.96 ± 0.21
grlD⁻	19.3 ± 3.4	1.55 ± 0.02***	143 ± 5*	13.5 ± 2.4	1.09 ± 0.02
grlE⁻	14.2 ± 1.6	1.15 ± 0.01	122 ± 5	11.7 ± 1.3	0.95 ± 0.00
grlH⁻	13.3 ± 1.0	0.98 ± 0.01*	150 ± 5**	8.9 ± 0.6	0.66 ± 0.01
fslA⁻	17.2 ± 3.0	1.31 ± 0.03***	136 ± 6	12.7 ± 2.2	0.97 ± 0.03
fslB⁻	14.0 ± 2.4	1.46 ± 0.06***	132 ± 3	10.7 ± 1.8	1.11 ± 0.05
fslK⁻	17.4 ± 3.0	1.60 ± 0.03***	167 ± 9***	10.4 ± 1.8	0.96 ± 0.02
fscE⁻	14.7 ± 1.7	1.33 ± 0.03***	131 ± 2	11.3 ± 1.3	1.02 ± 0.02

in protein accumulation. *grlH*⁻ cells accumulated more nuclei per hour than wild type cells. Together these data indicate that none of the mutants play a significant role in the growth of cells.

Table 18. The effect of GPCRs on mass and protein accumulation of cells. Doubling times from Table 15 were used to determine mass, protein, and nuclei accumulation per hour. Mean ± SEM, n ≥ 3. Values are statistically significant from wild type at * with p < 0.05 and ***with p < 0.001.

Cell type	Per 10^7 cells/hour			Per 10^7 nuclei/hour	
	Mass (mg)	Protein (µg)	Nuclei, x 10^{-5}	Mass (mg)	Protein (µg)
Wild-type	1.09 ± 0.21	78 ± 5	8 ± 1	0.90 ± 0.18	65 ± 4
$grlB^-$	1.72 ± 0.45	100 ± 10	10 ± 1	1.36 ± 0.36	80 ± 8
$grlD^-$	1.35 ± 0.27	109 ± 10	10 ± 1	0.94 ± 0.19	76 ± 8
$grlE^-$	1.31 ± 0.19	106 ± 9	11 ± 1	1.08 ± 0.16	87 ± 8
$grlH^-$	1.49 ± 0.31	110 ± 21	17 ± 3***	0.99 ± 0.21	73 ± 14
$fslA^-$	1.26 ± 0.24	96 ± 8	9 ± 1	0.93 ± 0.18	70 ± 7
$fslB^-$	0.91 ± 0.17	95 ± 7	9 ± 1	0.69 ± 0.13	72 ± 6
$fslK^-$	1.18 ± 0.23	108 ± 10	11 ± 1	0.71 ± 0.14	65 ± 7
$fscE^-$	1.28 ± 0.17	116 ± 8*	11 ± 1	0.98 ± 0.13	89 ± 6

Several GPCRs are important for spore development

The cost of lacking AprA or CfaD is a defect in spore viability, suggesting these proteins help regulate spore survivability (39, 40). $grlD^-$, $fslA^-$, and $fscE^-$ cells have a reduced ability to produce spores during development and their spores are less viable

than wild type spores (Table 19). Although $grlE^-$, $fslB^-$, and $fslK^-$ cells can produce a

normal number of spores, the spores are less viable than wild type spores (Table 19).

These data suggest that multiple GPCRs may be required for *Dictyostelium* spore

development and viability.

Table 19. The effect of GPCRs on spore development and viability. Percent of visible spores following 48 hours of developed were calculated from the input cells. Spores were treated with detergent, plated, and viable colonies were counted. Values are mean ± SEM, n=3 . ** and *** indicates differences are significantly different compared to wild-type with $p < 0.01$ and $p < 0.001$, respectively (one-way ANOVA).

Cell Type	Viable spores after development as a percent of input cell number	Detergent resistant spores as a percent of total spores
Wild-type	122 ± 11	124 ± 15
$grlB^-$	82 ± 16	127 ± 11
$grlD^-$	0.38 ± 0.20***	34 ± 16***
$grlE^-$	96 ± 20	47 ± 18**
$grlH^-$	148 ± 27	105 ± 16
$fslA^-$	0.14 ± 0.05***	62 ± 3**
$fslB^-$	60 ± 20	15 ± 6***
$fslK^-$	124 ± 8	14 ± 3***
$fscE^-$	24 ± 12**	39 ± 4***

Expansion of GPCR mutant colonies

$aprA^-$ cells have slowly expanding colonies and this slow expansion is not due to a defect in motility (46). The expansion of GPCR mutant colonies was measured daily. $grlB^-$, $grlH^-$, $fslA^-$, $fslB^-$, and $fslK^-$ colonies expanded slower than wild type cells as these colonies were smaller than wild type colonies on days 4, 5, and 6 (Figure 26). $grlD^-$ colonies were smaller than wild type colonies on day 4, but were similar to wild type colonies on all other days. $fscE^-$ colonies expanded similarly to wild type colonies but were significantly smaller on day 6. Slow colony expansion in $grlH^-$, $fslA^-$, $fslB^-$, and $fslK^-$ colonies may be due to slower motility seen in these strains (data not shown). GrlB may play a role in chemorepulsion as it has a slower expansion not due to a defect in cell motility.

*Several GPCRs appear to be necessary for AprA chemorepulsion*

Wild type cells move in a biased direction away from a source of AprA (48). We tested the ability of GPCR mutant cells to be chemorepulsed by AprA. As we have previously seen, wild type cells moved in a biased direction away from AprA (48). Likewise, $grlE^-$, $fslA^-$, and $fslK^-$ mutants respond to and move away from AprA (Figure 27). $grlB^-$, $grlD^-$, $grlH^-$, and $fslB^-$ are all insensitive to GPCRs may play a role in AprA chemorepulsion.
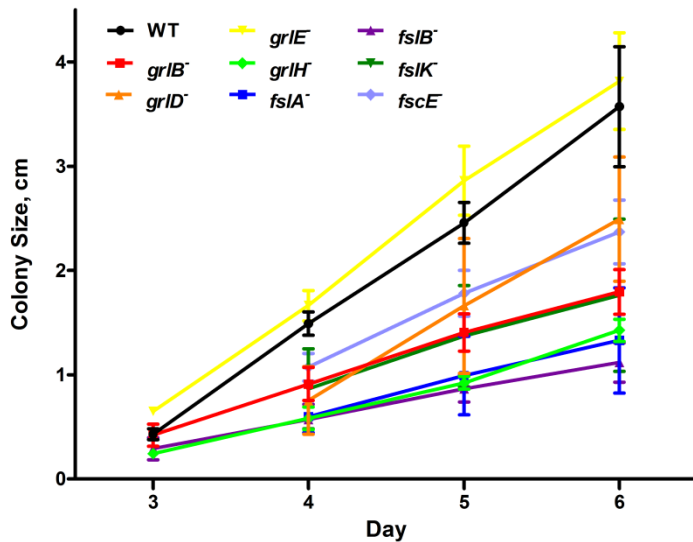
Figure 26: GPCR mutant colony expansion. Approximately 10 cells were plated onto plates containing *K. aerogenes* bacteria. At least 3 colonies were measured per time plate. After 6 days, individual wild type colonies were indistinguishable from each other. Values are mean ± SEM, n ≥ 3. The absence of error bars indicates the SEM was less than the size of the marker.

GrlB and GrlH are involved in cell dispersal at the edge of colonies

Cells at the edge of wild type colonies tend to move away from the cell dense center, while cells of an AprA mutant colony do not (46). AprA mutant colonies form a tight edge line (46). We screened GPCR mutant cells for their ability to spread out from the colony center. We would expect mutants of the AprA chemorepulsion pathway to display tight colony edges. As we have previously seen, wild type cells move away from the edge of colonies (46). *grlH⁻* and *grlB⁻* cells did not move outward from the dense colony center (Figure 28). The remainder of mutant cells spread away from the center

145
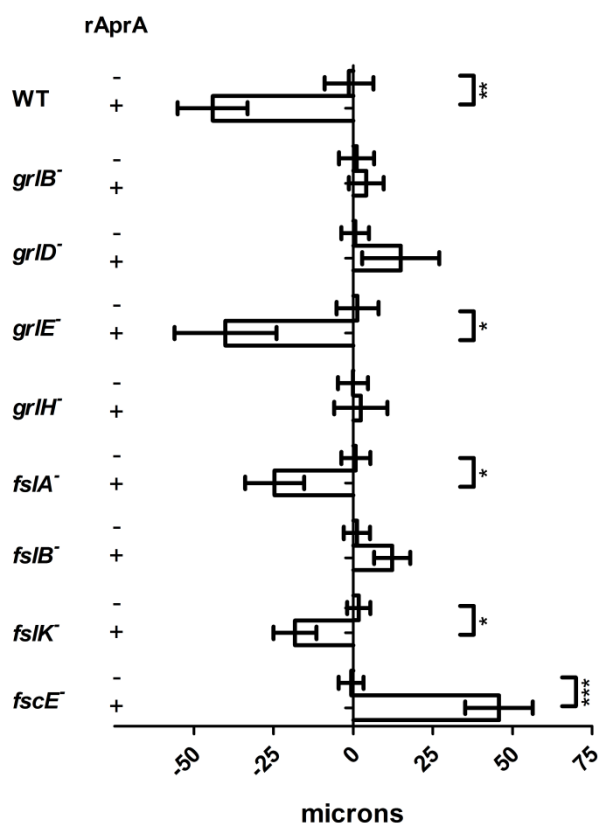
Figure 27: The effect of AprA on chemorepulsion in GPCR mutants. rAprA solution or an equivalent volume of buffer was added to one side of an Insall Chamber. Videomicroscopy was used to visualize the movement of cells which were then manually tracked. Migration along the x-axis is shown in microns (mean ± SEM, n ≥ 3). *, **, and *** indicate $p < 0.05$, $p < 0.01$, and $0 < 0.001$, respectively (t-test).

of the colony similar to wild type. These observations were supported by the average distances cells at the edge of colonies move. Cells at the edge of *grlH⁻* and *grlB⁻* colonies traveled significantly less distance than cells at the edge of wild type colonies (Table 20). These data indicates that GrlB and GrlH are good candidates for AprA signaling.
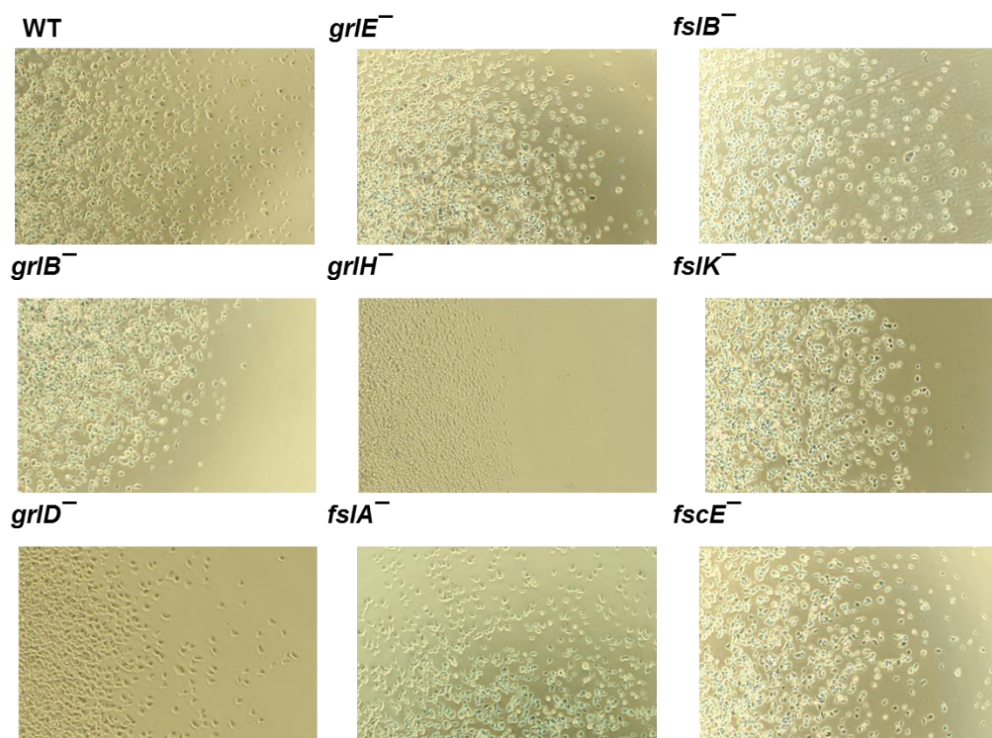
Figure 28: Colony edge formation of GPCR mutants. Colonies of cells were allowed to adhere to glass well slides. Fresh media was added to the wells and cells were left overnight to spread. The edges of colonies were imaged with a 20x phase contrast objective. The right colony edge is shown for all strains except *fslA*⁻ where the top colony edge is shown. Images are representative of at least three individual experiments.

Table 20. Distance traveled away from colony edge. The distance traveled from the colony edge at least 30 randomly chosen cells was measured from Figure 28 and data not shown. Values are mean ± SEM. *** indicates $p < 0.001$ (one-way ANOVA).

Cell Type	Average distance from colony edge (microns)
Wild-type	52 ± 7
grlB⁻	16 ±3***
grlD⁻	68 ± 7
grlE⁻	31 ± 4
grlH⁻	11 ± 1***
fslA⁻	36 ± 4
fslB⁻	37 ± 5
fslK⁻	61 ± 12
fscE⁻	42 ± 5

Discussion

In this section of the dissertation, I have characterized eight GPCRs and their sensitivity to AprA and CfaD. Here, I show that there are several candidates that may play a role in AprA and/or CfaD signaling. GrlB, GrlE, and GrlH are strong candidates for proliferation inhibition, while GrlB and GrlH are also candidates for chemorepulsion signaling.

Several mutants displayed proliferation slower than wild type. The slower proliferation of *fscE⁻* cells was due to an increased accumulation of AprA. Intriguingly, *grlD⁻* cells had significantly slower proliferation and increased accumulation but were insensitive to AprA and CfaD inhibition. *grlD⁻* cells were also found to be more multinucleate than wild type cells. Within the time course of 16 hours a defect in cytokinesis could explain why *grlD⁻* cells appeared to be insensitive to AprA and CfaD. *grlD⁻* cells contained more protein than wild type cells. When protein was corrected for the multinuclear phenotype, *grlD⁻* cells had similar amounts of protein to wild type cells. Additionally, *grlD⁻* cells have a significant defect in spore production and viability. This suggests that *grlD⁻* cells have an overall defect in proliferation, possibly due to cytokinesis disruption and viability. GrlD may be important for normal cellular function including viability.

GrlB, GrlE, and GrlH appear to be candidates for proliferation inhibition signaling. *grlE⁻* and *grlH⁻* cells have significantly faster doubling times and *grlB⁻* reaches a higher density than wild type cells. These are both phenotypes we have previously seen independent of each other for certain AprA and CfaD signaling components (45, 47). The increase in proliferation for these mutants was not due to higher accumulation of AprA or CfaD. Additionally, all three mutant strains were insensitive to the addition of AprA and *grlB⁻* and *grlE⁻* cells were insensitive to CfaD. Together this suggests that GrlB, GrlE, and GrlH are potential candidates for proliferation inhibition signaling components.

$grlB^-$, $grlD^-$, $grlH^-$, and $fslB^-$ appear to be insensitive to AprA chemorepulsion signaling. The edges of $grlB^-$ and $grlH^-$ colonies are tight while the edges of $grlD^-$ and $fslB^-$ cells disperse similar to wild type cells. This suggests that $grlD^-$ and $fslB^-$ cells can sense AprA and move outward at the colony edge. The insensitivity to rAprA may be an artifact in these strains or due to their slow motility. Together the data indicate that GrlB and GrlH are candidate components of AprA chemorepulsion signaling.

Conclusions and future directions

The work in this dissertation appendix shows that GrlB, GrlE, and GrlH are potential candidates for proliferation inhibition through AprA and CfaD while GrlB and GrlH are candidates for chemorepulsion signaling through AprA. Future work on these GPCRs should focus on rescuing the potential candidates to show that specific phenotypes are due to loss of the gene. Additionally, expressing the receptors in a heterologous system would allow us to study the binding of rAprA and rCfaD to these receptors.

APPENDIX D

PERITONEAL DIALYSIS FLUID AND SOME OF ITS COMPONENTS POTENTIATE FIBROCYTE DIFFERENTIATION

Summary

Work in this appendix was done as side project working with peripheral blood mononuclear cells, which our lab uses to study wound healing. Much of the intellectual design for the work in this section is credited to Katayoon Keyhanian when she brought the idea of studying fibrosis in dialysis patients. Additionally, and undergrad, Hannah Starke helped with a portion of the experiments within this section.

Long-term peritoneal dialysis often results in the development of peritoneal fibrosis. Submesotheium thickening, increased extracellular matrix deposition, and increased fibrotic tissue characterize peritoneal fibrosis. For many fibrosing diseases, monocytes enter the fibrotic lesion and differentiate into fibroblast-like cells called fibrocytes, which contribute to fibrosis. Peritoneal dialysis (PD) fluids contain glucose, a number of electrolytes, and buffers. Recently, high sodium chloride has been associated with an increase in fibrocyte differentiation. We report that PD fluid potentiates human fibrocyte differentiation *in vitro* and that sodium chloride and sodium lactate are responsible for this potentiation. In addition, PD fluid and sodium chloride decrease the ability of the plasma protein Serum Amyloid P (SAP) to inhibit fibrocyte differentiation. Together, these results suggest that PD fluid components contribute to the development of peritoneal fibrosis, and their ability to desensitize the SAP response may exacerbate the disease.

Introduction

For patients with end stage renal disease, the kidneys no longer function to properly remove wastes from the body (207). Peritoneal dialysis (PD) is the most cost-effective and easiest therapy available to replace kidney function (208-211). PD fluids contain a mixture of electrolytes to help maintain blood composition, an osmotic agent to facilitate the transport of water and other liquids through a membrane, and a buffer to maintain proper pH (209, 210). The commonly used peritoneal dialysis fluid Dianeal® contains the electrolytes sodium, chloride, calcium, and magnesium, the sugar D-glucose as an osmolyte, and a buffer containing lactate. PD fluid is injected via a permanent catheter into the peritoneal cavity (208, 212). The peritoneal membrane acts as a dialyzing membrane, allowing the removal of waste products from the body (210-212). Although peritoneal dialysis has many advantages to other treatments, the development of tissue remodeling such as angiogenesis, fibrosis and membrane failure are debilitating disadvantages (208, 210-214).

Peritoneal fibrosis is characterized by a thickening of the submesothelium, increased extracellular matrix deposition, the presence of myo-fibroblasts, and increased fibrotic (scar) tissue (208, 210-214). During an inflammation response, leukocytes leave the blood to the affected organ and may differentiate into fibroblast-like cells called fibrocytes (215). Like fibroblasts, fibrocytes can aid in wound healing by promoting scar tissue formation (215-217). Fibrocytes differentiate from CD14$^+$ monocytes and share characteristics of both blood leukocytes and tissue resident cells (218, 219). Fibrocytes can promote angiogenesis and secrete inflammatory cytokines and extracellular matrix

proteins (215, 220). Serum amyloid P (SAP) is a pentraxin protein, secreted by the liver into the plasma, which inhibits fibrocyte differentiation (216). The presence of fibroblasts in peritoneal fibrosis has been well documented, however the presence of fibrocytes has not (214, 221-225).

A number of factors including the presence of a catheter, uremia, peritonitis, and the PD fluid itself can contribute to development of peritoneal fibrosis. Glucose degradation products (GDP) (including 5-hydroxymethylfuraldehyde and 3,4-dideoxyglucosone-3-ene) that form during heat sterilization of the PD fluid have an adverse effect on the peritoneal membrane and can promote fibrosis. Recent studies using low-GDP fluids show a decrease in peritonitis however, they did not report whether peritoneal fibrosis was still observed in these patients. Although the effects of GDPs in PD fluid have been analyzed, little has been done to determine the effects of the remaining components of PD fluid.

In this report, we examine the effects of PD fluid and components of PD fluid on fibrocyte formation. Previously, we found that increased sodium chloride potentiates the differentiation of monocytes into fibrocytes (226). Our results indicate that PD fluid components sodium chloride and sodium lactate potentiate fibrocyte differentiation and the potentiation is not inhibited by SAP.

Methods

Cell culture and fibrocyte differentiation assays

Human blood was collected into heparin tubes (BD Bioscience, San Jose, CA) from adult volunteers who gave written consent and with specific approval from the Texas A&M University human subjects Institutional Review Board. Peripheral blood mononuclear cells (PBMC) were isolated as previously described (227).

PBMC were cultured in 96-well cell plates (Falcon) with peritoneal dialysis fluid (132 mM sodium, 96 mM chloride, 3.5 mM calcium, 0.5 mM magnesium, 40 mM lactate, and 1.5% D-glucose) or individual components of PD fluid (sodium chloride, calcium chloride, magnesium chloride, sodium lactate, or D-glucose) in RPMI-1640 medium. One molar solutions of sodium chloride, calcium chloride, magnesium chloride, D-glucose and sodium lactate were prepared in water and filter sterilized as previously described (226). Solutions were added to the wells at the indicated concentrations. 5×10^4 cells in 100 μL of RPMI-1640 were added to each well. Cells were incubated for five days with 5% CO_2 at 37°C. Following incubation, cells were fixed with methanol for ten minutes and stained with a Hema 3 staining Kit (Thermo Fisher Scientific, Milwaukee, WI). Fibrocytes were identified by their spindle-shape morphology and counted in five 900-μm fields of view.

SAP ranging from 5μg/mL to 0.04μg/mL was co-incubated with 12.5% PD fluid, 12.5 mM sodium chloride, 5 mM sodium lactate (all in RPMI-1640), or RPMI-1640 alone. Fibrocytes were incubated, stained, and counted as stated previously.

154

Collagen and DAPI Staining

Collagen staining was done as previously described with the exception that the primary antibody was 2.5 µg/ml rabbit anti-collagen I (Abcam, Cambridge, MA) (228).

Plates from the fibrocyte differentiation assays were stained with 2 µg/ml DAPI (Sigma Aldrich), imaged, and analyzed with CellProlifer analysis software (229).

Statistics

Data were analyzed using t-tests and calculating IC_{50}s with Prism (GraphPad software, San Diego, CA).

Results

PD fluid potentiates fibrocyte differentiation

The use of PD fluid is associated with peritoneal fibrosis, and fibrocytes contribute to fibrosis (212, 213, 216). To determine if PD fluid affects the differentiation of monocytes into fibrocytes, human PBMCs were incubated with various concentrations of PD fluid for 5 days. The number of fibrocytes present after 5 days in PD fluid was determined and normalized to the number of fibrocytes without PD fluid. In the presence of 12.5% PD fluid, the number of fibrocytes was significantly increased (Figure 29). $[Na^+]$ and $[Cl^-]$ are 134 mM and 107 mM, respectively in RPMI medium. In RPMI medium, 12.5% PD fluid corresponds to an additional 16.5 mM sodium and an additional 12 mM chloride, making the $[Na^+]$ 150.5 mM and the $[Cl^-]$ 119 mM. These concentrations are comparable to previous findings where sodium chloride potentiated

fibrocyte differentiation (226). $[Ca^{2+}]$ and $[Mg^{2+}]$ are 0.42 mM and 0.4 mM, respectively in RPMI medium. In RPMI medium, 12.5% PD fluid corresponds to an additional 0.44 mM calcium and an additional 0.06 mM magnesium making the $[Ca^{2+}]$ 0.86 mM and the $[Mg^{2+}]$ 0.46 mM. A 0.18% addition of glucose from 12.5% PD fluid to the 0.2% in RPMI medium results in a total of 0.38% glucose. RPMI does not contain lactate, therefore the final concentration of lactate from 12.5% PD fluid is 5 mM. The number of fibrocytes was significantly decreased in the presence of 50% PD fluid. These results indicate that PD fluid can potentiate the differentiation of fibrocytes.

Some, but not all, components of PD fluid potentiate of fibrocyte differentiation

PD fluid is composed of glucose, sodium chloride, magnesium chloride, calcium chloride, and sodium lactate. To determine which component(s) of PD fluid are responsible for the potentiation of fibrocyte differentiation, the individual components were incubated with PBMCs for 5 days. Glucose, calcium chloride, and magnesium chloride did not potentiate fibrocyte differentiation. Sodium chloride and sodium lactate potentiated fibrocyte differentiation at 12.5 mM and 5 mM, respectively (Figure 30). In RPMI medium, an additional 12.5 mM sodium chloride equals a $[Na^{+}]$ of 146.5 mM and a $[Cl^{-}]$ of 119.5 mM. These concentrations are similar to previous findings and to the
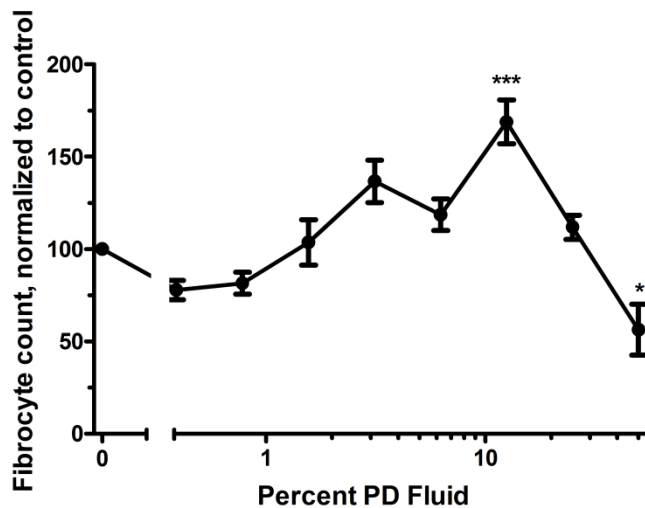
Figure 29: PD fluid potentiates the differentiation of fibrocytes. PBMC were incubated with the indicated concentrations of PD fluid for 5 days. The cells were then stained and counted. Values are mean ± SEM, n=6. * and *** indicate statistical significance with $p < 0.05$ and $p < 0.001$, respectively (one-way ANOVA).

concentrations in 12.5% PD fluid (226). An additional 5 mM sodium lactate in RPMI medium yields a $[Na^+]$ of 141 mM and a lactate concentration of 5 mM. Again, the sodium concentration is similar to previous observations where fibrocyte differentiation was potentiated (226).
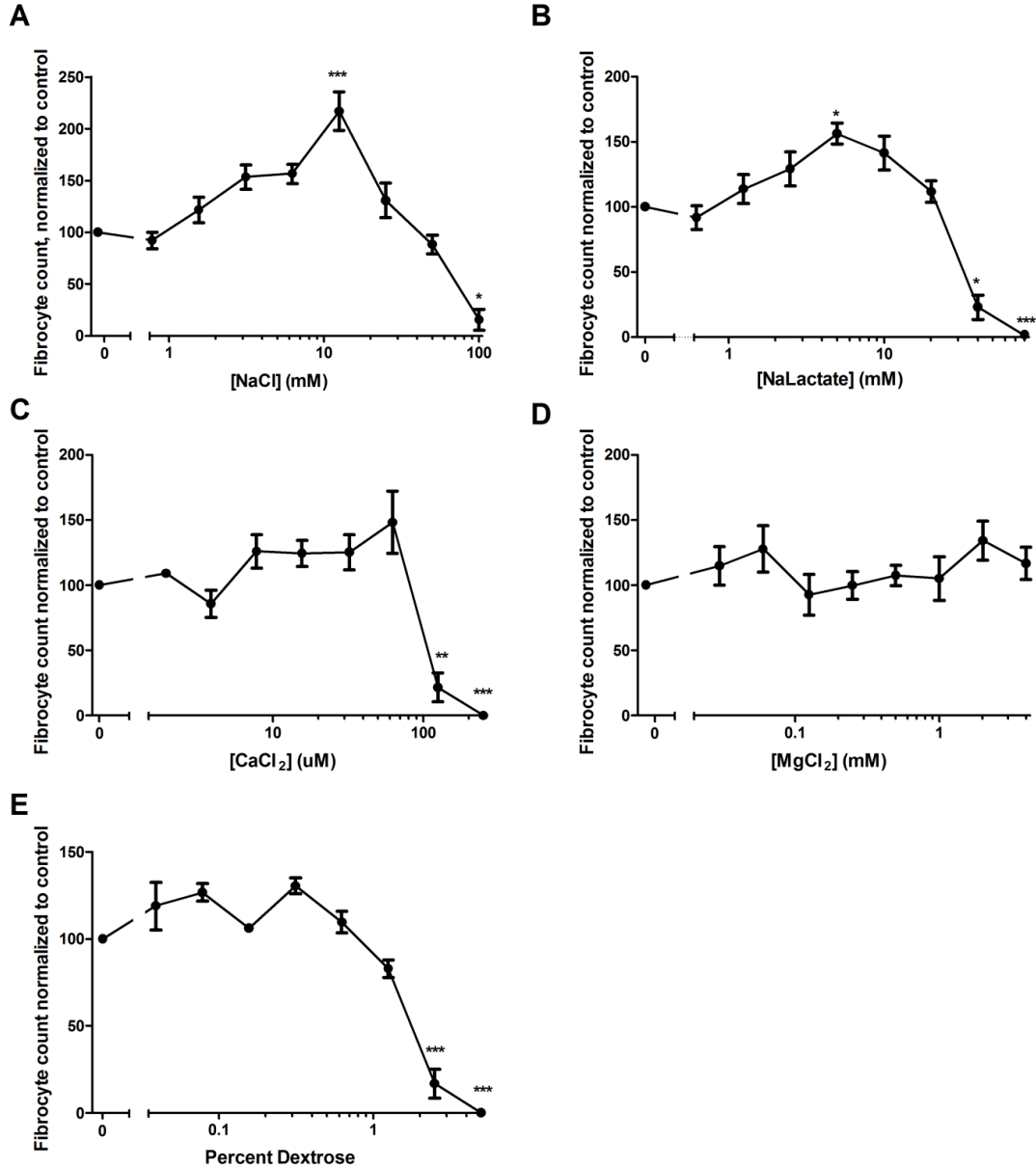
Figure 30: The PD fluid components sodium chloride and sodium lactate potentiate fibrocyte differentiation. PBMC were incubated with the indicated PD fluid components with the indicated concentrations added to the medium for 5 days, after which cells were stained and counted. Values are mean ± SEM n=3. *, **, and *** indicate significant difference in fibrocyte numbers compared to control with $p < 0.05$, $p < 0.01$, and $p < 0.001$, respectively (t-test). The absence of an error bar indicates that the error was smaller than the plot symbol.
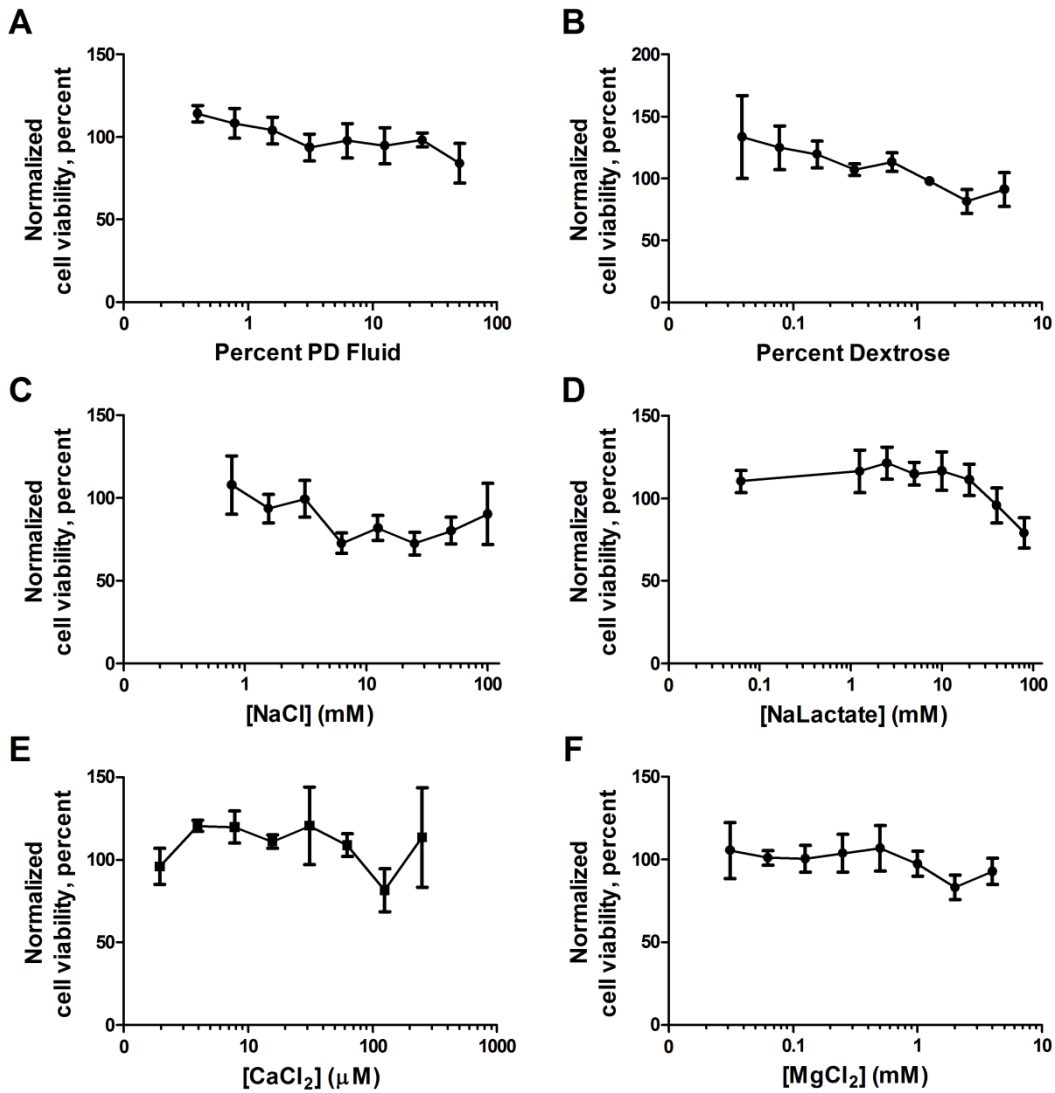
Figure 31: PD fluid and its components do not affect cell viability. PBMC were incubated with the indicated PD fluid components with the indicated concentrations added to the medium for 5 days, after which cells were stained and counted. Values are mean ± SEM n=3. The absence of an error bar indicates that the error was smaller than the plot symbol.

159

One reason for the increase in fibrocyte number could be an increase in the number of adherent cells. After counting the number of fibrocytes, plates were stained with DAPI and the total number of viable adherent cells was analyzed via Cell Profiler. There was no significant increase or decrease in adherent cells that could attribute for the increase of fibrocytes (Figure 31). Together these data indicate that some, but not all, of the components of PD fluid potentiate fibrocyte differentiation.

The expression of collagen is increased by PD fluid, sodium chloride, and sodium lactate

Collagen is expressed by fibrocytes and used as a marker of these cells (228, 230). To verify that the cells we counted were indeed fibrocytes, PBMCs were cultured with PD fluid, sodium chloride, or sodium lactate for 5 days. The cells were then stained for collagen I and analyzed by flow cytometry. PD fluid, sodium chloride, and sodium lactate all significantly increased the expression of collagen in these cells compared to cells in buffer alone (Figure 32). The presence of increased collagen in the cells indicates that PD fluid, sodium chloride, and sodium lactate potentiate fibrocyte differentiation.
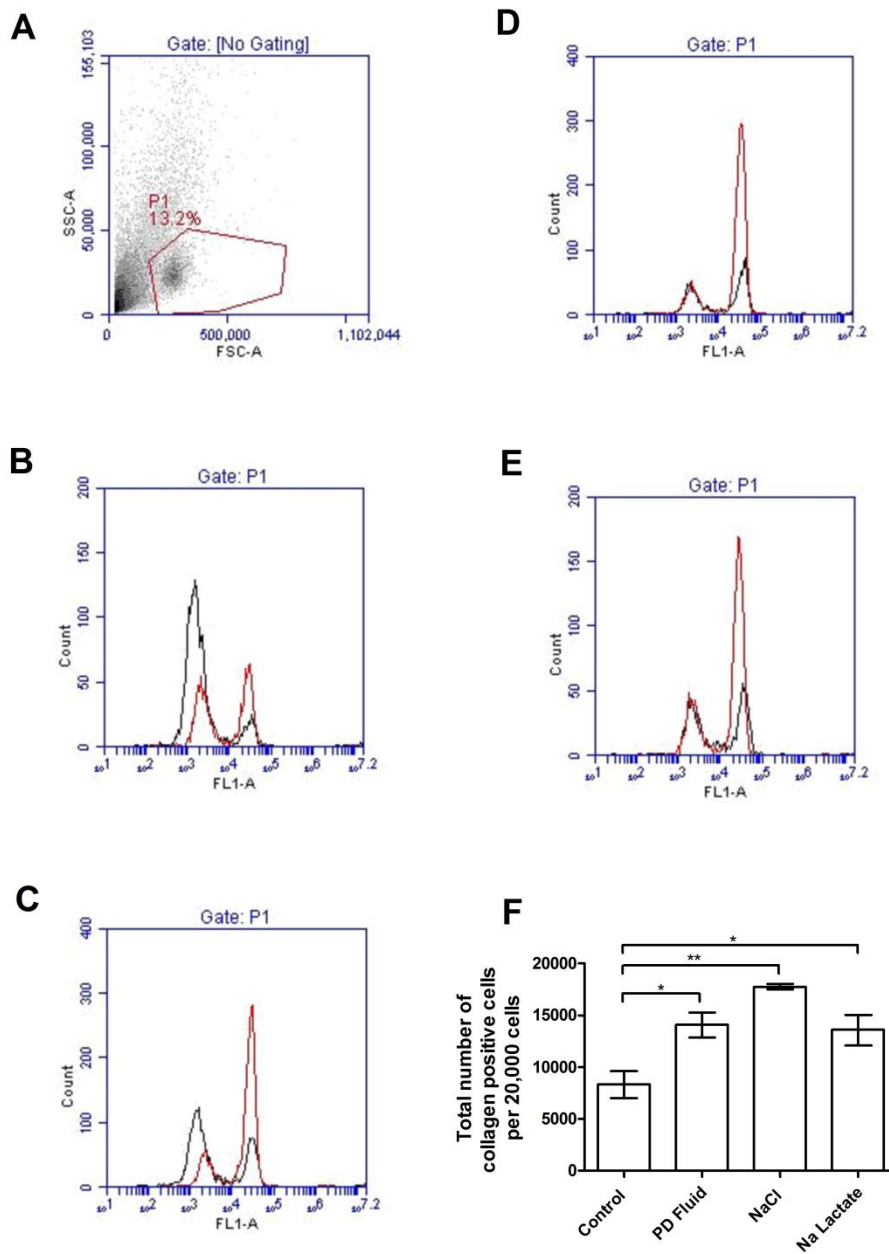
Figure 32: PD fluid, sodium chloride, and sodium lactate increase the expression of collagen. Cells were stained with polyclonal rabbit antibodies for collagen I. A) Forward and side scatter properties of 5 day cultured cells. Histograms show the fluorescent intensities of rabbit IgG control (black line) and collagen I (red line) for media alone (B), PD fluid (C), sodium chloride (D), and sodium lactate (E). F) The total number of collagen positive cells was calculated from the percentage of positive cells within the region P1. Values are mean ± SEM, n≥3. *, p < 0.05; **, p < 0.01 (t-test).

PD fluid and some of its components effect the sensitivity of SAP

SAP is secreted from the liver and inhibits fibrocyte differentiation (156, 216, 231). PBMC were incubated with or without SAP in the presence of PD fluid, sodium chloride, and sodium lactate at the concentrations that caused the highest potentiation of fibrocytes (Figure 33). IC_{50} values showed that PD fluid and sodium chloride significantly desensitized PBMC to SAP (Table 21). Although sodium lactate with SAP had an increased IC_{50} compared to SAP alone, the difference was not significant. These data indicate that PD fluid and sodium chloride interfere with the ability of SAP to inhibit fibrocyte differentiation, while sodium lactate only potentiates fibrocyte differentiation.

Table 21: IC50 values for PD fluid, sodium chloride, and sodium lactate in the presence of SAP. IC_{50} values were obtained by fitting a sigmoidal dose response curve to the data from Figure 33. Values mean ± SEM. ** indicates a significant difference from the control with $p < 0.01$.

Solution	IC_{50} (μg/ml)
Control	0.26 ± 0.03
PD Fluid	0.45 ± 0.06*
Sodium chloride	0.37 ± 0.03**
Sodium lactate	0.32 ± 0.05
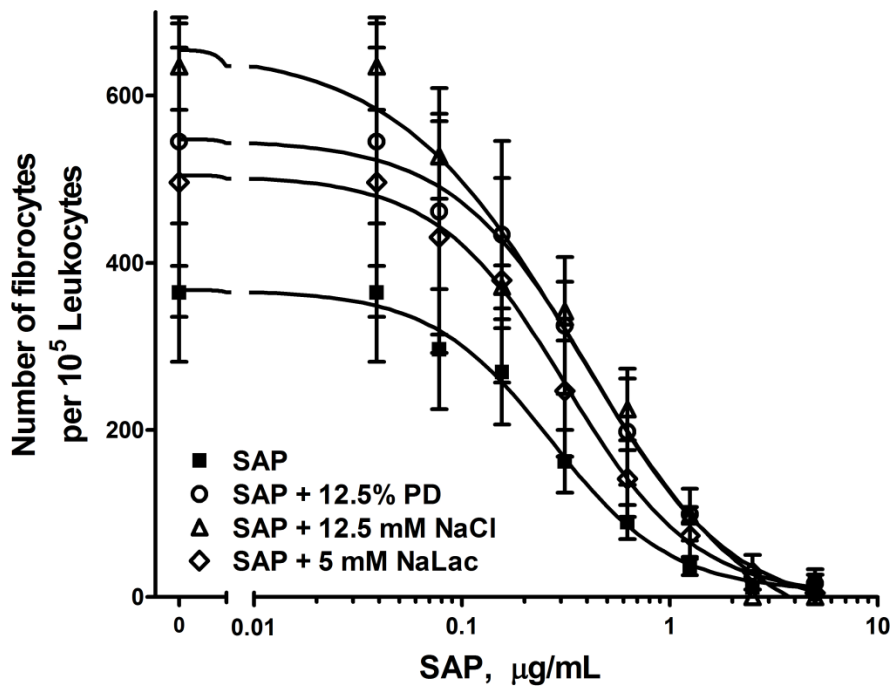
Figure 33. Sodium chloride and PD fluid, but not sodium lactate, interfere with the ability of SAP to inhibit fibrocyte differentiation. Cells were incubated in PD fluid or its components with and without various concentrations of SAP for 5 days. The number of fibrocytes were counted and normalized to the fibrocyte count without SAP. Values are mean ± SEM, n=3.

Discussion

Fibrocytes derived from monocytes are commonly found in fibrosing diseases such as congestive heart disease and renal fibrosis (232, 233). Long-term peritoneal dialysis often results in the formation of fibrotic tissue within the peritoneum (208, 210-214). Here we show that fibrocyte differentiation is potentiated by PD fluid and two of its components, sodium chloride and sodium lactate. PD fluid and sodium chloride appear to block the ability of serum amyloid P (SAP) to inhibit fibrocyte differentiation.

163

Sodium lactate potentiates fibrocyte differentiation in a mechanism independent of SAP inhibition.

PD fluid, sodium chloride, and sodium lactate potentiated fibrocyte differentiation. Cells were confirmed to be fibrocytes due to the increase in collagen observed after PD fluid, sodium chloride, and sodium lactate incubation. An increase of any cell type could be due to an increase in cell proliferation. Previous work with fibrocytes did not identify any changes in fibrocyte or fibrocyte precursor proliferation (234). We analyzed the number of adherent, and therefore viable, cells to determine if there was an increase in proliferation after 5 days with PD fluid or its components. We did not observe any differences in proliferation with any of the solutions used. Therefore, the increase in fibrocyte number is not due to an increase in total cell number.

Previously our lab observed that ~155 mM of sodium and ~130 mM of chloride potentiated fibrocyte differentiation (226). We saw that PD fluid corresponding to a [Na^+] of 150.5 mM and a [Cl^-] of 119 mM potentiated fibrocyte formation. With the addition of sodium chloride alone, a [Na^+] of ~146 mM and a [Cl^-] of ~120 mM were able to potentiate fibrocyte differentiation. Additionally, when sodium lactate was added, a sodium concentration of 141 mM was able to potentiate fibrocyte differentiation. Potentiation of fibrocyte differentiation by sodium lactate was probably due to increases in sodium as the lactate concentration for potentiation was only 5 mM and PD fluid contains 40 mM lactate. These are comparable to our previous findings (226).

Peritoneal dialysis fluid pumped into the peritoneum contains 132 mM sodium chloride. The transport of ions across the peritoneal membrane has been shown to be dependent on the glucose concentration in the peritoneal dialysis fluid (235). Typical dwell times (time allowed for exchange to occur across the membrane) are 4-10 hours. With 1.5% glucose and a 4-hour dwell time, approximately 13.2 mM of additional sodium would be reabsorbed from the blood. This corresponds to approximately 145 mM total sodium in the peritoneum. Assuming the same parameters, an additional 14 mM of chloride would be reabsorbed, resulting in 111 mM chloride in the peritoneum retention fluid. 145 mM sodium and 111 mM chloride could cause potentiation of fibrocyte differentiation which would likely occur in the peritoneum over long-term treatment.

Serum amyloid P (SAP) inhibits the differentiation of fibrocyte by interacting with FCγRI on monocytes (236). Both PD fluid and sodium chloride influence the ability of SAP to inhibit fibrocyte differentiation. For unknown reasons, sodium lactate did not significantly influence SAP activity. This could be due to the necessity of chloride or a secondary effect of having lactate present. Alternatively, sodium lactate fibrocyte potentiation could be through a mechanism independent of SAP inhibition. Blocking SAP inhibition leads to an increased number of fibrocytes. Peritoneal fibrosis could be potentiated by inhibiting SAP in the peritoneum by whole PD fluid and specifically sodium chloride. Conversely, peritoneal fibrosis may be alleviated in patients undergoing long-term peritoneal dialysis by altering the sodium chloride levels in the PD fluid such that SAP is no longer inhibited.

165

APPENDIX E

RBLA IS REQUIRED FOR APRA PROLIFERATION INHIBITION AND

CHEMOREPULSION[1]

Summary

Retinoblastoma (RB) is a tumor suppressor that regulates cell proliferation. This is a target effector we would expect a signal that inhibits cell proliferation to activate. Work on the *Dictyostelium* knockout of RB , *rblA⁻,* was completed by several members of our lab. The following dissertation appendix gives a summary of our findings, a short introduction about RB, and the results from the portion of the manuscript I completed myself.

We found that the loss of RblA results in a higher maximum density of cells in shaking culture, due to increase cytokinesis and a low accumulation of the chalone CfaD. Cell lacking RblA are insensitive to AprA, but not CfaD. *rblA⁻* cells proliferate slower on bacterial lawns. RblA does not affect cell growth. In addition to its role in proliferation inhibition, RblA is necessary for the chemorepulsion by AprA.

_____

Introduction

RB is a tumor suppressor gene that regulates cell proliferation through controlling the entry of cells into S phase (237). RB typically binds to and blocks the transcription factors that are needed for S phase to begin (237). When the cell cycle is promoted, cyclin-dependent kinases phosphorylate RB to inhibit its binding (238). Cells then transcribe the necessary components to enter S phase (238). The loss of RB leads to the formation of retinoblastomas (239).

In *Dictyostelium*, the retinoblastoma gene, RblA, also seems to regulate S phase mediators (240). Previous work has shown that cells lacking RblA had normal proliferation, but overexpression of RblA caused slower proliferation (240). We therefore, examined the role of RblA in the chalone signaling pathways for AprA and CfaD.

Methods

Proliferation on bacterial lawns was done as previous described (132) and colony size determination was done following Phillips (46).

Results

To determine if like *aprA*⁻ and *cfaD*⁻ colonies, *rblA*⁻ colonies expanded more slowly than wild type colonies, cells were plated and the average colony diameters were measured daily (46). *rblA*⁻ colonies were significantly smaller than wild type colonies (Figure 34A). Interestingly, the colonies appeared to increase at the same rate, with

167

rblA⁻ cells having a delay in colony formation (Figure 34A). One explanation for slow colony expansion would be slow proliferation. We examined the proliferation of *rblA⁻* on bacterial lawns. At 24 hours after plating, wild type and *rblA⁻* cell density was similar (Figure 34B). However, at 48 and 72 hours after plating, there were significantly less cells than wild type. Together, this indicates that RblA aids is proliferation and colony expansion on bacterial lawns and the loss of this protein disrupts the ability of cells to proliferate and expand on bacteria.
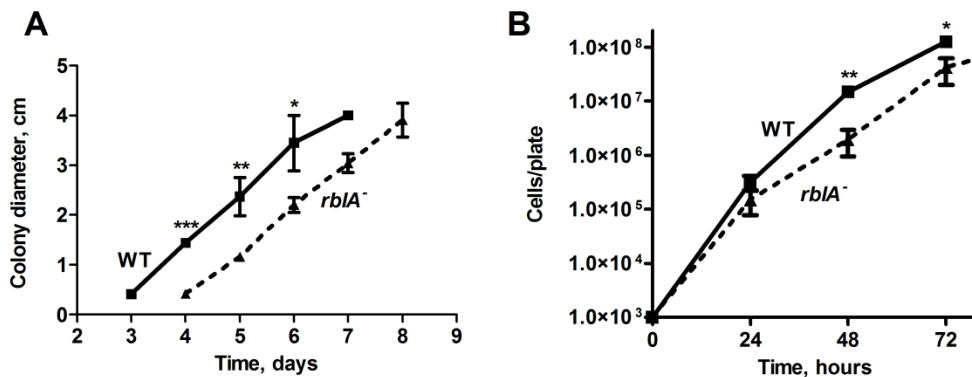
Figure 34: RblA facilitates bacterial proliferation and colony expansion. (A) Dilutions of log-phase cells were mixed with bacteria and spread on SM/5 plates. Well-spaced colonies were imaged daily and the average colony diameter was measured. Before day 3 for wild-type cells, and day 4 for *rblA⁻* cells, no clearing of the bacterial lawn was observed. **(B)** 10^3 cells were plated on bacterial lawns and the number of *Dictyostelium* cells was counted daily. For A and B, values are mean ± SEM, n = 7, the absence of error bars indicates that the error was smaller than the plot symbol, * indicates $p < 0.05$, ** indicates $p < 0.01$, and *** indicates $p < 0.001$ (t-test).

Discussion

We found that rblA- cell proliferation is significantly slower on bacterial lawns. To date, no other mutants ($aprA^-$, $cfaD^-$, $cnrN^-$, $qkgA^-$, or $bzpN^-$) we have screened within the chalone pathways have this phenotype (39, 40, 45, 46, 132). RblA regulates cell-cycle genes (237). There are three types of cytokinesis in Dictyostelium cells, at least one of which is dependent on substrate attachment . Therefore, it is possible that the loss of RblA disrupts a gene or protein necessary for substrate cell division and thus causes the slow proliferation and colony expansion on bacterial plates. It is also possible that RblA mutants have a defect in the ability to ingest or digest bacteria and therefore fail to clear plates as rapidly as wild type cells.

The inactive state of RblA would be un phosphorylated. RblA either lies within the AprA pathway itself or is acted up on by a component of the AprA pathway. AprA could active a kinase to phosphorylate RblA and therefore inhibit the transcription of factors leading to cell cycle progression. Future work will determine whether AprA acts directly or indirectly on RblA.

APPENDIX F

A MECHANISTIC VIEW OF DPPIV CHEMOREPULSION

Summary

The work in this section of the dissertation is a compilation of elucidating the mechanism of DPPIV and examining the ability of DPPIV to act as a therapeutic for ARDS.

Here we find that DPPIV can bind human neutrophils and that binding is affected by the addition of a DPPIV-enzymatic inhibitor. Gradients of DPPIV increase the number of cells with actin localized away from the source of DPPIV. Various concentrations of rDPPIV effectively reduce neutrophil accumulation in the lungs of mice. Additionally, nebulized rDPPIV chemorepulses human neutrophils and reduces neutrophils in mouse lungs. Together, gives insight into the mechanism used by DPPIV to induce chemorepulsion.

Introduction

ARDS has a mortality rate of ~40% (101). It is characterized by neutrophil damage to the tissue and a loss of lung integrity due to edema and epithelial cell damage (106). Neutrophils release proteases and reactive oxygen species that damage the tissue (105, 106). One mechanism to resolve neutrophil damage would be to chemorepulse neutrophils from the lung tissue.

DPPIV is an enzyme found on epithelial cells and some immune cells and as a soluble form in many bodily fluids (75, 82). We previously found that DPPIV acts as a chemorepellent of human neutrophils (187). DPPIV functions in a range above, below, and within the physiological concentration (400-800 ng/ml) of DPPIV. The enzymatic activity of DPPIV is necessary for neutrophil chemorepulsion. DPPIV does not cleave components of the media or neutrophil products that then act as chemorepellents. Oropharyngeal aspiration of DPPIV in a mouse model of ARDS reduces the accumulation of neutrophils in the lungs. Less neutrophils are present in the alveolar space and the lung epithelial tissue with DPPIV treatment. DPPIV does not inhibit or promote apoptosis *in vitro* and the reduction of neutrophils in the lungs of mice is not due to increased apoptosis. DPPIV acts as a chemorepellent and has the potential for a therapeutic of ARDS.

Here we show that DPPIV can bind to neutrophils and like the chemorepulsion, is mediated by enzymatic activity. Gradients of DPPIV increase the number of neutrophils with actin polarized away from the source of DPPIV.

171

Methods

Dilutions of Alexa647 labeled DPPIV were incubated with human neutrophils for 10 minutes, cells were collected, excess DPPIV removed, and fluorescence was measured by flow cytometry. Binding assays using DPPIV enzyme inhibitor (DPPIV 1cHCl) were done similarly, except DPPIV was pre-incubated with the inhibitor before added to the cells. For actin localization, 8-well glass slides were coated with 20 µg/ml human fibronectin at 37°C for 30 minutes and wash twice with PBS. Human neutrophils at 3 x 10^6 cells/ml were plated in 200 µl volumes into each well. Cells were allowed to adhere to plates for 15-20 minutes, non-adherent cells were washed off, and remaining cells were left to settle for another 15 minutes at 37°C. A gradient of DPPIV was created by placing a drop of rDPPIV in one corner of the well. After 40 minutes, cells were fixed with 4% paraformaldehyde for 10 minutes, washed with PBS, incubated with 0.1% Triton X-100 for 2 minutes, washed and blocked with 1% BSA/PBS for 10 minutes. Cells were stained with Alexa-488 conjugated phalloidin for 20 minutes and mounted with DAPI. Cells were imaged with a 100x objective. Actin localization toward or away from the source of DPPIV was analyzed for one hundred or more cells using a 60x objective.

Results

rDPPIV binds neutrophils

One way DPPIV could cause chemorepulsion is through binding to neutrophils. To determine if DPPIV could bind neutrophils, cells were incubated with labeled DPPIV

(DPPIV-Alexa) and fluorescence measured by flow cytometry. We found that DPPIV

bound neutrophils (Figure 35). Intriguingly, there were two populations of binders.

Some donors more strongly bound DPPIV (Figure 35C) than others (Figure 35B). This

indicates that DPPIV can bind neutrophils.
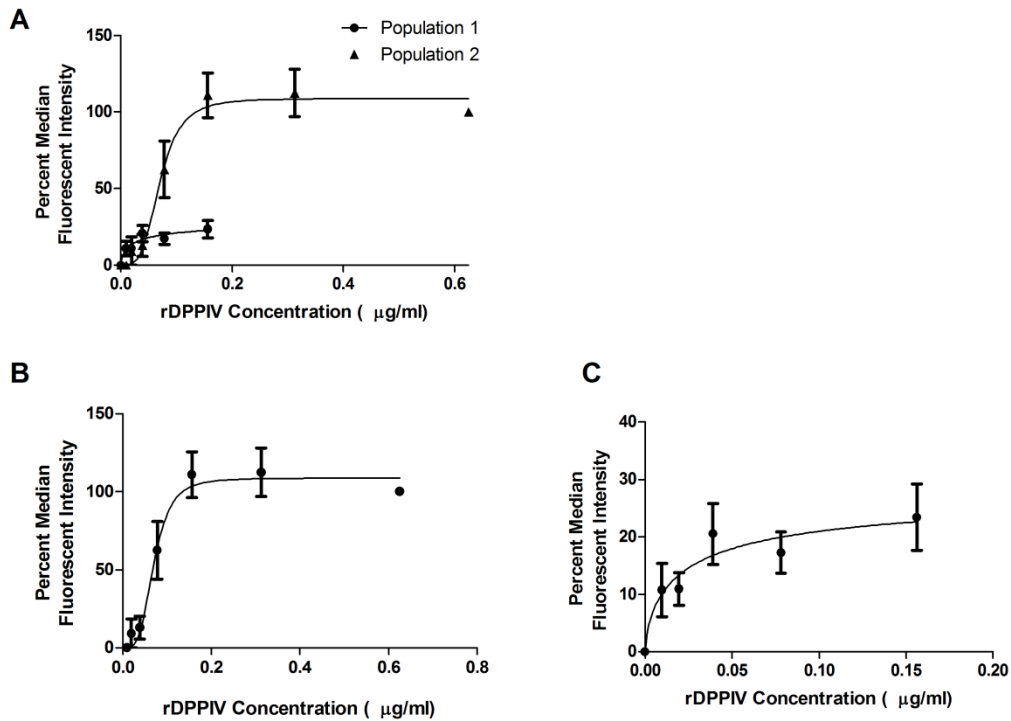
Figure 35: DPPIV binds human neutrophils. Neutrophils were incubated with various concentrations of DPPIV-Alexa and examined for the ability to bind DPPIV by flow cytometry. (A) Two populations of donors. (B) and (C) each population individually. Values are mean ± SEM (n≥5).

*DPPIV binding is effected by DPPIV enzymatic inhibitors*

We previously saw that the chemorepulsion of neutrophils by DPPIV was dependent on its enzymatic activity (187). Binding assays were repeated with a DPPIV enzymatic inhibitor to determine if enzymatic activity was necessary for binding of DPPIV. The binding of DPPIV to neutrophils was affected by the addition of a DPPIV enzymatic inhibitor (Figure 36). This is supported by a significantly lower Bmax and increase in K_D in the presence of the inhibitor. This indicates binding of neutrophils to DPPIV is dependent on the enzyme activity of DPPIV.
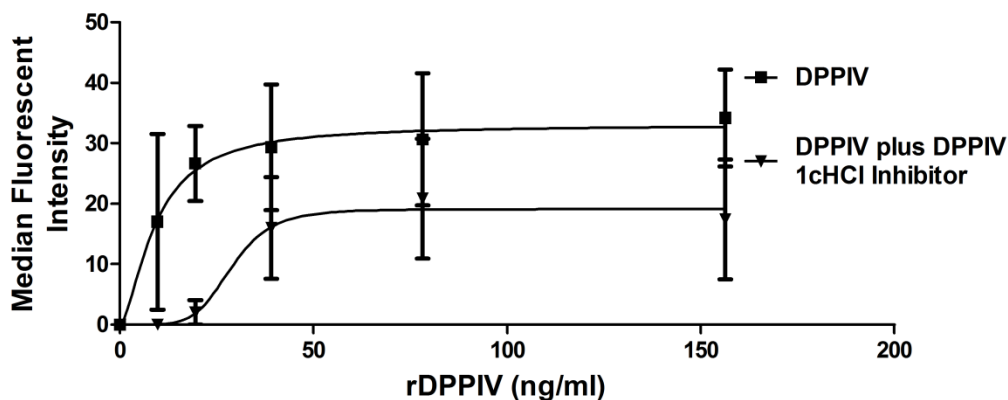
Figure 36: DPPIV enzyme activity is necessary for binding neutrophils. Binding assays were repeated with an inhibitor of DPPIV enzyme activity. Curves are fit to one-site with Hill-coefficient. Values are mean ± SEM, n ≥ 5.

DPPIV effects the localization of actin

Chemoattractants signal to reorganize actin filaments (61). Actin filaments in actively chemotaxing cells are localized to the leading edge (61). In the case of a chemoattractant, this would be the edge closest to the attractant. One would expect if chemorepellents use similar mechanisms, the actin would localize at the leading edge, in this case the edge facing away from the repellent source. Neutrophils in a gradient of DPPIV were fixed and stained with phalloidin-Alexa488 to observe actin localization. Localization was visualized and polarized cells were imaged and counted. The percent of cells moving up and down the gradient were counted. Here, 'toward' indicates actin is polarized closest to the source of DPPIV and 'away' indicates actin was polarized at the cell edge farthest from the source of DPPIV. In both the control and gradient wells, approximately 11% of cells had actin polarization in the toward direction (Figure 37). In the control well, 6% of cells had actin polarized away. This increased to ~26% in DPPIV gradient wells. This suggests that DPPIV may use actin dynamics to regulate chemorepulsion.
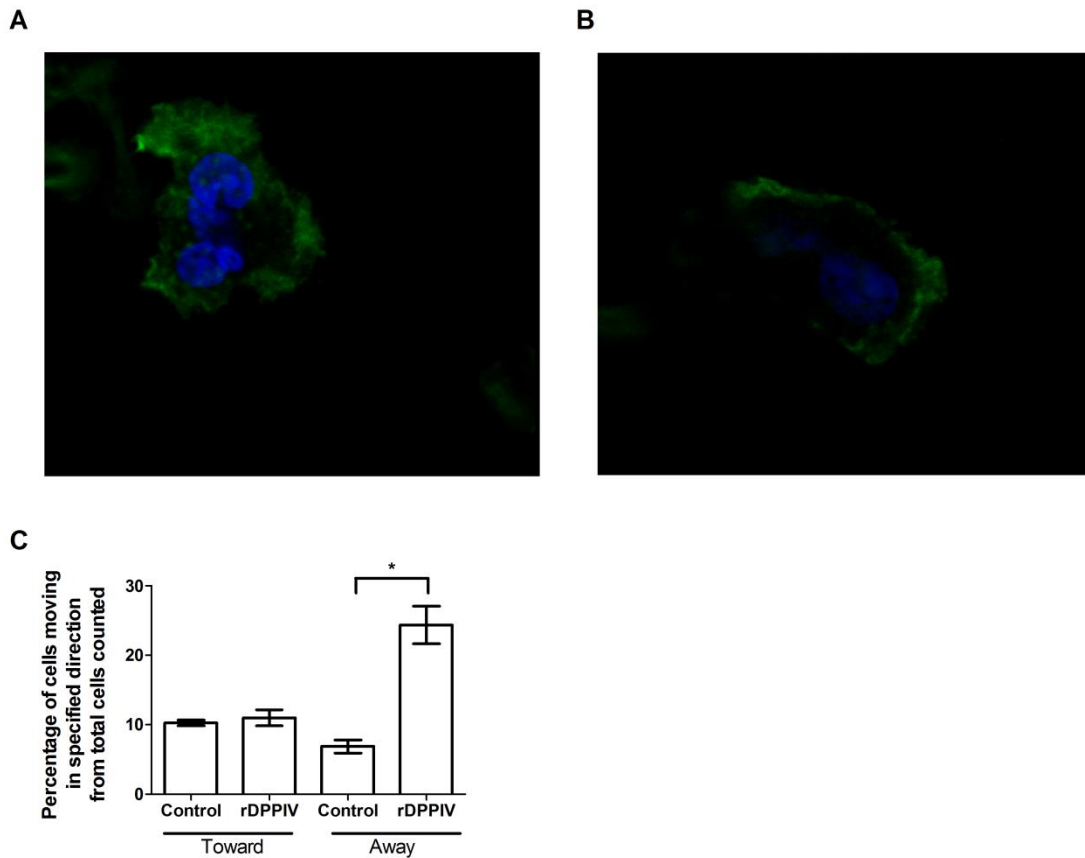
Figure 37: DPPIV affects actin polarization. Human neutrophils were fixed and labeled with phalloidin-Alexa488. **(A)** A representative image from control well and **(B)** a representative image of a cell moving away from DPPIV in the gradient well are shown. **(C)** Quantification of phalloidin localization. Percentage of cell polarized toward or away from DPPIV out of total cells in shown. Values are mean ± SEM (n=3). $p < 0.05$ (t-test).

Discussion

The work in this section of the dissertation examines the mechanism through which DPPIV acts as a chemorepellent. We found that DPPIV can bind to human neutrophils and that this binding is affected by the addition of enzyme inhibitors of

DPPIV enzymatic activity. Gradients of DPPIV increase the number of cells that have actin polarized away from the source of the DPPIV.

DPPIV enzyme activity is required for the chemorepulsion of human neutrophils (187). There was heterogeneity in the binding properties of DPPIV. We found that enzymatic activity is also necessary for neutrophil binding of DPPIV. It is unclear whether DPPIV is actually cleaving a membrane component of neutrophils or the substrate pocket is just necessary for neutrophil binding. DPPIV contains a caveolin binding domain in the substrate pocket including Ser630, part of the enzymatic triad (241). This evidence suggests that DPPIV could be using the substrate pocket without cleaving. Blocking the site with inhibitors, could prevent binding of DPPIV to neutrophils.

Chemoattractants cause polarization of cell components. Cells in a gradient of chemoattractant have PTEN localized to the rear of the cell (the part farthest away from the chemoattractant) to prevent pseudopod formation in the wrong direction (38, 51, 58-60). At the leading edge (the edge closest to the chemoattractant), PIP_3 and Rac are enriched, leading to actin polymerization and pseudopod formation (61). Evidence suggests that chemorepellents function in a reverse of this mechanism where PTEN would be localized closest to the repellent to prevent movement toward it (38, 51, 58-60). Here we found that the chemorepellent DPPIV uses actin dynamics for cells movement. A general increase in actin polarization at the membrane is seen in gradients of DPPIV. Additionally, gradients of DPPIV increase the number of cells with actin localized farthest from the source of DPPIV. Based on the actin localization, these cells

would be moving away from the DPPIV. This suggests that DPPIV chemorepulsion affects actin dynamics.

Conclusions and future directions

Work done in this section of the dissertation analyzes the mechanism of DPPIV-induced chemorepulsion. DPPIV can bind neutrophils in an enzyme-dependent manner. Future work on DPPIV binding will focus on identifying the receptor or binding partner of DPPIV. It will also determine whether DPPIV cleaves the partner or if the substrate pocket is necessary for binding. Future work on the mechanism will examine other known components of chemotaxis pathways such as PTEN for their localization in response to DPPIV gradients.